CR 73046

DEVELOPMENT OF A HOT JET PUMP BLC SYSTEM (JET INDUCED LIFT SYSTEM) PHASE I : BENCH TESTING OF AN EXPERIMENTAL JET PUMP

N67 15159 (ACCESSION NUMBER)

99 (PAGES)

CR-73046 (NASA CR OR TMX OR AD NUMBER)

1 (THRU)

(CODE)

15 (CATEGORY)

FACILITY FORM 602

NASA CR-

DEVELOPMENT OF A HOT JET PUMP BLC SYSTEM

(JET INDUCED LIFT SYSTEM)

PHASE I: BENCH TESTING OF AN EXPERIMENTAL JET PUMP

By Randall J. Seaver

Prepared under Contract No. NAS2-2518 by

SUNRISE AIRCRAFT CORPORATION OF AMERICA

La Mesa, California

for Ames Research Center

NATIONAL AERONAUTICS AND SPACE ADMINISTRATION

For sale by the Clearinghouse for Federal Scientific and Technical Information. Springfield, Virginia 22151-Price

FOREWARD

This document comprises the final report prepared by Sunrise Aircraft Corporation of America for Ames Research Center, Moffett Field, California 94035, under Contract NAS2-2518. The Phase I of this multi-phased program includes design, fabrication and bench testing of an experimental jet pump. The program is intended to lead to wind-tunnel testing of a jet pump powered, boundary layer control system, known as the Jet Induced Lift (JIL) system, as applied to a large scale aircraft model such as the Ames Deflected Slipstream STOL model.

The work on this contract was supervised by Mr. Fred G. Wagner. The subcontractor, Dynatech Corporation of Cambridge, Massachusetts, made valuable contributions in theoretical analysis and experimental techniques.

TABLE OF CONTENTS

ILLUSTRATIONS

Figure

Page

SUMMARY

An experimental jet pump utilizing high energy compressed air as the driving fluid was developed and bench tested. The configuration is typical of the requirements for a jet-induced-high-lift wing system, and is applicable as a boundary layer control device utilizing suction and blowing.

The jet pump was operated continuously for extended periods of time (up to eight hours in several runs) over a wide range of primary jet total pressures and temperatures. Test runs were conducted with six different nozzle sets, each specifically designed for a given input primary jet total pressure and total temperature. The maximum primary jet total pressure was 410 psia, while the maximum total temperature (at the nozzle throat) was 2590°F. The Dynatech Corporation combustor unit installed in the compressed air line was operated at temperatures up to 3560°F.

Induced (suction) airflow of up to 2.433 lb/sec were measured during this investigation. A mass augmentation ratio (blowing slot airflow over compressed air weight flow) of 22.2 for the above suction flow was obtained. The maximum mass augmentation was 28.9 (at a low blowing slot airflow, however). A maximum thrust augmentation (blowing slot thrust over primary jet nozzle thrust) of $\tau = 1.32$ was measured. Using the reference areas of the NASA Ames Deflected Slipstream STOL model wing, maximum BLC flow coefficients of $C_{Q_S} = .032$ (suction flow coefficient) and $C_\mu = .26$ (blowing momentum coefficient) were obtained, at an assumed freestream dynamic pressure, $q_o = 4.5$ lb/ft^2.

Jet pump performance was adversely affected by the total pressure losses caused by an unstreamlined primary jet feedpipe and nozzle cluster obstruction in the suction duct, and duct wall flow separation encountered in the blowing duct. These losses must be reduced in order to achieve the pre-test design point performance $C_{Q_S} = .050$, $C_\mu = .55$.

Tests made with wooden inserts in the suction and blowing ducts improved the duct flow and the loss characteristics. A bellmouth inlet to the mixing

tube was fabricated to evaluate the extent of the total pressure losses caused by the nozzle cluster. Improved performance resulted from the decrease in total pressure loss. Converging (sonic) nozzle operation and extensive off-design point operation resulted in a wide range of data. The flow (or velocity) distribution at the suction (inlet) and blowing (exit) slots were satisfactory, although uneven.

The test results reported herein support the proposition that a high lift system utilizing multiple jet pump represents a feasible means of boundary layer control for Short Take-off and Landing (STOL) aircraft. Further development work is required to improve the jet pump duct configuration in order to attain higher BLC performance at primary jet pressures and temperatures obtainable at the present state-of-the-art.

INTRODUCTION

The jet pump, when utilized as a boundary layer control device, produces suction at the flap hinge over one portion of a wing and ejects a blowing jet sheet over the flaps on another portion of the wing, thereby providing the high lift coefficients necessary for Short Take-off and Landing (STOL) aircraft. Figures 2 and 3 show the jet pump in a BLC application.

The purpose of this program is to generate sufficient data and knowledge to enable design and fabrication of jet pump hardware suitable for future wind tunnel programs. The bench testing of an experimental jet pump represents the initial phase of a possible multi-phased program which may include wind-tunnel testing of a jet pump powered boundary layer control system applied to a large scale aircraft model such as the NASA Ames Deflected Slipstream STOL model.

The present report covers the results of the experimental investigations performed, and presents methods of theoretical and test data analysis.

NOMENCLATURE

Symbols

A	cross-sectional area, ft^2
b	span, ft
c	wing chord, ft
c_p	specific heat at constant pressure Btu/lb°R
C_W	nozzle discharge coefficient
C_Q	BLC air volume flow coefficient, $= \frac{Q}{v_o S_{ref}}$ (at density ρ_o)
C_μ	blowing momentum coefficient $= \frac{W_B v_B}{q_o S_B g}$
C_1, C_2, etc	constants
d	diameter, ft
g	gravitational acceleration, ft/sec^2
h	enthalpy, Btu/lb
h_{RP}	enthalpy of combustion, Btu/lb
J	Joules mechanical equivalent of heat, ft-lb/Btu
k	ratio of specific heats $= c_p/c_v$
l	length, ft
m	entrainment ratio $= \frac{W_S}{W_{PJ}}$
M	Mach number
p	pressure, lb/ft^2 or psia
P	power, hp
q	dynamic pressure $= \frac{1}{2}\rho v^2$, lb/ft^2
Q	air volume flow, ft^3/sec
R	gas constant, ft.lb/lb°R
s	slot width, ft
S	wing area, ft^2
T	temperature, °R or °F

u	mixing efficiency.
v	velocity, ft/sec
W	BLC air weight flow rate, lb/sec
α	velocity ratio = $\frac{v_{SJ}}{v_{PJ}}$ at station I
α	coefficient of linear expansion, per °R
β	velocity ratio = $\frac{v_M}{v_{PJ}}$ at station M
γ	specific weight, lb/ft^3
ε	slot velocity distribution correction factor
Δ	change, difference
η	jet pump efficiency
ρ	mass density = $\frac{\gamma}{g}$, $\frac{lb.sec^2}{ft^4}$
ϕ	nozzle area ratio at station I = $\frac{A_{PJ}}{A_{SJ}}$
τ	thrust augmentation ratio

Subscripts

avg	average
B	blowing
BIT	burner inlet
Bu	burner
D	duct
E	entrance, suction slot
ex	excess
f	flap
fuel	fuel
i	ideal = theoretical
I	primary nozzle plane, Station I
in	input
j	index for summation
JP	jet pump
M	mixture or mixing

o	freestream, ambient, stagnation
out	output
PJ	primary jet
PO	primary driving gas (compressed air) before expansion in primary nozzle
ref	reference
s	static
S	suction
SJ	secondary jet
t	total

Superscripts

*	critical conditions (primary nozzles : throat)
-	average

Constants

A_B	.18680 ft^2
A_{D_B}	.15635 ft^2
A_E	.29514 ft^2
A_I	.08726 ft^2
A_M	.08275 ft^2
c_{p_o}	.240 Btu/lb °R (ambient air)
$c_{p_{avg}}$	.265 Btu/lb°R (combustion tests)
g	32.174 ft/sec^2
h_{RP_o}	19,200 Btu/lb (kerosene)
J	778.16 ft. lb/Btu
p_o	2116 lb/ft^2
R	53.35 ft. lb/lb°R
$T_{t_{BIT}}$	100°F

T_o 70°F (530°R)

α 10.6×10^{-6} /°F (310 stainless steel)

WORK ACCOMPLISHED

Experimental Jet Pump and Test Stand

Dimensions and instrumentation - The experimental jet pump was intended for application to the NASA Ames Deflected Slipstream STOL model. Figure 4 shows the jet pump configuration in the model wing. The basic dimensions of the jet pump and the internal dimensions of the primary jet nozzles are given in figures 5 and 6.

The instrumentation of the experimental jet pump provided for measurement of the primary air mass flow rate, total temperature and total pressure; the secondary air mass flow rate; mixing tube and diffuser total pressure profiles; static pressure profiles across the inlet (suction) slot and in the ducts and mixing sections from wall taps at various locations along and transverse to the duct axis. Total pressure distributions were taken at the exit (blowing) slot, and flow angles at the exit slot were measured. The methods and parameters affected are summarized in table 1. A summary schematic of the instrumentation is shown in figure 7.

Fabrication - The basic components of the jet pump are the suction duct and slot, mixing tube, downstream conical diffuser, and the blowing diffuser duct and slot. The suction and blowing ducts were constructed of laminated fibreglass. The mixing tube and conical diffuser were made of 15ST aluminum. The primary jet feedpipe and nozzle cluster assembly were fabricated with Hastelloy "C" nickel alloy, while the nozzle tips were fabricated of a variety of materials (see figure 6), generally depending upon the temperature range involved. A bellmouth entrance was constructed of laminated wood for the tests conducted with the suction duct removed.

TABLE 1. - DATA ACQUISITION

	Flow Parameters	Instrumentation Used to Measure	Required for Determining
Primary jet	$p_{t_{PO}}$	Bourdon tube gage	Jet pump input conditions
	$T_{t_{PO}}$	Heater tests: Thermocouple and bridge Burner tests: not measured	Jet pump inlet conditions
	$W_{air_{PJ}}$	Flow meter and panel gage	Jet pump performance
	$W_{fuel_{PJ}}$	Rotameter	Jet pump performance
Secondary flow	p_o	Barometer	Suction slot inlet total pressure Blowing slot exit static pressure
	T_o $p_{t_{D_B}}, T_{t_{D_B}}$ or p_{t_M}, T_{t_M}	Thermometer Total pressure probe and Kiel temperature traverse	Suction slot inlet total temperature $\bar{p}_{t_{D_B}}$ or $\bar{p}_{t_M}$ Jet pump performance
	p_E	Static pressure taps along suction slot and traversing static probe	W_{SJ}, suction slot velocity distribution
	p_{t_B}	Total pressure rake traverse (Blowing duct)	Blowing duct losses $\bar{p}_{t_M} - \bar{p}_{t_B}$ Blowing slot velocity distribution
	Wall static pressure distribution	U-tube and well-type manometers	Static pressure survey throughout the suction duct, mixing tube and diffuser and blowing duct

Primary air supply system - The tests were performed at the subcontractor's test facility (Dynatech Corporation of Cambridge, Massachusetts). The tests conducted can be placed in two categories: 1) cold and electrically heated compressed air tests; 2) combustion heated compressed air tests. The primary air flow loop schematic of the test facility is shown in figure 8.

The primary air in all tests was supplied by a two-stage reciprocating compressor which can deliver over 6 lb/min at a pressure of 425 psig. When desired, the air is heated after leaving the compressor by two 240V, 25 kw electric heaters in a series flow arrangement. The temperature of the air leaving the heaters can be controlled to $\pm$ 20°F within the range from 200° to 1200°F. Heater discharge pressure can be controlled to $\pm$ 2 psi within the range 50 to 410 psig.

For use in the testing above 1200°F, Dynatech developed a combustor heating system which delivered the compressed air at temperatures up to 3560°F at the combustor outlet. This burning chamber was originally designed by General Electric Company for jet engine starter service. By modifying the combustor fuel nozzles, ignition system and starting procedures, Dynatech achieved reliable operation at the .11 lb/sec flow rate, which is 1/7 of the combustor design flow rate. The combustor fuel (kerosene) was provided by a nitrogen-pressurized fuel system, regulated by a precision needle valve and measured by a rotameter flow meter. The fuel system is shown schematically in figure 8, and a cutaway view of the combustor is shown in figure 9.

Test stand - The jet pump was mounted on a test stand (figure 10). The low temperature feedpipe (60-1200°F) and the high temperature combustion chamber are shown in figures 11 and 13. The installation of the primary jet nozzle cluster and supporting strut (with the top of the suction duct removed) is presented in figure 12. The bellmouth entrance to the mixing tube (suction duct removed) is shown in figure 14. The manometer bank (figure 15) concludes the test set-up.

Experimental Investigations

Primary jet nozzles - The six primary jet nozzles design points cover the spectrum of operating conditions as shown below:

TABLE 2. - PRIMARY JET DESIGN POINTS

Nozzle Set	Primary Jet Total Pressure $P_{t_{PO}}$, psia	Primary Jet Total Temperature $T_{t_{PO}}$, °F
1	100	60
2	350	60
3	100	1200
4	350	1200
5	100	3000
6	400	3000

The nozzle sets bench tested were numbers 2, 3, 4 and 6; two other nozzle sets were fabricated. One nozzle set, designated 4A, was a set of converging (sonic) nozzles having the same throat area as the set 4 primary jet nozzles. The other nozzle set, designated 6R, was fabricated with the nozzle set 6 dimensions but with more suitable material.

Bench tests - 38 test runs were conducted using the six different nozzle sets. Tables 3 and 4 summarize the primary jet total pressure and total temperature for the pertinent tests performed. For the combustion tests, the total temperature of the combustor is given. In the first test run (number 3-1), at least one nozzle in the set was blocked by small pieces of ceramic material from the upstream heater insulation. A filter was placed in the line for following tests. A test under the nozzle set 4 conditions was run with five nozzles blocked (designated test run 4P), in order to determine the effect of the number of operating nozzles on jet pump performance.

TABLE 3 - ELECTRICALLY HEATED AIR TESTS

Test Run	Primary Jet Total Pressure $P_{t_{PO}}$, psia	Primary Jet Total Temperature $T_{t_{PO}}$, °F	Remarks
2-1	350	144	Design point
2-2	300	114	
2-3	250	150	
2-4	200	150	
3-1	100	1180	2 nozzles blocked
4-1	350	1200	Design point
4-2	300	1200	
4-3	260	1200	
4-4	225	1200	
4A-1	345	1150	Sonic nozzle test
4A-2	265	1200	Sonic nozzle test
4A-3	215	1200	Sonic nozzle test
4A-4	170	1130	Sonic nozzle test
4P-1	350	1200	4 nozzles blocked
4P-2	300	1200	4 nozzles blocked
4P-3	260	1200	4 nozzles blocked
4B-1	350	1170	Bellmouth entrance
4B-2	300	1195	Bellmouth entrance
4B-3	260	1240	Bellmouth entrance
4B-4	350	1200	Nozzle cluster moved 1 inch back from original station I
			Bellmouth entrance

TABLE 4 - COMBUSTOR HEATED AIR TESTS

Test Run	Primary Jet Total Pressure $P_{t_{PO}}$, ~~°F~~ psia	Primary Jet Total Temperature (calculated) $T_{t_{PO}}$, °F	Burner Total Temperature $T_{t_{Bu}}$, °F	Remarks
3-2	102	1650	2050	
3-3	102	1950	2440	
4-5	350	1840	2200	
4-6	346	2240	2930	
4-7	350	2590	3340	
4A-5	345	2110	2330	
4A-6	349	2450	2790	
6-1	350	2140	2890	
6-2	393	2220	2960	
6R-1	410	1670	2070	
6R-2	410	1600	2100	Suction duct insert
6R-3	410	1640	2230	Suction and Blowing inserts
6R-4	410	2050	2910	" " "
6R-5	410	2250	3240	" " "
6R-6	410	2590	3560	" " "

In several of the nozzle set 6R tests, wooden inserts were placed in the suction and blowing ducts in an effort to improve the flow characteristics and to reduce the total pressure losses. In order to determine the total pressure losses due to the nozzle cluster obstruction, tests (designated 4B) were performed with the suction duct removed and a straight bellmouth type entrance installed. Another test was made with the nozzle cluster backed off one inch from the design position (Station I in figure 14).

TEST RESULTS

The bench test results of the jet pump can be presented in terms of the input (primary) conditions, the output (exit slot) conditions, and the pertinent relationships between the input and output parameters. Table 5 summarizes the jet pump performance for each nozzle set design point (or the test nearest the design point). For results of all tests performed, Appendix B presents the analytical methods and the test data in tabular form.

ANALYSIS AND DISCUSSION

Jet Pump Design Point

Aerodynamic coefficients - Using dimensions of the existing NASA Ames Deflected Slipstream STOL Model wing (envisioned with four jet pumps per wing panel), the most outboard jet pump was chosen for the design of the experimental jet pump to be bench tested (see figure 4). The aircraft (or large scale wind tunnel model) design conditions for this jet pump are (Ref.1):

Design freestream dynamic pressure . . . . . $q_o = 4.5$ lb/ft^2

Suction reference wing area . . . . . $S_S = 16.178$ ft^2

Blowing reference wing area . . . . . $S_B = 14.707$ ft^2

The following BLC flow coefficients (based on the model dimensions) were considered desirable for obtaining STOL performance:

Suction flow coefficient $C_{Q_S} = .050$

Blowing momentum coefficient $C_\mu = .55$

TABLE 5 - SUMMARY OF DESIGN POINT
JET PUMP PERFORMANCE

Test run	2-1	3-2	4-1	4A-1	6R-6
Remarks	-	-	-	convergent (sonic) nozzles	suction and blowing duct inserts
Primary jet total pressure, $p_{t_{PO}}$, psia	350	102	350	345	410
Primary jet total temperature, $T_{t_{PO}}$, °F	144	1650	1200	1200	2590
Primary jet weight flow rate, W_{PJ}, lb/sec.	.123	.101	.107	.123	.097
Primary jet exit velocity, v_{PJ}, ft/sec.	2092	3530	3581	3515	5164
Blowing jet sheet weight flow rate, W_B, lb/sec.	1.823	2.018	2.082	2.093	2.483
Blowing jet sheet velocity, v_B, ft/sec.	131	166	167	167	213
Blowing jet sheet temperature, T_{s_B}, °F	74	153	136	132	176
Mass augmentation, $\frac{W_B}{W_{PJ}}$	14.82	20.05	19.49	16.97	25.69
Thrust augmentation $\tau = \frac{W_B v_B}{W_{PJ} v_{PJ}}$	.928	.940	.907	.808	1.056
Suction flow coefficient, C_{Q_S}	.0223	.0252	.0259	.0259	.0314
Blowing momentum coefficient,	.112	.157	.163	.164	.248

Jet pump parameters - The experimental jet pump was designed for the nozzle set 6 primary jet conditions of $p_{t_{PO}}$ = 400 psia, $T_{t_{PO}}$ = 3000°F. The nozzle sets for the other cases were dimensional for producing (as closely as possible) the same BLC flow coefficients. Table 6 is a brief summary of the predicted design point conditions for the nozzle sets 4 and 6 tests (Ref. 1 and 2).

TABLE 6 - PREDICTED PERFORMANCE

Parameter	Nozzle Set 4	Nozzle Set 6
Primary jet total pressure, $p_{t_{PO}}$, psia	350	400
Primary jet total temperature, $T_{t_{PO}}$, °F	1200	3000
Primary jet airflow rate, W_{PJ}, lb/sec.	.115	.095
Entrainment ratio, $m = \frac{W_S}{W_{PJ}}$	31.9	40
Secondary jet suction airflow rate, W_S, lb/sec	3.669	3.800
Velocity ratio, $\alpha = \frac{v_{SJ}}{v_{PJ}}$ (at station I)	.183	.130
Blowing (slot) dynamic pressure, q_B, lb/ft^2	95	95
Suction duct total pressure loss, $\Delta p_{t_{SJ}}$, lb/ft^2	8	8
Blowing duct total pressure loss, $\Delta p_{t_{D_B}}$, lb/ft^2	9.5	9.5
Thrust augmentation, $\tau = \frac{W_B v_B}{W_{PJ} v_{PJ}}$	2.50	2.31
Suction flow coefficient, $C_{Q_S} = \frac{W_S}{\rho_o v_o S_S g}$	.050	.050
Blowing momentum coefficient, $C_\mu = \frac{W_B v_B}{g q_o S_B}$	.550	.550

Jet Pump Performance

Total pressure rise - In a jet pump, the thermal (potential) energy converted to kinetic energy by the primary jet nozzles will act to increase the pressure of the secondary air stream. This increase in pressure is dependent upon the primary jet momentum, which is a function of the primary jet total pressure and total temperature.

TABLE 7 - TOTAL PRESSURE RISE

Test Run	Primary Jet Total Pressure $p_{t_{PO}}$, psia	Primary Jet Total Temperature $T_{t_{PO}}$, °F	Jet Pump Total Pressure Rise $\Delta p_{t_{JP}}$, lb/ft^2
2-1	350	144	83
4-1	350	1200	115
4-7	350	2590	120
3-2	102	1650	101
6R-3	410	1640	138

The preceding table 7 shows the results obtained in selected bench tests. The jet pump total pressure rise, $\Delta p_{t_{JP}}$, can be expressed as :

$$\Delta p_{t_{JP}} = u\,(\Delta p_{t_{JP_i}}),\ \text{lb/ft}^2 \quad \ldots\ldots\ldots\ldots\ldots\ldots\ldots\ldots \quad (3)$$

The mixing efficiency, u, is discussed in detail in another section. In the following analysis, the mixing efficiency is assumed to be equal to 1.00. The ideal total pressure rise, $\Delta p_{t_{JP_i}}$, is that pressure rise which would be achieved if wall friction losses are negligible within the mixing tube, the flow is well mixed at the mixing tube discharge, and the primary jet adjusts isentropically to the secondary jet static pressure.

The ideal total pressure rise may be plotted as a function of entrainment ratio, following the calculation procedure given in Appendix A. For the primary jet input total pressure, $p_{t_{PO}}$ = 350 psia and total temperature, $T_{t_{PO}}$ = 1200°F, table 8 indicates that the ideal jet pump total pressure rise decreases as the entrainment ratio (and total airflow) increases. This is reasonable, since the

same input energy must raise the pressure of a larger air mass.

TABLE 8 - IDEAL TOTAL PRESSURE RISE

Entrainment Ratio, $m = \frac{W_S}{W_{PJ}}$	Ideal Jet Pump Total Pressure Rise, $\Delta p_{t_{JP_i}}$, lb/ft^2
15	120.5
18.5 (Test point)	115
20	114
30	93
35	69
Note: $p_{t_{PO}} = 350$ psia, $T_{t_{PO}} = 1200°F$, $W_{PJ} = .107$ lb/sec	

Entrainment ratio - In jet pumps, secondary fluid flows at a relatively low head output are induced by a high pressure primary fluid (at a low flow rate). The ratio of this induced airflow rate (suction flow rate, W_S) to the driving fluid flow rate (primary jet flow rate, W_{PJ}) is the entrainment ratio, m.

$$m = \frac{W_S}{W_{PJ}} \quad \ldots\ldots\ldots\ldots\ldots\ldots\ldots\ldots\ldots\ldots \quad (4)$$

It can be shown that the entrainment ratio is dependent upon the total pressure rise of the mixed streams (and therefore dependent upon the primary jet total temperature and pressure), by applying the continuity relationship at the blowing slot,

$$W_B = \rho_B v_B A_B g = (m + 1)\, W_{PJ}, \text{ lb/sec} \quad \ldots\ldots\ldots\ldots\ldots \quad (5)$$

and the fact that the dynamic pressure at the blowing slot, q_B, can be defined as

$$q_B = \Delta p_{t_{JP}} - \Delta p_{t_{loss}} = \frac{1}{2} \rho_B v_B^2, \frac{lb}{ft^2} \quad \ldots\ldots\ldots\ldots\ldots \quad (6)$$

where:

$\Delta p_{t_{loss}}$ is the total pressure loss of the entire system.

Rearranging equation (6):

$$v_B = \sqrt{\frac{2}{\rho_B}\left[\Delta p_{t_{JP}} - \Delta p_{t_{loss}}\right]}, \text{ ft/sec} \quad \ldots\ldots\ldots\ldots\ldots\ldots \quad (7)$$

Substituting equation (7) into equation (5),

$$m = \sqrt{2\rho_B\left[\Delta p_{t_{JP}} - \Delta p_{t_{loss}}\right]}\,\frac{A_B g}{W_{PJ}} - 1 \quad \ldots\ldots\ldots\ldots\ldots\ldots \quad (8)$$

Equation (8) shows that the entrainment ratio is also a function of the total pressure losses in the system. Therefore, the greatest effort must be made to minimize the total pressure losses in the ducts.

Figure 16 presents the variation of the dynamic pressure at the blowing slot, q_B, with the entrainment ratio for the test run 4-1. A similar curve could be drawn to show the relationship of the blowing momentum coefficient, C_μ, to the entrainment ratio. By calculating the ideal jet pump total pressure rise (as outlined in Appendix A), and applying the mixing efficiency, u, definition as the ratio of actual jet pump total pressure rise to the ideal total pressure rise, a family of curves as drawn in figure 16 may be presented as a function of entrainment ratio. The significance of figure 16 is that it can completely define the performance of the jet pump for

1) given input parameters (W_{PJ}, $p_{t_{PO}}$, $T_{t_{PO}}$)
2) given mixing efficiency, u
3) given jet pump geometry.

For example, for test run 4-1, at an entrainment ratio of m = 18.5, the total pressure rise in the jet pump (assuming u = 1.00) will be 116 lb/ft^2, from figure 16. The blowing slot dynamic pressure, q_B, at m = 18.5 is 29 lb/ft^2. The total pressure losses in the duct system, $\Delta p_{t_{loss}}$, is therefore 87 lb/ft^2, by equation (6). With the same nozzle set, it can be seen that increased jet pump performance will be realized with a lower loss characteristic.

Total pressure losses - The total pressure losses in the suction and blowing ducts incurred in the bench test series adversely affect the performance of the jet pump. The suction duct total pressure losses are caused by suction slot entrance losses, air diffusion, air turning, air friction on the duct walls, and the pressure losses due to the primary jet feedpipe and nozzle cluster obstruction. The last factor comprises the largest portion of the suction duct total pressure losses. Surface friction, abrupt duct area (and velocity) changes and the turbulent wake in the mixing tube caused by the feedpipe, nozzle cluster, and support rod are the major components of the total pressure losses due to this nozzle cluster assembly. The predicted value of the suction duct total pressure losses (8 lb/ft^2 at a flow rate of 3.80 lb/sec) was based on experimental evidence obtained in prior tests (Ref 1) having a different feedpipe and nozzle cluster design.

The pressure losses in the blowing duct are caused by blowing air diffusion (including wall separation), turning and friction. The predicted total pressure loss (Ref. 1) was 9.5 lb/ft^2, but no allowance was made for some duct wall flow separation experienced in the bench tests. Figure 17 shows the total pressure losses in the blowing duct (downstream of Station M - see figure 1) incurred in the bench tests. In the test run 6R, a sanded wooden insert was installed in the blowing duct to improve the flow characteristics and to decrease the losses (also in figure 17).

The suction duct losses cannot be accurately determined at this time, due to an apparent error in the static tap 21 measurement of static pressure in the mixing section. However, the losses can be estimated if the mixing efficiency of the jet pump can be ascertained. By calculating the ideal jet pump total pressure rise for each case (using the measured pressure p_{SJ} (tap 21)) and subtracting the test value of $(p_{t_M} - p_o)$ which represents the excess total pressure at the end of the mixing tube, an approximation of the suction duct total pressure loss curve may be made for a mixing efficiency value, u = 1.00. Another difficulty in accurately defining the losses is incomplete mixing at the end of the mixing tube (as "Flow Characteristics" section), hence the total pressure value at the end of the mixing tube, p_M, may not be correct.

Taking these factors into account, the curve of suction duct total pressure loss as a function of airflow rate is drawn in figure 17. The most obvious anomalies are the nozzle set 4P and 6R series. The 4P test series was run with four blocked nozzles (reduced mixing efficiency), while the 6R test series was run with a sanded wooden insert in the suction duct, which caused a reduction in the losses.

One test run (not summarized in the Appendices) was made with a 17-foot long pipe of 6-inch diameter connected to the mixing tube inlet. A comparison of the suction duct total pressure losses of this test with those encountered in tests with the suction duct attached and the bellmouth inlet attached is given in the table below:

Parameter	Suction duct on	Bellmouth entrance	Pipe entrance
Test run	4-1	4B-1	-
Suction airflow rate, W_S, lb/sec	1.975	2.343	1.933
Suction duct total pressure losses, $\Delta p_{t_{SJ}}$, lb/ft^2	66	44	73

For the pipe entrance, the calculated pressure loss due to wall friction was 10 lb/ft^2. Hence, the total pressure loss due to the nozzle cluster in the axial flow was 63 lb/ft^2. If a relationship such as

$$\Delta p_{t_{SJ}} = C\, W_S^2, \text{ lb/ft}^2 \quad \ldots\ldots\ldots\ldots\ldots\ldots\ldots\ldots \quad (9)$$

is assumed, the constant C for the long pipe entrance (removing the wall friction effect) is 16.9. For the test run 4-1, C is also calculated to be 16.9. It should be noted that in tests with the suction duct on, the total secondary airflow does not pass over the nozzle cluster in an axial direction, and that some losses occur in the ducts due to friction, turning, and diffusion. However, it can be said that a large percentage of the suction duct total pressure loss is due to the nozzle cluster and primary feedpipe.

By taking the difference between the $\Delta p_{t_{JP}}$ and q_B curves in figure 16, the relationship between the total pressure losses and entrainment ratio can be found, as shown in figure 18. From this figure, table 9 can be generated.

TABLE 9 - EFFECT OF TOTAL PRESSURE LOSSES

Parameter	Test Run 4-1	Ideal Case (Hypothetical)
Total pressure loss, $\Delta p_{t_{loss}}$, lb/ft^2	87	0
Entrainment ratio, m	18.5	32.9
Suction flow coefficient, C_{Q_S}	.0259	.0462
Blowing momentum coefficient, C_μ	.163	.463
Thrust augmentation, τ	.907	2.576

The above table illustrates the important and over-riding part that the total pressure losses play in determining jet pump performance. The ideal case of table 9 is the theoretical maximum performance obtainable with the nozzle set 4 at design point input conditions.

By streamlining the nozzle cluster and feedpipe, and by improving the duct flow with inserts in both the suction and blowing ducts, the total pressure losses will be substantially reduced, and improved jet pump performance will be obtained.

Mixing efficiency - The mixing efficiency, u, may be presented as:

$$u = \frac{\Delta p_{t_{JP}}}{\Delta p_{t_{JP_i}}} \quad \text{. . . . .} \quad (10)$$

The equation (10) states that only a percentage of the ideal jet pump total pressure rise is accomplished in the real case, due to imperfect mixing, wall friction losses, and "accommodation" losses due to the shock and expansion waves induced by unequal static pressure at the nozzle plane (i.e., $p_{PJ} \neq p_{SJ}$). Unfortunately, no meaningful mixing efficiency data may be gleaned

from the bench tests performed. As shown in the following section, the static pressure at the mixing (or nozzle) plane (p_{SJ}), was not correctly measured, hence all total pressure loss (and therefore all total pressure rise) measurements are, at best, only estimates. For the design point tests, the mixing efficiency is approximately u = 1.00. For the off-design pressure runs, u will be less than 1.0 due to the "accommodation" necessary to equalize $p_{PJ} = p_{SJ}$.

Static pressure tap 21 - The static pressure tap 21 at the mixing tube entrance (see figure 1 - station I) was suspected to have given a reading too low. Therefore, accurate measurement of the suction duct total pressure loss and the jet pump total pressure rise were not possible; reliance must be placed upon the ideal case.

The evidence for the above statement is this: Under the test run 4-1 conditions, the calculated value of $\Delta p_{t_{JP}}$, based upon the indicated static pressure is 143 lb/ft^2 (see Table B5). However, the ideal jet pump total pressure rise is calculated to be only 115 lb/ft^2 (see Table A1). Since an "ideal" jet pump can produce only 115 lb/ft^2 at this entrainment ratio, the actual value of $\Delta p_{t_{JP}}$ must be less than 115 lb/ft^2. This means that the true value of p_{SJ}(tap 21) must be higher than the static pressure indicated. It should be noted that tap 21 is in a region of curving streamlines and rapidly changing pressures (see figure 23), thus it is not surprising that tap 21 might be inaccurate. It is likely that the true value of static pressure of the secondary (suction) air lies between that indicated by the taps 18 and 21.

Bellmouth entrance - The bellmouth entrance (suction duct removed) increased the performance of the jet pump. The decrease in total pressure losses resulting from the suction duct being removed is the reason for the increased performance. Figure 19 compares this data with previous test points, on an entrainment vs. primary jet total pressure basis. Since the higher entrainment ratio and the relatively equal primary airflow result in a higher secondary airflow rate, the true effect of the bellmouth entrance is somewhat obscured. A true comparison can be made by assuming the secondary flow rates of test 4B-1 through 4B-3 are equal to those of the test series 4-1 through

4-3, respectively, and calculating entrainment ratios by the methods of the "Performance Prediction" section (also in figure 19).

In the test designated 4B-4, the nozzle cluster was moved out of the mixing tube in small increments. The maximum entrainment ratio was attained when the nozzle plane was one inch upstream of the original nozzle plane (station I on figure 1). The maximum entrainment obtained with this "telescoping" action was m = 21.9; if the secondary flow were to be assumed equal to that of test 4-1, and the entrainment calculated (discussed above), the resulting entrainment ratio would be m = 27.4 for a jet pump designed for the secondary mass flow of test 4-1.

The static pressure distribution in the mixing tube (bellmouth entrance tests) was comparable to previous tests. However, the static pressure recovery in the conical diffuser was less than in previous tests. For typical pressure profiles, see figure 23 in the "Flow Characteristics" section.

Sonic nozzle operation - Sonic (converging) nozzle operation results in slightly lower entrainment ratios, compared to supersonic (converging - diverging) nozzles, at high primary jet total pressure. Table 10 compares the test run 4A-1 (sonic nozzles) to the run 4-1 (supersonic nozzles) data.

The table shows the differences in entrainment ratio and thrust augmentation obtained with sonic nozzles. The estimated mixing efficiency was calculated by summing the terms q_B (table B6), $\Delta p_{t_{SJ}}$ (figure 17), and $\Delta p_{t_{D_B}}$ (figure 17), to obtain the actual jet total pressure rise, $\Delta p_{t_{JP}}$, and dividing by the ideal jet pump total pressure rise, $\Delta p_{t_{JP_i}}$, from table A1.

Off design point operation - When the primary nozzles are operated at a total pressure lower than the design pressure, a decrease in jet pump performance (C_{Q_S}, C_μ) results. Table 11 gives the pertinent performance data for the test series 4-1 thru 4-4.

TABLE 10 - SONIC NOZZLE OPERATION

Parameter	Test run 4A-1	Test run 4-1
Primary jet total pressure, $p_{t_{PO}}$, psia	345	350
Primary jet total temperature, $T_{t_{PO}}$, °F	1200	1200
Primary jet weight flow rate, W_{PJ}, lb/sec	.123	.107
Secondary air weight flow rate, W_S, lb/sec	1.970	1.975
Entrainment ratio, $m = \frac{W_S}{W_{PJ}}$	15.97	18.49
Estimated mixing efficiency, u	.84	1.00
Thrust augmentation, τ	.808	.907

TABLE 11 - OFF DESIGN POINT OPERATION

Parameter	Test run			
	4-1	4-2	4-3	4-4
Primary jet total pressure, $p_{t_{PO}}$, psia	350	300	265	225
Primary jet total temperature, $T_{t_{PO}}$, °F	1200	1200	1200	1200
Primary jet weight flow rate, W_{PJ}, lb/sec	.107	.096	.077	.067
Secondary air weight flow rate, W_S, lb/sec	1.975	1.822	1.750	1.608
Entrainment ratio, $m = \frac{W_S}{W_{PJ}}$	18.49	19.07	22.83	24.12
Suction airflow coefficient, C_{Q_S}	.0259	.0239	.0230	.0211
Blowing momentum coefficient, C_μ	.164	.138	.124	.103

Number of nozzles - The effect of the number of nozzles on jet pump performance was tested. In the test series 4P, four nozzles were plugged, leaving five in operation (resulting in 5/9 of the 9-nozzles airflow rate). The resulting mixing efficiencies are on the order of 80% (see table 12 below). A true correlation of data would be made only if a 5 nozzle cluster was fabricated for the 9 nozzle airflow rate; with such a configuration, u might have higher values.

TABLE 12 - EFFECT OF NUMBER OF NOZZLES

Parameter	Test run	
	4-1	4P-1
Number of primary nozzles	9	5
Primary jet total pressure, $p_{t_{PO}}$, psia	350	350
Primary jet total temperature, $T_{t_{PO}}$, psia	1200	1200
Primary jet weight flow rate, W_{PJ}, lb/sec	.107	.061
Secondary air weight flow rate, W_S, lb/sec	1.975	1.427
Entrainment ratio, $m = \frac{W_S}{W_{PJ}}$	18.49	23.39
Estimated mixing efficiency, u	1.00	.81
Thrust augmentation, τ	.907	.787

Flow Characteristics

Suction slot and duct - The spanwise velocity distribution at the suction slot was satisfactory. Figure 20 shows the velocity profile for the test run 4-1. It is a typical plot (i.e., the other test runs produced essentially the same spanwise distribution). It can be seen that the highest velocities are attained at that portion of the slot nearest the mixing tube. The small sanded wooden insert placed in the suction duct ramp (outlined in figure 20) did not improve the spanwise velocity distribution.

The flow within the suction duct can best be described as complex. After entering the slot, the air enters the chordwise flow suction duct in which it flows nearly perpendicular to the mixing tube axis. A 70° turn is then made (in the ideal case) into the spanwise suction duct which carries the air past the obstruction of the nozzle cluster into the mixing tube. Probing within the duct indicated a turbulent area where the sanded insert was placed in the nozzle set 6R tests (figure 20).

Mixing tube and conical diffuser - Extensive total pressure and temperature probing was made in the mixing tube and conical diffuser at three different stations. The figures 21 show the velocity profile near the end of the mixing tube and near the end of the diffuser for the test run 4-1. Three different traverse angles are presented. Figures 22a and 22c show the temperature profiles for the same stations and traverse angles. In some cases, for example, figure 21a, the probe was not centered on the primary jet, and the influence of the nozzle is not reflected in the profiles. It should be noted that the temperature of the air in this test was below 300°F in the mixing tube and below 200°F in the diffuser. Neither the mixing tube or diffuser were too warm to touch in any test.

The static pressure distribution in the jet pump for test 4-1 is given in figure 23. The large total pressure loss occurring in the suction duct is indicated on the plot at tap 21, the nozzle exit plane. Downstream of the nozzle exit plane, the static pressure is recovered by expansion in the conical diffuser, and in most test runs, the static pressure within the duct equalled the atmosphere pressure at the end of the conical diffuser.

Downstream diffuser and blowing duct - After the air streams are mixed and expanded, the mixture must be turned into the blowing slot before flowing over the hypothetical deflected flap (aileron). Further diffusion and turning is accomplished with the downstream diffuser. The sharp bend in the duct between static taps 3 and 4 causes the air to separate from the lower surface of the duct. The total pressure loss caused by this separation is shown in figure 24. The effect of the sanded wooden insert in the blowing duct is also shown in figure 24; the separation from the duct wall is delayed until between

static taps 4 and 5.

Blowing slot - The spanwise velocity distribution of the blowing jet sheet (test run 4-1) is satisfactory (figure 25). The centrifugal action caused by the large turning angle in the blowing duct forces higher velocities outboard. No back-flow was noted along the blowing slot span.

The flow profile vertically across the slot is given in figure 26. From this and similar plots, the blowing slot profile correction factor ϵ_B, may be calculated (see figure 27).

Performance Prediction

Empirical relationships - On the basis of the test data obtained, the performance of the jet pump (m, $\Delta p_{t_{JP}}$) can be predicted by equations (11) through (17) for the design point and combustion chamber (high temperature) data. The duct characteristic equations are determined by the duct configuration (e.g., suction duct removed, inserts added, etc).

$$\Delta p_{t_{JP}} = CW_S^2, \text{ lb/ft}^2 \quad \ldots\ldots\ldots\ldots\ldots\ldots\ldots\ldots \quad (11)$$

where:

C = 30.0 for test runs 2, 3, 4 and 6 (original duct system - no inserts)

C = 24.0 for test run 6R (sanded wooden inserts improve flow characteristics)

C = 22.4 for test run 4B (bellmouth entrance)

The jet pump total pressure rise may also be expressed, as a first approximation, as a function of the primary jet momentum, $W_{PJ}v_{PJ}$; the assumption is valid when $[(m + 1)\, v_M - mv_{SJ}] \ll v_{PJ}$

$$\Delta p_{t_{JP}} = C_1 \frac{W_{PJ}v_{PJ}}{g}, \text{ lb/ft}^2 \quad \ldots\ldots\ldots\ldots\ldots\ldots\ldots\ldots \quad (12)$$

and substituting:

$$W_{PJ} = \frac{C_2 P_{t_{PO}} C_W A_{PJ}^*}{\sqrt{T_{t_{PO}}}}, \text{ lb/sec} \quad \ldots\ldots\ldots\ldots\ldots\ldots \quad (13)$$

$$v_{PJ} = M_{PJ}\, a_{PJ} = M_{PJ} \sqrt{kgRT}_{s_{PJ}} = C_3 M_{PJ}^* \sqrt{T_{t_{PO}} \frac{2}{k+1}}, \text{ ft/sec} \quad \ldots \quad (14)$$

where:

$M_{PJ}^* = \frac{v_{PJ}}{a_{PJ}^*}$; a_{PJ}^* = speed of sound at nozzle throat conditions.

so that:

$$\Delta p_{t_{JP}} = C_4 P_{t_{PO}} C_W A_{PJ}^* M_{PJ}^*, \text{ lb/ft}^2 \quad \ldots\ldots\ldots\ldots\ldots \quad (15)$$

where:

$P_{t_{PO}}$ is in psia

A_{PJ}^* is in ft^2

C_4 is in Table 13 below.

Combining equations (11) and (15), the secondary flow rate is:

$$W_S^2 = C_5 P_{t_{PO}} C_W A_{PJ}^* M_{PJ}^*, \frac{lb^2}{sec^2} \quad \ldots\ldots\ldots\ldots\ldots\ldots \quad (16)$$

where:

C_5 is in Table 13 below.

Finally, the entrainment ratio can be predicted by the following equation, utilizing equations (13) and (16):

$$m = \frac{W_S}{W_{PJ}} = C_6 \sqrt{\frac{T_{t_{PO}} M_{PJ}^*}{P_{t_{PO}} C_W A_{PJ}^*}} \quad \ldots\ldots\ldots\ldots\ldots\ldots \quad (17)$$

where:

C_6 is in Table 13 below.

TABLE 13 - CONSTANTS FOR EMPIRICAL EQUATIONS

Test Run	Constant C_4	Constant C_5	Constant C_6	Remarks
2, 3, 4, 4A, 6	1060	35.33	.0776	Original duct system
6R	1000	41.67	.0843	Original duct system with sanded wooden inserts added
4B	1025	45.75	.0883	Bellmouth entrance

In figure 28, the predicted suction airflow (calculated by equation 16) is compared with test data for each case. The major difference between prediction and test values are in the test runs 2 and 4A data. The consistent deviation from prediction for set 2 may be due to the effect of moisture condensation shock waves.

The dependence of jet pump performance upon the primary jet total pressure and total temperature is shown in figure 29, in terms of entrainment ratio vs. $p_{t_{PO}}$ and $T_{t_{PO}}$, using equation (17). For purposes of illustration, and to eliminate the effect of the variation in primary jet flow rate, it is assumed that the primary jet nozzles are dimensioned so that a primary jet flow rate of W_{PJ} = .100 lb/sec is obtained at each $p_{t_{PO}}$ and $T_{t_{PO}}$ combination. These curves are based on extrapolated test data.

Pre-test performance prediction - In order to accurately predict the jet pump performance of an untested configuration, graphs similar to figures 16 and 18 must be developed for the nozzle set and duct geometry to be tested. An estimate of the duct total pressure losses, or a single test point, results in the predicted entrainment ratio. Figures 30-32 give data similar to figure 16 for nozzle sets 2, 3 and 6R.

Potential jet pump performance - From figures 16 and 30-32, the maximum possible entrainment ratio and blowing momentum coefficient for each nozzle set is given in Table 14 (determined at $\Delta p_{t_{loss}} = 0$ lb/ft^2).

TABLE 14 - MAXIMUM POSSIBLE JET PUMP PERFORMANCE

Nozzle set	Primary Jet Total Pressure $p_{t_{PO}}$, psia	Primary Jet Total Temperature $T_{t_{PO}}$, °F	Maximum Entrainment Ratio m	Maximum Blowing Momentum Coefficient C_μ
2	350	144	26.0	.364
3	100	1200	30.7	.432
4	350	1200	32.9	.463
6R	410	2590	38.0	.532

By reducing the total pressure losses, a higher level of performance can be attained. With a streamlined nozzle cluster and feedpipe assembly (drag coefficient $C_D \approx .20$ for a streamlined body of this type), the suction duct total pressure losses can be decreased to $\Delta p_{t_{SJ}} = 20$ lb/ft^2 (at a flow rate of $W_S = 3.10$ lb/sec). By preventing flow separation in the blowing duct, it is estimated that the blowing duct loss can be reduced to $\Delta p_{t_{D_B}} = 10$ lb/ft^2. The resulting characteristic equation (equation (16)) will have a $C_5 = 100.0$. With these loss characteristics, the predicted maximum jet pump performance (in terms of C_μ) can be determined as a function of $p_{t_{PO}}$ and $T_{t_{PO}}$, as in figure 33.

Jet Pump Application

Thrust augmentor - The jet pump can be used as a thrust augmentation device. The ratio τ_1 of the thrust obtained from the blowing slot to the thrust which would be obtained from the primary nozzles when the back pressure is atmospheric, can be expressed as:

$$\tau_1 = \frac{W_B v_B}{W_{PJ} v_{PJ}} \quad \ldots\ldots\ldots\ldots\ldots\ldots\ldots\ldots\ldots\ldots \quad (18)$$

Figure 34 shows the thrust augmentation as a function of primary jet total pressure (at a constant primary jet total temperature, $T_{t_{PO}}$ = 1200 °F) for the original duct system, the bellmouth inlet system, and with the jet pump loss characteristics defined on page 29 and figure 33. The curves are based on extrapolated data using the assumptions and procedures outlined on page 28.

BLC system - The experimental jet pump tested was designed for use as part of a boundary-layer-control system. A comparison between an all-blowing BLC system, applied to the same model wing, and the suction-blowing jet pump system illustrates the over-all superiority of the jet pump system. For the all-blowing system, it will be assumed that the same quantity of high energy compressed air is expanded through perfect supersonic slots with no duct losses. The jet pump system produces a suction flow coefficient, C_{Q_S}, over the suction portion of the wing matched with a blowing momentum coefficient, C_μ, that produces an equal lift coefficient over the blowing portion of the wing. However, to keep the power input over the entire wing constant for both BLC systems, the reference area for the all-blowing system must be the sum of the suction and blowing reference areas of the jet pump system. Hence, the ratio, τ_2, of thrust obtained by the jet pump system to the thrust of this hypothetical all-blowing system can be expressed as:

$$\tau_2 = \frac{W_B v_B}{W_{PJ} v_{PJ}} \frac{(S_S + S_B)}{S_B} \quad \ldots\ldots\ldots\ldots\ldots\ldots\ldots \quad (19)$$

Figure 35 shows the relative values of the blowing momentum coefficient as a function of the primary jet total pressure and total temperature, (based on the extrapolation of test data) for the original jet pump system, the bellmouth inlet-jet pump system, and the hypothetical all-blowing system. The momentum ratio, τ_2, is shown in figure 36 for a constant $T_{t_{PO}}$ = 1200°F.

Jet pump potential performance - The maximum performance of the jet pump was not attained in the bench tests, due to a number of factors. The discrepancy between the predicted test results (table 6) and the test results (Appendix B) can be attributed to the geometrical restrictions imposed by the wing envelope, the need for adaptability to a number of nozzle sets, and the unstreamlined nozzle cluster and feedpipe assembly. With the resulting high total pressure losses, a maximum thrust augmentation of $\tau_1 = 1.06$ was obtained with the original duct system. In the bellmouth tests, the thrust augmentation was increased to over $\tau = 1.30$. For an ideal jet pump duct system (minimum losses), the thrust augmentation would be increased to $\tau = 2.3$ for a $T_{t_{PO}} = 1200°F$.

Jet Pump Component Reliability

The total run time for the experimental jet pump in the bench test series was approximately 90 hours, of which approximately 2.5 hours were with the hot burning chamber in operation. The nozzle set 4 was in use over 70% of the total run time.

After an accumulated run time of approximately 40 hours for the nozzle cluster assembly (including 2.5 hours at the extremely high temperatures), leakage of primary air was observed at the primary nozzle threads and at the junction of the "gooseneck" and the large Hastelloy flange. This leakage amounted to less than 5% of the total flow.

As a result of permanent dimensional changes during the burning chamber tests, the nozzle cluster had a different orientation on the "gooseneck" pipe. Over the extended test period, the blowing slot lips were slightly warped, resulting in a reduction in blowing slot area of 7% (affected the bellmouth tests only).

The jet pump demonstrated its performance repeatability in tests over 6 months apart (see figure 19 for respective data points for the 3/17/66 and 9/19/66 bench tests). In all test runs with the suction duct on, the flow was steady (i.e. there were no rapid or violent fluctuations of pressure indicated on the manometer board). In the bellmouth inlet tests, the secondary

flow oscillated considerably, and the data taken were average values. The instrumentation functioned well, with the exception of the static pressure tap 21. The total pressure and temperature probes in the mixing tube were difficult to center on a primary jet, due to either the slight thermal expansion of the nozzle cluster unit and/or the deflection of the probes due to the impingement of the jets.

CONCLUSIONS

The experimental jet pump investigations demonstrated the reliability, performance capability, performance repeatability, and extended component life of the jet pump. The test results provided maximum BLC coefficients (referred to the wing of the NASA Deflected Slipstream STOL model) of C_{Q_S} = .0320 (suction flow coefficient) and C_μ = .256 (blowing momentum coefficient). These coefficients are adequate for Short-Take-off and Landing (STOL) aircraft.

The following statements can be made about the performance characteristics of the jet pump:

1) The entrainment ratio ($m = \frac{W_S}{W_{PJ}}$) is dependent upon the total pressure ~~rise~~ rise accomplished by the jet pump, $\Delta p_{t_{JP}}$, and the total pressure losses encountered in the duct system, $\Delta p_{t_{loss}}$. Accurate prediction of m is possible only if these two factors can be determined.

2) The total pressure rise in the jet pump caused by the energy exchange between the primary and secondary jets can be analytically predicted for a given primary jet total pressure, $p_{t_{PO}}$, total temperature, $T_{t_{PO}}$, and flow rate, W_{PJ}, and a given jet pump geometry.

3) The total pressure loss in the jet pump must be reduced for increased jet pump performance. The losses due to the un-streamlined nozzle cluster assembly constitute a large percentage of the pressure losses in the system, and can be reduced by improving the aerodynamic cleanliness of the

cluster.

4) The mixing efficiency, u, of the jet pump was not accurately measured in these bench tests, due to an apparent error in a static pressure tap. Indications are that u = 1.00 is a good approximation for design point nozzle operation.

5) The tests conducted with the bellmouth entrance (suction duct removed) resulted in increased jet pump performance, due to the decreased total pressure losses. These tests gave a quantitative evaluation of the pressure losses due to the nozzle cluster in axial flow.

6) The small wooden inserts improved the duct flow characteristics, and improved jet pump performance.

7) Operation with converging (sonic) nozzles resulted in lower performance than that of converging-diverging primary jet nozzles, due to a loss in mixing efficiency.

8) Tests run with five nozzles in operation (four nozzles plugged) resulted in a mixing efficiency of approximately 80% of the mixing efficiency of the nine nozzle configuration tests.

9) The suction slot airflow was not evenly distributed across the span, but the distribution is satisfactory from a BLC point of view. Likewise in the blowing slot, the distribution is satisfactory, although uneven along the span. The flow within the duct was steady in all test runs except the bellmouth tests. Wall separation in the blowing duct diffuser contributed to the high total pressure losses and to the uneven blowing slot spanwise distribution.

Increased jet pump performance will be obtained by reducing the total pressure losses resulting from the un-streamlined primary jet feedpipe and nozzle cluster in the suction duct and the wall separation encountered in the blowing duct diffusion process. Due to the high pressure losses, the full po-

tential of the jet pump unit was not attained. With a reduced loss characteristic, the B[illegible] flow coefficients and thrust augmentation will be substantially increased.

The performance of the jet pump unit can be predicted analytically, and the analysis can be applied to future jet pump design work. The discrepancy between the pre-test predicted performance (table 6 in text) and the actual performance (summarized in table 5 in text) is due to the unexpected high total pressure losses.

The bench tests have demonstrated the feasibility of the application of the jet pump as a combined suction and blowing boundary layer control system. Suction and blowing are accomplished over different portions of the wing, with the benefits of a minimum of moving parts, no external (to the wing) parts (since the jet pump units are within the wing envelope) and a conventional flap and/or aileron configuration.

RECOMMENDATIONS

Further design and bench testing is recommended in an effort to reduce the high total pressure losses encountered in the Phase I bench tests of the jet pump. The work envisioned includes aerodynamic fairing of the nozzle cluster assembly, redesign of the blowing duct diffuser, and bench tests designed to optimize the jet pump performance. Concurrent with this design effort, further development and testing of a high temperature combustion chamber (providing compressed air at temperatures up to 3000°F) is recommended.

The ultimate goal of this project is the installation and wind tunnel testing of a jet pump BLC system in the NASA Ames Deflected Slipstream STOL Model. A design effort is recommended for the jet pump system installation and static testing in the wing, including all necessary ducting, instrumentation, controls and primary jet air supply power unit-compressor combination.

REFERENCES

1. R.G. Wilcox and F.G. Wagner, "Theoretical Analysis and Predesign of An Experimental Jet Pump For the Wing of The Ames Short-Haul Transport Model", Sunrise Aircraft Corp. of America, Report 04-65, August, 1965.

2. R.G. Wilcox and F.G. Wagner, "Notes on Detail Design of An Experimental Jet Pump For The Wing of The Ames Short-Haul Transport Model", Sunrise Aircraft Corp. of America, Report 05-65, September, 1965.

3. J.H. Keenan and J. Kaye, "Gas Tables", John Wiley & Sons, Inc., 1948.

4. Dr. K.E. Hickman, "Analytical Prediction of Jet Pump Performance", Dynatech Corporation, Report 635, April, 1966.

5. G.V. Lachmann (Editor), "Boundary Layer and Flow Control", Volumes 1 and 2, Pergamon Press, 1961.

6. H.B. Helmbold, "Contributions to Jet Pump Theory", Wichita State University, Engineering Report 294, 1957.

7. Society of Automotive Engineers (SAE), "Aero-Space Applied Thermodynamics Manual", Committee A-9, Aero-Space Environmental Systems, 1960.

8. M.E. Morrison, Jr. and F.G. Wagner, "Low Speed Wind Tunnel Tests on A Convair Type P6Y Seaplane With A Combined Suction-Blowing BLC System And An All-Blowing BLC System In Combination With Propeller Slipstream", Convair, San Diego, Report CVAL 267, A,B, 1959.

9. F.G. Wagner, "Theoretical And Experimental Investigations of Constant-Pressure And Constant-Diameter Jet Pumps", Wagner Aircraft Co., Inc. Report 02-63, 1963.

10. United States Letter Patents (Inventor Fred G. Wagner)
    (a) #3,093349 "Duct Arrangement For Aircraft Boundary Layer Control"
    (b) #3,085,740 "End Inlet Jet Pump For Boundary Layer Control System"
    (c) #3,149,805 "Jet Curtain V/STOL System" (co-inventor Peter J. Frey)

APPENDIX A - JET PUMP PERFORMANCE THEORY

Total Pressure Rise (Table A1)

Assumptions - The assumptions made in this analysis are:

1) Ideal gases
2) Completely mixed flow at station M
3) The primary flow static pressure, p_{PJ}, is assumed to adjust to match the static pressure of the secondary flow by an isentropic expansion or compression process at a point downstream of the nozzle plane (station I). The adjustment process takes place before any mixing occurs between the two streams
4) The expansion or compression of the primary flow within the adjustment region is assumed to have a negligible effect on the static pressure and the flow area of the secondary jet
5) Wall friction forces in the mixing tube and the diffuser are negligible compared to pressure and momentum forces in the primary and secondary flows
6) adiabatic flow throughout the mixing region and diffuser
7) k = constant = 1.40

Ideal jet pump total pressure rise - A measure of the jet pump performance is the total pressure rise of the mixed stream resulting from the energy released in the primary jet nozzles. Using the relationships of conservation of momentum, energy and continuity, this ideal total pressure rise may be calculated. For a jet pump, the momentum equation is (see figure 1 for stations):

$$A_{SJ}p_{SJ}+A_{PJ}p_{PJ}-A_{M}p_{M} - F_{D} = \frac{1}{g}\left(W_{M}v_{M} - W_{S}v_{SJ} - W_{PJ}v_{PJ}\right), \text{ lb} \quad \ldots\ldots \quad \text{(A-1)}$$

where: F_D is the duct force due to the pressure force on the walls of the mixing tube.

$$F_{D} = \int_{\text{Sta I}}^{\text{Sta M}} p\,dA_{\text{walls}}, \text{ lb} \quad \ldots\ldots\ldots\ldots\ldots\ldots\ldots \quad \text{(A-2)}$$

As an approximation: $F_D = \frac{P_{SJ} + P_M}{2} (A_I - A_M)$, lb . . . . . (A-3)

By assumption 3) above, $p_{PJ} = p_{SJ}$.

By the continuity relationship:

$$W_S + W_{PJ} = W_M = \rho_M A_M v_M g, \text{ lb/sec} \quad . . . . . \quad (A-4)$$

and by the conservation of energy theorem:

$$W_S h_{t_{SJ}} + W_{PJ} h_{t_{PO}} = W_M h_{t_M}, \text{ Btu/sec} \quad . . . . . \quad (A-5)$$

Hence,

$$h_{t_M} = \frac{m h_{t_{SJ}} + h_{t_{PO}}}{m + 1}, \text{ Btu/lb} \quad . . . . . \quad (A-6)$$

or,

$$T_{t_M} = \frac{m T_{t_{SJ}} + \frac{h_{t_{PO}}}{c_{p_M}}}{m + 1}, \quad ^\circ R \text{ [assuming } c_{p_M} = c_{p_{t_{SJ}}} \text{]} \quad . . . . . \quad (A-7)$$

Utilizing equations (A-1), (A-4) and (A-7), and defining the following variables,

$$\alpha = \frac{v_{SJ}}{v_{PJ}} \quad . . . . . \quad (A-8)$$

$$\beta \equiv \frac{v_M}{v_{PJ}} = \frac{W_{PJ} (m + 1) R T_{s_M}}{p_M v_{PJ} A_M} \quad . . . . . \quad (A-9)$$

where:

$$T_{s_M} = T_{t_M} - \frac{v_M^2}{2 g J c_{p_M}}, \quad ^\circ R \quad . . . . . \quad (A-10)$$

a solution for p_M may be obtained :

$$p_M = \left(\frac{A_I}{A_M}\right) p_{SJ} + \frac{W_{PJ} v_{PJ}}{gA_M}(1 + m\alpha - (m+1)\beta) - \frac{(p_{SJ}+p_M)}{2A_M}(A_I - A_M), \text{ lb/ft}^2 \quad \text{(A-11)}$$

Substituting for α and β, an equation of the form

$$p_M^2 - C_1 p_M + C_2 = 0 \quad \text{(A-12)}$$

may be formed, where,

$$C_1 = p_{SJ} + \frac{2W_{PJ} v_{PJ}(1+m\alpha)}{g(A_I+A_M)}, \text{ lb/ft}^2 \quad \text{(A-13)}$$

$$C_2 = \frac{2\,(m+1)^2 W_{PJ}^2 RT_{s_M}}{gA_M\,(A_I+A_M)}, \ \frac{\text{lb}^2}{\text{ft}^4} \quad \text{(A-14)}$$

Solving equation (A-12), one gets:

$$p_M = \frac{C_1 + \sqrt{C_1^2 - 4C_2}}{2} \quad \text{(A-15)}$$

An iterative procedure is being used to determine values of p_M. The known variables are W_{PJ}, p_{SJ}, W_{PJ}, m, v_{PJ} α, A_I, A_M, c_{p_M}, $T_{t_{PO}}$. The iteration routine is:

1) Assume a value for v_M
2) Solve for T_{s_M} by equation (A-10)
3) Solve for p_M by equation (A-15)
4) Solve for ρ_M by : $\rho_M = \frac{p_M}{gRT_{s_M}}, \ \frac{\text{lb-sec}^2}{\text{ft}^4}$

5) Solve for v_M by : $v_M = \frac{W_{PJ}(m+1)}{gA_{M}}$, ft/sec

6) Iterate to step 1 until successive v_M values are close.

Utilizing the last v_M calculated above, the total pressure at station M is then found by:

$$p_{t_M} = p_M + \frac{1}{2}\rho_M v_M^2, \text{ lb/ft}^2 \quad \ldots\ldots\ldots\ldots\ldots\ldots \quad \text{(A-16)}$$

Finally, the ideal total pressure rise is calculated by:

$$\Delta p_{t_{JP}} = p_{t_M} - p_{t_{SJ}}, \text{ lb/ft}^2 \quad \ldots\ldots\ldots\ldots\ldots\ldots \quad \text{(A-17)}$$

Table A1 summarizes the theoretical jet pump performance for each test run, based on test values of pressures, temperatures, flow rates and velocities.

Efficiencies

Jet pump efficiency - The efficiency of the jet pump, η, can be defined as the ratio of useful power obtained (output) to the power input of the primary jet. The power input to the jet pump is:

$$P_{PJ} = W_{PJ}\Delta h \frac{J}{550} = 1.415\ W_{PJ}\Delta h, \text{ HP} \quad \ldots\ldots\ldots\ldots\ldots\ldots \quad \text{(A-18)}$$

The "experimental", or useful, output power is:

$$P_{PJ_{out}} = \frac{1}{550} Q_M \Delta p_{t_{JP}}, \text{ HP} \quad \ldots\ldots\ldots\ldots\ldots\ldots \quad \text{(A-19)}$$

Where:

Q_M is the volume flow rate at the end of the mixing tube

$\Delta p_{t_{JP}}$ is the total pressure rise of the jet pump in the mixing tube

Hence,

$$\eta = \frac{P_{PJ_{out}}}{P_{PJ_{in}}} = \frac{\frac{1}{550}\frac{W_{PJ}}{\rho_M g}(m+1)\Delta p_{t_{JP}}}{1.415\, W_{PJ}\, \Delta h} = \frac{(m+1)\Delta p_{t_{JP}}}{\rho_M g J \Delta h} \quad \ldots\ldots\ldots \quad (A\text{-}20)$$

Ideal efficiency - The ideal efficiency relates the maximum power output (perfect mixing) to the power input of the jet pump. The maximum power output can be expressed as

$$P_{PJ_{out}} = \frac{1}{550} Q_M \Delta p_{t_{JP_i}}, \quad hp \quad \ldots\ldots\ldots\ldots\ldots\ldots\ldots \quad (A\text{-}21)$$

where:

$\Delta p_{t_{JP_i}}$ is the ideal total pressure rise, calculated by equation (A-17)

It follows that:

$$\eta_i = \frac{(m+1)\Delta p_{t_{JP_i}}}{\rho_M g J \Delta h} \quad \ldots\ldots\ldots\ldots\ldots\ldots\ldots \quad (A\text{-}22)$$

Mixing efficiency - The mixing efficiency is the ratio of the jet pump efficiency, η, to the ideal jet pump efficiency, η_i.

$$u = \frac{\eta}{\eta_i} = \frac{\Delta p_{t_{JP}}}{\Delta p_{t_{JP_i}}} \quad \ldots\ldots\ldots\ldots\ldots\ldots\ldots \quad (A\text{-}23)$$

TABLE A1 - IDEAL JET PUMP PERFORMANCE*

Test Run	Velocity, v_M, ft/sec	Pressure, p_M, lb/ft^2	Total Pressure p_{t_M}, lb/ft^2	Jet Pump Total Pressure Rise $\Delta p_{t_{JP}}$, lb/ft^2	Ideal Efficiency η_i
2-1	305	2032	2136	83	.1251
2-2	283	2042	2133	68	.1221
2-3	256	2055	2129	55	.1130
2-4	227	2068	2126	42	.1003
3-1	337	2019	2133	74	.0861
3-2	393	1988	2137	101	.0844
3-3	389	1989	2131	104	.0778
4-1	396	1982	2137	115	.0885
4-2	361	2008	2138	103	.0832
4-3	336	2018	2133	80	.0775
4-4	305	2033	2130	70	.0732
4-5	412	1971	2133	124	.0781
4-6	412	1973	2132	119	.0686
4-7	421	1969	2132	120	.0638
4B-1	466	1937	2154	123	.1073
4B-2	424	1954	2136	100	.0966
4B-3	389	1979	2134	85	.0893
4B-4	461	1996**	2215**	99**	.0668
4P-1	265	2063	2137	71	.0647
4P-2	244	2069	2132	63	.0610
4P-3	228	2072	2127	52	.0569
4A-1	390	2007	2160	135	.0920
4A-2	345	2026	2148	103	.0832
4A-3	307	2041	2140	69	.0669
4A-4	270	2054	2132	59	.0701
4A-5	409	1997	2153	132	.0702
4A-6	411	2001	2154	135	.0650
6-1	458	1939	2137	137	.0756
6-2	485	1920	2141	157	.0799
6R-1	492	1903	2130	140	.0915
6R-2	509	1880	2124	137	.0959
6R-3	501	1883	2118	138	.0927
6R-4	513	1875	2115	135	.0819
6R-5	516	1882	2123	134	.0779
6R-6	525	1881	2125	134	.0726

* Based on test values of pressures, temperatures flow rates and velocities
** Based on $p_{t_{SJ}}$ = 2116 lb/ft^2, since no pressure data available.

APPENDIX B - ANALYSIS OF JET PUMP TEST DATA

Primary Jet Parameters (Tables B1 and B2)

Primary jet total pressure - The primary jet total pressure, $p_{t_{PO}}$, is a controlled parameter, measured by a Bourdon tube gauge located upstream of the primary pipe entrance in the suction duct.

Primary jet total temperature - The primary jet total temperature, $T_{t_{PO}}$, is a controlled parameter for the "hot and cold jet" tests ($T_{t_{PO}} \geq 1200°F$), $T_{t_{PO}}$ was calculated by using the Fleigner formula, evaluated at the nozzle throat (for k = 1.30).

$$\sqrt{T_{t_{PO}}} = \frac{.523\ p_{t_{PO}}\ A^*_{hot} C_W}{W_{PJ}} \quad \ldots\ldots\ldots\ldots\ldots\ldots\ldots\ldots \quad (B\text{-}1)$$

where:

$$A^*_{hot} = A^*_{cold}\left[1+\alpha\ (T_{t_{PO}} - T_o)\right]^2,\ ft^2 \quad \ldots\ldots\ldots\ldots\ldots \quad (B\text{-}2)$$

A^*_{cold}: measured throat area of nozzles, ft^2

α : coefficient of linear expansion/°R

$$W_{PJ} = W_{air_{PJ}} + W_{fuel_{PJ}},\ lb/sec \quad \ldots\ldots\ldots\ldots\ldots\ldots\ldots \quad (B\text{-}3)$$

C_W = nozzle discharge coefficient determined by cold air tests

TABLE B1 - PRIMARY JET NOZZLES

Nozzle Set	Nozzle Throat Area A^*, ft^2 (9 Nozzles)	Nozzle Area Ratio A^*/A	Nozzle Discharge Coefficient, C_W	Jet Pump Area Ratio $\phi = \frac{A_{PJ}}{A_{SJ}}$
2	1.084×10^{-4}	.3229	.935	.00389
3	6.05×10^{-4}	.5885	.965	.01195
4	1.75×10^{-4}	.2578	.935	.00786
4A	1.952×10^{-4}	1.000	.935	.00201
6	1.948×10^{-4}	.2151	.935	.00971
6R	1.80×10^{-4}	.2151	.915	.00971

Burner total temperature - For all burner tests, the burner total temperature, $T_{t_{Bu}}$, was calculated using the following equation:

$$W_{PJ}\, c_{p_{avg}} (T_{t_{Bu}} - T_{t_{BIT}}) = W_{fuel_{PJ}}\, h_{RP_o}, \text{ Btu/sec} \quad \ldots\ldots\ldots \quad (B\text{-}4)$$

Primary jet weight flow rate - The primary air jet weight flow rate is measured by a flowmeter and panel gage. For the burner tests,

$$W_{PJ} = W_{fuel_{PJ}} + W_{air_{PJ}}, \text{ lb/sec} \quad \ldots\ldots\ldots\ldots\ldots\ldots \quad (B\text{-}5)$$

The kerosene flow was measured by a rotameter. The minimum air/fuel ratios were approximately 200% theoretical air.

Secondary Jet Parameters (Table B3)

Assumptions - Assumptions made in this analysis are:

1) $p_o = 2116$ lb/ft^2 (constant)

2) $T_o = 530°R$ (constant)

TABLE B2 - PRIMARY JET INPUT PARAMETERS

Run No.	Primary Jet Total Pressure $P_{t_{PO}}$, psia	Burner Total Temperature $T_{t_{Bu}}$, °F	Primary Jet Total Temperature $T_{t_{PO}}$, °F	Primary Jet Flow Rate W_{PJ}, lb/sec
2-1	350	-	144	.123
2-2	300	-	114	.104
2-3	250	-	150	.081
2-4	200	-	150	.065
3-1	100	-	1180	.084
3-2	102	2050	1650	.101
3-3	102	2440	1950	.095
4-1	350	-	1200	.107
4-2	300	-	1200	.096
4-3	260	-	1200	.077
4-4	225	-	1200	.067
4-5	350	2200	1840	.093
4-6	346	2940	2240	.085
4-7	350	3340	2590	.082
4B-1	350	-	1170	.112
4B-2	300	-	1195	.094
4B-3	200	-	1240	.079
4B-4	350	-	1200	.111
4P-1	350	-	1200	.061
4P-2	300	-	1200	.055
4P-3	260	-	1200	.046
4A-1	345	-	1150	.123
4A-2	265	-	1200	.094
4A-3	215	-	1200	.073
4A-4	170	-	1130	.059
4A-5	345	2330	2110	.097
4A-6	349	2790	2450	.093
6-1	350	2890	2140	.103
6-2	393	2960	2220	.113
6R-1	410	2070	1670	.113
6R-2	410	2100	1600	.115
6R-3	410	2230	1640	.114
6R-4	410	2910	2050	.106
6R-5	410	3240	2250	.102
6R-6	410	[illegible]	2590	.097

Secondary jet weight flow rate - The secondary jet (suction air) weight flow rate was calculated:

$$W_S = \rho_E g \int_{\text{spanwise}} v_E dA_E, \text{ lb/sec} \quad \ldots \quad \text{(B-6)}$$

where:

$dA_E = s db_S$, s = slot depth perpendicular to span

db_S = increment of span

$$v_E = \frac{1}{b_S} \sum_{j=1}^{11} v_{E_j} \Delta b_{S_j}, \text{ ft/sec} \quad \ldots \quad \text{(B-7)}$$

j = location of static pressure tap in slot; j runs from 1 to 11.

$$v_{E_j} = \sqrt{\frac{2}{\rho_E} (p_o - p_{s_{E_j}})} \quad [\text{assume } \rho_E = \rho_o], \text{ ft/sec} \quad \ldots \quad \text{(B-8)}$$

where:

$(p_o - p_{s_{E_j}})$ is the dynamic pressure measured at station j in suction slot.

A plot of v_{E_j} vs. $\int_{j=1}^{11} sdb$ is graphically integrated to obtain the suction air flow rate, W_S.

Static pressure at station I - The static pressure at the nozzle plane (station I - exit of the primary nozzles) was measured by static pressure tap 21 in the mixing tube. [Note: data analysis and comparison with theory reveals that tap 21 does not accurately measure p_{SJ}. However, this analysis will assume that tap 21 is not faulty.]

Secondary jet velocity - The secondary jet velocity at station I, v_{SJ}, was calculated in the following way:

TABLE B3 - SECONDARY JET PARAMETERS

Run No.	Secondary Jet Weight Flow Rate W_S, lb/sec	Entrainment Ratio $m = \frac{W_S}{W_{PJ}}$	Static Pressure at Station I p_{SJ}, lb/ft^2	Total Pressure at Station I $p_{t_{SJ}}$, lb/ft^2	Secondary Jet velocity v_{SJ}, ft/sec	Velocity Ratio $\alpha = \frac{v_{SJ}}{v_{PJ}}$	Total Pressure loss in Suction Duct $\Delta p_{t_{SJ}}$, lb/ft^2
2-1	1.700	13.82	1968	2053	279	.1334	63
2-2	1.598	15.37	1990	2065	260	.1295	51
2-3	1.465	18.09	2012	2074	236	.1165	42
2-4	1.310	20.15	2035	2084	209	.1060	32
3-1	1.720	20.48	1971	2059	282	.0931	57
3-2	1.917	19.05	1924	2036	322	.0912	80
3-3	1.850	19.45	1923	2027	311	.0815	89
4-1	1.975	18.49	1903	2022	334	.0933	94
4-2	1.822	19.07	1936	2035	304	.0862	81
4-3	1.750	22.83	1962	2053	288	.0830	63
4-4	1.608	24.12	1984	2060	262	.0767	56
4-5	2.000	21.43	1886	2009	342	.0797	107
4-6	1.968	23.11	1895	2013	332	.0706	103
4-7	1.970	24.07	1893	2012	335	.0660	104
4B-1	2.343	21.02	1862	2031	401	.1128	85
4B-2	2.190	23.30	1890	2036	371	.1051	80
4B-3	2.042	25.74	1924	2049	341	.0968	67
4B-4	2.423	21.87	data not available				
4P-1	1.427	23.39	2007	2066	231	.0648	50
4P-2	1.318	24.26	2019	2069	212	.0604	47
4P-3	1.248	26.94	2030	2075	200	.0578	41
4A-1	1.970	15.97	1909	2025	330	.0939	91
4A-2	1.790	19.04	1951	2045	295	.0848	71
4A-3	1.633	22.35	1984	2061	265	.0780	55
4A-4	1.467	25.07	2011	2073	235	.0731	43
4A-5	1.937	19.97	1908	2021	325	.0707	95
4A-6	1.960	20.43	1911	2019	318	.0644	97
6-1	2.130	20.78	1853	1995	369	.0795	121
6-2	2.250	19.85	1824	1984	395	.0827	132
6R-1	2.347	20.70	1816	1991	412	.0981	126
6R-2	2.433	21.16	1798	1987	431	.1045	129
6R-3	2.360	20.85	1798	1979	422	.1012	136
6R-4	2.383	22.58	1798	1979	422	.0913	136
6R-5	2.383	23.48	1808	1988	420	.0870	127
6R-6	2.387	24.69	1810	1991	420	.0813	125

$$v_{SJ} = \frac{W_S}{\rho_{SJ} A_{SJ} g} = \frac{W_S R T_{s_{SJ}}}{P_{SJ} A_{SJ}}, \text{ ft/sec} \quad \ldots\ldots\ldots\ldots\ldots\ldots \quad (B\text{-}9)$$

where:

$$T_{s_{SJ}} = T_{t_{SJ}} - \frac{v_{SJ}^2}{2gJc_{p_o}}, \ ^\circ R \quad \ldots\ldots\ldots\ldots\ldots\ldots\ldots\ldots \quad (B\text{-}10)$$

$$A_{SJ} = \frac{A_I}{1 + \phi}, \text{ ft}^2 \quad \ldots\ldots\ldots\ldots\ldots\ldots\ldots\ldots\ldots\ldots \quad (B\text{-}11)$$

Total pressure at station I - The total pressure at station I, $p_{t_{SJ}}$, is analyzed as:

$$p_{t_{SJ}} = p_{SJ} + \frac{1}{2} \rho_{SJ} v_{SJ}^2 = p_{SJ} + \frac{W_S^2 R T_{s_{SJ}}}{2g P_{SJ} A_{SJ}^2}, \text{ lb/ft}^2 \quad \ldots\ldots \quad (B\text{-}12)$$

Total pressure loss in the suction duct - The total pressure loss in the suction duct, $\Delta p_{t_{SJ}}$, was calculated by:

$$\Delta p_{t_{SJ}} = p_o - p_{t_{SJ}}, \text{ lb/ft}^2 \quad \ldots\ldots\ldots\ldots\ldots\ldots\ldots\ldots \quad (B\text{-}13)$$

[Note: The data in figure 17 was estimated by

$$\Delta p_{t_{SJ}} = \Delta p_{t_{JP}} - (p_{t_M} - p_o), \text{ lb/ft}^2$$

since the static pressure tap 21 does not accurately measure p_{SJ}. Hence, the tabular values of $\Delta p_{t_{SJ}}$ in table B3 are different from those estimated in figure 17].

Primary Jet Exit Conditions (Table B4)

Assumptions - Assumptions made in this section are:

1) There is a point downstream (accommodation point) of the nozzle plane (station I) where the static pressure of the primary jet, P_{PJ}, equalizes with p_{SJ}, resulting in a constant pressure profile

across the mixing tube

2) $k = 1.40$ = constant

Primary jet Mach number - The primary jet Mach number, M_{PJ}, is a function of the pressure ratio $\frac{p_{PJ}}{p_{t_{PO}}}$ $(= \frac{p_{SJ}}{p_{t_{PO}}})$. For a given p_{SJ}, M_{PJ} can be found from a table of one dimensional isentropic compressible flow functions (see table in Ref. 3).

Primary jet static temperature - The static temperature of the primary jet is calculated using the pressure ratio, $\frac{p_{SJ}}{p_{t_{PO}}}$, utilizing the perfect gas tables to obtain the ratio $T_{s_{PJ}}/T_{t_{PO}}$.

Primary jet enthalpy change - The primary jet enthalpy change is

$$\Delta h = h_{t_{PO}} - h_{s_{PJ}}, \text{ Btu/lb} \quad \ldots\ldots\ldots\ldots\ldots\ldots \quad (B\text{-}14)$$

where:

$h_{t_{PO}}$ and $h_{s_{PJ}}$ are found in Table 1 of Reference 3 for the temperatures $T_{t_{PO}}$ and $T_{s_{PJ}}$ respectively.

Primary jet velocity - The primary jet velocity, v_{PJ}, was calculated by using the Bernoulli equation for isentropic compressible flow:

$$v_{PJ} = \sqrt{2gJ\,\Delta h}, \text{ ft/sec} \quad \ldots\ldots\ldots\ldots\ldots\ldots \quad (B\text{-}15)$$

TABLE B4 - PRIMARY JET EXIT CONDITIONS

Run No.	Pressure Ratio $\frac{p_{SJ}}{p_{t_{PO}}}$	Mach Number, M_{PJ}	Temperature ratio $\frac{T_{s_{PJ}}}{T_{t_{PO}}}$	Primary Jet Exit Static Temp. $T_{s_{PJ}}$, °R	Enthalpy change Δh, Btu/lb	Primary Jet Velocity v_{PJ}, ft/sec
2-1	.03905	2.762	.39592	239	87.4	2092
2-2	.04606	2.655	.41498	238	80.5	2007
2-3	.05589	2.530	.43856	268	81.9	2025
2-4	.07066	2.381	.46864	286	77.6	1972
3-1	.13688	1.956	.56651	929	183.1	3028
3-2	.13099	1.984	.55952	1181	248.9	3530
3-3	.13092	1.984	.55952	1348	290.7	3815
4-1	.03776	2.784	.39214	651	256.1	3581
4-2	.04481	2.672	.41188	684	248.1	3525
4-3	.05240	2.571	.43066	715	240.6	3471
4-4	.06123	2.471	.45021	747	232.9	3415
4-5	.03742	2.790	.39111	900	372.6	4319
4-6	.03803	2.780	.39282	1061	447.1	4732
4-7	.03756	2.782	.39248	1197	515	5078
4B-1	.03694	2.798	.38969	635	251.8	3550
4B-2	.04375	2.688	.40901	677	248.5	3528
4B-3	.05139	2.584	.42823	728	248.3	3526
4B-4	data not available				(Estimated:	3556)
4P-1	.03982	2.749	.39819	661	253.7	3564
4P-2	.04674	2.645	.41686	692	246.2	3511
4P-3	.05422	2.54[illegible]	.43493	722	239.0	3459
4A-1	.03843	2.773	.39402	634	246.8	3515
4A-2	.05113	2.587	.42762	710	241.8	3480
4A-3	.06408	2.442	.45606	757	230.5	3397
4A-4	.08215	2.283	.48962	778	206.6	3216
4A-5	.03841	2.773	.39402	1013	421.6	4595
4A-6	.03803	2.780	.39282	1143	487.5	4941
6-1	.03677	2.801	.38924	1012	430.5	4643
6-2	.03223	2.888	.37480	1004	455.6	4776
6R-1	.03076	2.919	.36995	788	352	4199
6R-2	.03045	2.926	.36893	760	339.4	4123
6R-3	.03045	2.926	.36892	774	347	4168
6R-4	.03045	2.926	.36892	926	426.3	4620
6R-5	.03062	2.922	.36937	1001	465	4825
6R-6	.03056	2.921	.36950	1127	532.5	5164

Primary jet input power - The primary jet input power, P_{PJ}, is:

$$P_{PJ} = 1.415\ W_{PJ}\Delta h,\ hp \quad \ldots\ldots\ldots\ldots\ldots\ldots\ldots\ldots \quad (B\text{-}16)$$

where:

1.415 = conversion factor (hp/Btu).

Dimensionless Performance Parameters

Entrainment ratio - The entrainment ratio, m, (table B3) is:

$$m = \frac{W_S}{W_{PJ}} \quad \ldots\ldots\ldots\ldots\ldots\ldots\ldots\ldots \quad (B17)$$

Area ratio - The nozzle areas ratios, $\phi = \frac{A_{PJ}}{A_{SJ}}$, are shown in Table B1.

Velocity ratio - The velocity ratios, $\alpha = \frac{v_{SJ}}{v_{PJ}}$, are tabulated in Table B3.

Completely Mixed Flow Conditions (Station M) (Table B5)

Assumptions: -

1) The flow is completely mixed at the end of the mixing tube (station M)
2) Ideal gas
3) The velocity at station M is constant across the diffuser

Weight flow rate - The rate of flow at station M is the sum of the primary and secondary air weight flow rates:

$$W_M = W_S + W_{PJ},\ lb/sec \quad \ldots\ldots\ldots\ldots\ldots\ldots\ldots \quad (B\text{-}18)$$

Static pressure - The static pressure at station M, p_M, is found from the static pressure profiles for each test run.

Static temperature - The static temperature at station M, T_{s_M} is:

TABLE B5 - COMPLETELY MIXED FLOW CONDITIONS

Run No.	Weight Flow Rate W_M, lb/sec	Static pressure p_M, lb/ft^2	Velocity v_M, ft/sec	Total pressure p_{t_M}, lb/ft^2	Total Temperature T_{t_M}, °R	Excess Total Pressure $\Delta p_{t_{ex}}$, lb/ft^2	Jet Pump Total Pressure Rise $\Delta p_{t_{JP}}$, lb/ft^2
2-1	1.823	2049	302	2152	535.0	36	99
2-2	1.702	2054	281	2144	532.7	28	79
2-3	1.546	2066	255	2140	534.2	24	66
2-4	1.375	2075	226	2133	533.8	17	49
3-1	1.804	2043	333	2156	594.4	40	97
3-2	2.018	2017	388	2164	614.7	48	128
3-3	1.945	2022	384	2162	630.4	46	135
4-1	2.082	2012	390	2165	598.3	49	143
4-2	1.918	2030	357	2158	596.3	42	123
4-3	1.827	2042	332	2156	586.0	40	103
4-4	1.675	2053	302	2148	583.2	32	88
4-5	2.093	2007	405	2166	615.8	50	157
4-6	2.053	2009	405	2165	629.6	49	152
4-7	2.052	1999	415	2159	642.7	43	147
4B-1	2.484	1982	456	2195	582.1	79	164
4B-2	2.284	2302	415	2180	578.6	64	144
4B-3	2.121	2013	383	2165	576.0	49	116
4B-4	2.533	data not available			581.8	-	-
4P-1	1.488	2066	265	2140	516.3	24	74
4P-2	1.373	2071	243	2134	574.7	18	65
4P-3	1.295	2077	227	2132	570.4	16	57
4A-1	2.093	2013	389	2166	593.6	50	141
4A-2	1.884	2037	344	2159	586.4	43	114
4A-3	1.708	2052	306	2150	518.4	34	89
4A-4	1.526	2066	269	2143	570.7	27	70
4A-5	2.034	2017	405	2172	637.1	56	151
4A-6	1.993	2017	407	2169	653.9	53	150
6-1	2.236	1979	450	2168	634.7	52	173
6-2	2.368	1965	485	2181	644.0	65	197
6R-1	2.460	1968	476	2188	609.4	72	198
6R-2	2.548	1949	492	2185	604.7	69	198
6R-3	2.548	1949	485	2177	607.3	61	197
6R-4	2.489	1944	496	2176	622.1	60	196
6R-5	2.485	1950	499	2183	628.6	67	194
6R-6	2.483	1950	508	2187	640.0	71	196

$$T_{s_M} = T_{t_M} - \frac{v_M^2}{2gJc_{p_M}}, \ ^\circ R \quad \ldots\ldots\ldots\ldots\ldots\ldots\ldots \quad (B\text{-}19)$$

where:

T_{t_M} was obtained from the energy equation:

$$W_M c_{p_M} T_{t_M} = W_{PJ} c_{p_{t_{PO}}} T_{t_{PO}} + W_S c_{p_o} T_{t_{SJ}}, \ \text{Btu/sec} \quad \ldots\ldots\ldots\ldots \quad (B\text{-}20)$$

$$T_{t_M} = \frac{\left(\frac{c_{p_{t_{PO}}}}{c_{p_o}}\right) T_{t_{PO}} + m\, T_{t_{SJ}}}{m + 1}, \ ^\circ R \ (\text{assumed: } c_{p_M} = c_{p_o}) \quad \ldots\ldots \quad (B\text{-}21)$$

Note: It is necessary to iterate between T_{s_M} and v_M to solve for T_{s_M}

Velocity - The velocity, v_M, at station M is:

$$v_M = \frac{W_M R\, T_{s_M}}{p_M A_M}, \ \text{ft/sec} \quad \ldots\ldots\ldots\ldots\ldots\ldots \quad (B\text{-}22)$$

Total pressure - The total pressure, p_{t_M}, at station M is:

$$p_{t_M} = p_M + \frac{1}{2}\rho_M v_M^2, \quad \text{lb/ft}^2 \quad \ldots\ldots\ldots\ldots\ldots\ldots \quad (B\text{-}23)$$

Jet Pump Pressure Rise (Table B5)

Excess total pressure - The excess total pressure, $\Delta p_{t_{ex}}$, is:

$$\Delta p_{t_{ex}} = p_{t_M} - p_o, \ \text{lb/ft}^2 \quad \ldots\ldots\ldots\ldots\ldots\ldots \quad (B\text{-}24)$$

Jet pump total pressure rise - The jet pump total pressure rise (to station M) $\Delta p_{t_{JP}}$, was computed in the following way:

$$\Delta p_{t_{JP}} = \Delta p_{t_{SJ}} + \Delta p_{t_{ex}}, \text{ lb/ft}^2 \quad \ldots\ldots\ldots\ldots\ldots\ldots \quad \text{(B-25)}$$

Blowing Slot Conditions (Table B6)

Blowing slot airflow rate - The blowing slot airflow rate, W_B, was calculated by:

$$W_B = \varepsilon_B \, g \, \rho_B \int v_B \, dA_B, \text{ lb/sec} \quad \ldots\ldots\ldots\ldots\ldots\ldots \quad \text{(B-26)}$$

where:

ε_B is the blowing slot velocity profile correction factor. Results from boundary layer displacement thickness and flow angles not perpendicular to the slot. ε_B is plotted in figure 27

$dA_B = s_B db_B$

s_B = slot depth perpendicular to span

b_B = spanwise dimension from one end of slot

W_B is obtained by graphical integration using a plot of v_{B_j} vs $\int_{j=1}^{j=11} s_B db_B$

Blowing slot velocity - The blowing slot velocity at each station j along the span, v_{B_j}, was calculated by:

$$v_{B_j} = \sqrt{\frac{2}{\rho_B} (p_{t_{B_j}} - p_o)}, \text{ ft/sec} \quad \ldots\ldots\ldots\ldots\ldots\ldots \quad \text{(B-27)}$$

where:

$p_{t_{B_j}} - p_o$ = dynamic pressure at station j along the span, lb/ft^2.

The average blowing velocity, $\bar{v}_B$, was calculated by:

$$\bar{v}_B = \frac{\varepsilon_B}{A_B} \int_{j=1}^{j=11} v_{B_j} \, dA_B, \text{ ft/sec} \quad \ldots\ldots\ldots\ldots\ldots\ldots \quad (B\text{-}28)$$

Total pressure - The blowing total pressure, p_{t_B}, was presented by:

$$p_{t_B} = p_B + \frac{1}{2} \rho_B \bar{v}_B^2, \text{ lb/ft}^2 \quad \ldots\ldots\ldots\ldots\ldots\ldots \quad (B\text{-}29)$$

where:

$$p_B = p_o, \text{ lb/ft}^2$$

$$\rho_B = \frac{p_o}{gRT_{s_B}}, \frac{\text{lb-sec}^2}{\text{ft}^4} \quad \ldots\ldots\ldots\ldots\ldots\ldots \quad (B\text{-}30)$$

$$T_{s_B} = T_{t_B} - \frac{\bar{v}_B^2}{2gJc_{p_o}}, \text{ °R} \quad \ldots\ldots\ldots\ldots\ldots\ldots \quad (B\text{-}31)$$

Total pressure losses in the blowing duct - The total pressure losses in the blowing duct, $\Delta p_{t_{D_B}}$, are:

$$\Delta P_{t_{D_B}} = p_{t_M} - p_{t_B}, \text{ lb/ft}^2 \quad \ldots\ldots\ldots\ldots\ldots\ldots \quad (B\text{-}32)$$

Jet Pump Performance Parameters (Table B7)

Suction flow coefficient - The suction flow coefficient, C_{Q_S}, relates the suction airflow rate to the aircraft freestream conditions by:

$$C_{Q_S} = \frac{W_S}{\rho_o v_o g S_S} \quad \ldots\ldots\ldots\ldots\ldots\ldots \quad (B\text{-}33)$$

Blowing momentum coefficient - The blowing momentum coefficient, C_μ,

TABLE B6 - BLOWING SLOT EXIT CONDITIONS

Run No.	Blowing Jet Velocity $\bar{v}_B$, ft/sec	Blowing Jet Static Temp. T_{s_B}, °R	Blowing Jet Dynamic Pressure q_B, lb/ft^2	Blowing Duct Total Pressure Loss $\Delta p_{t_{D_B}}$, lb/ft^2
2-1	131	533.6	19.8	16
2-2	122	531.5	17.2	11
2-3	111	533.2	14.3	10
2-4	99	533.0	11.3	6
3-1	144	592.7	21.6	20
3-2	166	612.4	27.9	20
3-3	165	628.1	26.7	19
4-1	167	596.0	29	20
4-2	154	594.3	24.5	17
4-3	144	584.3	21.9	18
4-4	131	581.8	18.3	14
4-5	173	613.3	30.2	20
4-6	173	627.0	29.6	19
4-7	177	640.1	30.2	13
4B-1	202	578.7	43.6	35
4B-2	185	575.8	36.7	27
4B-3	171	573.6	31.5	18
4B-4	206	578.3	45.3	-
4P-1	115	575.2	14.3	10
4P-2	106	573.8	12.1	6
4P-3	99	569.6	10.7	5
4A-1	167	591.3	29.1	21
4A-2	149	584.6	23.3	20
4A-3	133	576.9	18.8	15
4A-4	117	569.6	14.9	12
4A-5	174	634.6	29.5	26
4A-6	175	651.3	29.0	24
6-1	191	631.7	35.4	17
6-2	204	640.5	40.3	25
6R-1	201	606.0	41.1	31
6R-2	207	601.2	43.8	23
6R-3	203	603.8	42.3	19
6R-4	208	618.5	43.0	17
6R-5	209	624.9	43.2	24
6R-6	213	636.2	44.0	27

relates the blowing air flow momentum to the aircraft freestream conditions by:

$$C_\mu = \frac{W_B v_B}{g q_o S_B} \quad \ldots\ldots\ldots\ldots\ldots\ldots\ldots\ldots\ldots\ldots \quad (B\text{-}34)$$

Mass augmentation - The mass augmentation is the ratio of the output airflow to the input airflow.

$$M.A. = \frac{W_B}{W_{PJ}} = (m + 1) \quad \ldots\ldots\ldots\ldots\ldots\ldots\ldots\ldots\ldots\ldots \quad (B\text{-}35)$$

Thrust augmentation - The thrust augmentation, τ, is defined as the ratio of thrust obtained at the blowing slot to that of the primary jets.

$$\tau = \frac{W_B v_B}{W_{PJ} v_{PJ}} \quad \ldots\ldots\ldots\ldots\ldots\ldots\ldots\ldots\ldots\ldots \quad (B\text{-}36)$$

TABLE B7 - JET PUMP PERFORMANCE PARAMETERS

Test Run	Suction flow coefficient, C_{Q_S}	Blowing momentum coefficient, C_μ	Mass augmentation, m + 1	Thrust augmentation, τ
2-1	.0223	.112	14.82	.928
2-2	.0210	.097	16.37	.995
2-3	.0192	.081	19.09	1.046
3-1	.0226	.122	21.48	1.021
3-2	.0252	.157	20.05	.940
3-3	.0243	.151	20.45	.885
4-1	.0259	.164	19.49	.907
4-2	.0239	.138	20.07	.873
4-3	.0230	.124	23.83	.984
4-4	.0211	.103	25.12	.959
4-5	.0263	.170	22.43	.901
4-6	.0259	.167	24.11	.883
4-7	.0259	.170	25.07	.872
4B-1	.0308	.246	22.02	1.262
4B-2	.0288	.207	24.30	1.274
4B-3	.0268	.178	26.74	1.302
4B-4	.0318	.256	22.87	1.322
4P-1	.0187	.081	24.39	.787
4P-2	.0173	.068	25.26	.754
4P-3	.0164	.060	27.94	.806
4A-1	.0259	.164	16.97	.808
4A-2	.0235	.132	20.04	.858
4A-3	.0215	.106	23.35	.915
4A-4	.0193	.084	26.07	.941
4A-5	.0254	.167	20.97	.794
4A-6	.0250	.164	21.43	.759
6-1	.0280	.200	21.78	.893
6-2	.0296	.227	20.85	.895
6R-1	.0308	.232	21.70	1.042
6R-2	.0320	.247	22.16	1.142
6R-3	.0313	.239	21.85	1.088
6R-4	.0313	.243	23.58	1.057
6R-5	.0313	.244	24.48	1.055
6R-6	.0314	.248	25.69	1.056

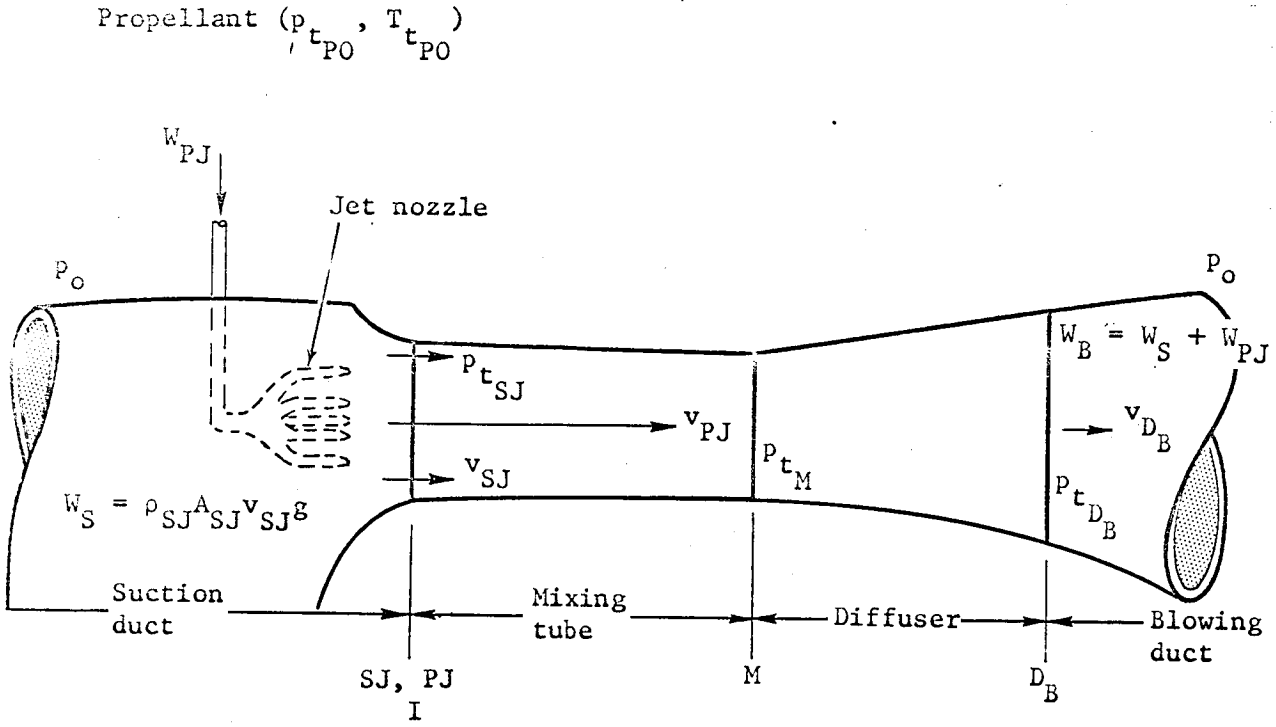

Total Pressures:

p_o = ambient total pressure, lb/ft^2

$p_{t_{PO}}$ = primary jet total pressure, lb/ft^2

$p_{t_{SJ}}$ = secondary jet total pressure, lb/ft^2

p_{t_M} = mixing tube total pressure, lb/ft^2

$p_{t_{D_B}}$ = blowing diffuser total pressure, lb/ft^2

$\Delta p_{t_{JP}}$ = jet pump total pressure rise, lb/ft^2

Jet Pump Parameters:

Velocity Ratio $\alpha = \dfrac{v_{SJ}}{v_{PJ}}$

Entrainment Ratio $m = \dfrac{W_S}{W_{PJ}}$

Efficiency $\eta = \dfrac{(m+1)\Delta p_{t_{JP}}}{Jg\,\rho_M\,\Delta h}$

Figure 1.- Jet pump definitions.

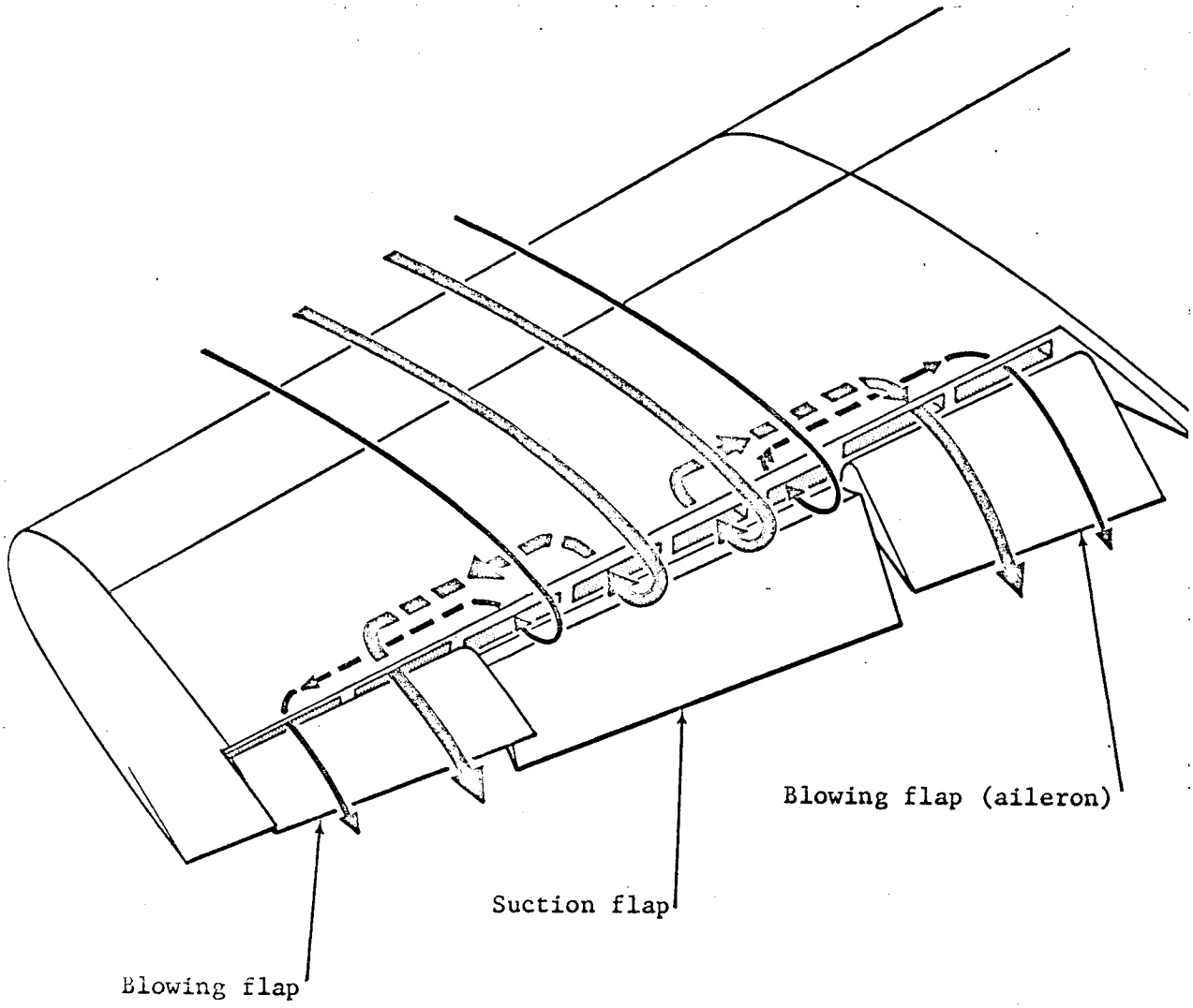

Figure 2.- Schematic of JIL airflow.

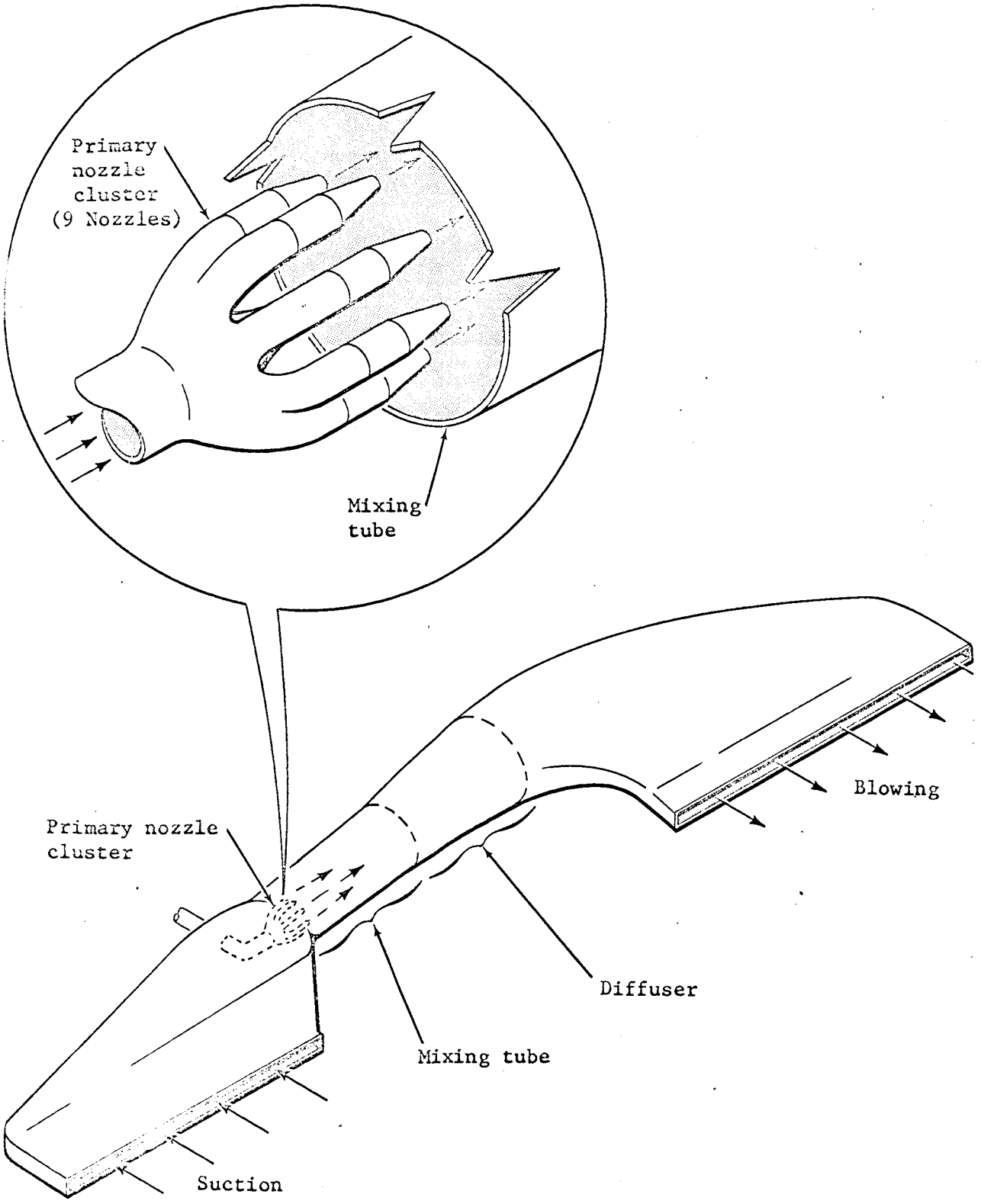

Figure 3.- BLC jet pump duct arrangement.

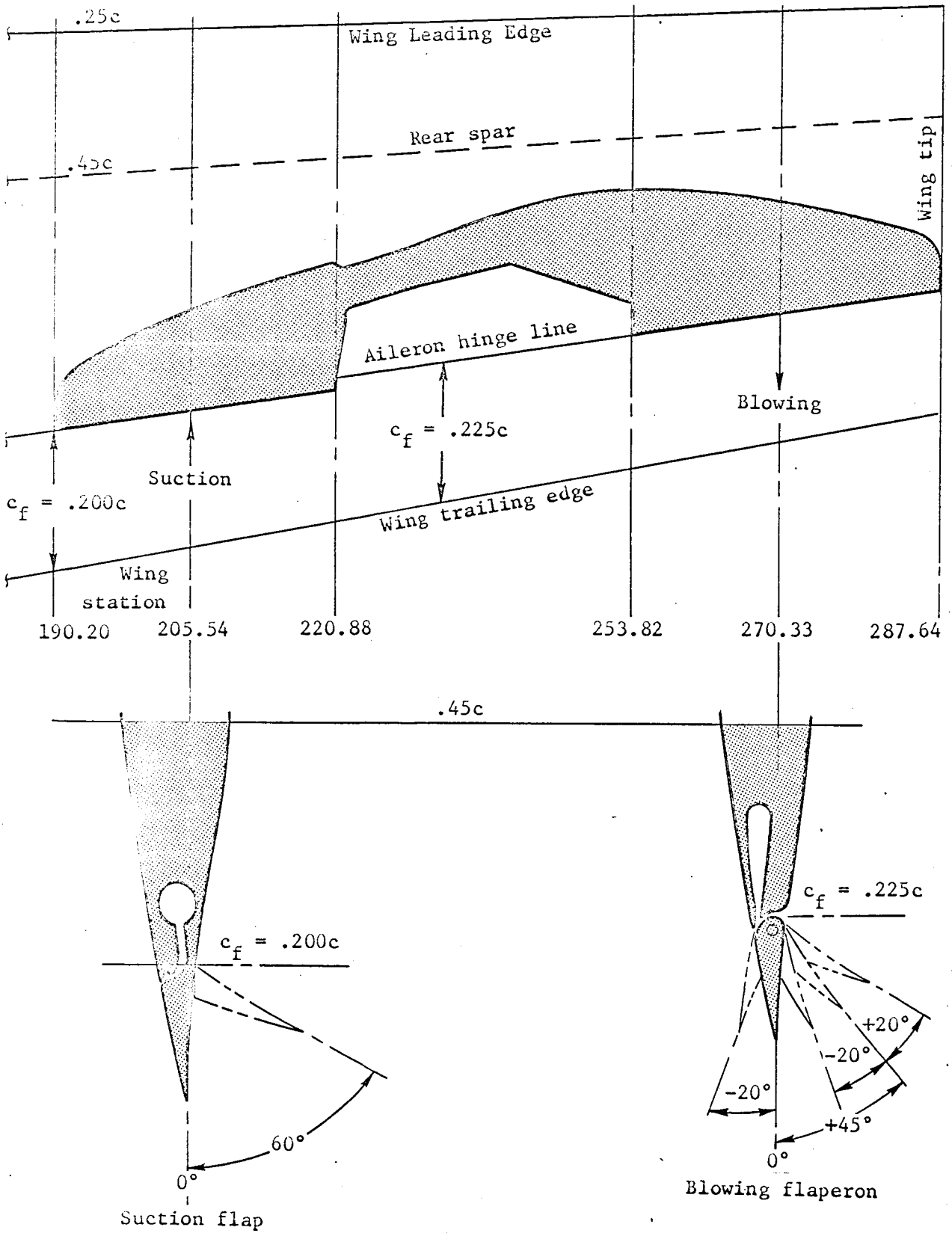

Figure 4.- Jet pump layout in NASA-Ames Deflected Slipstream STOL model.

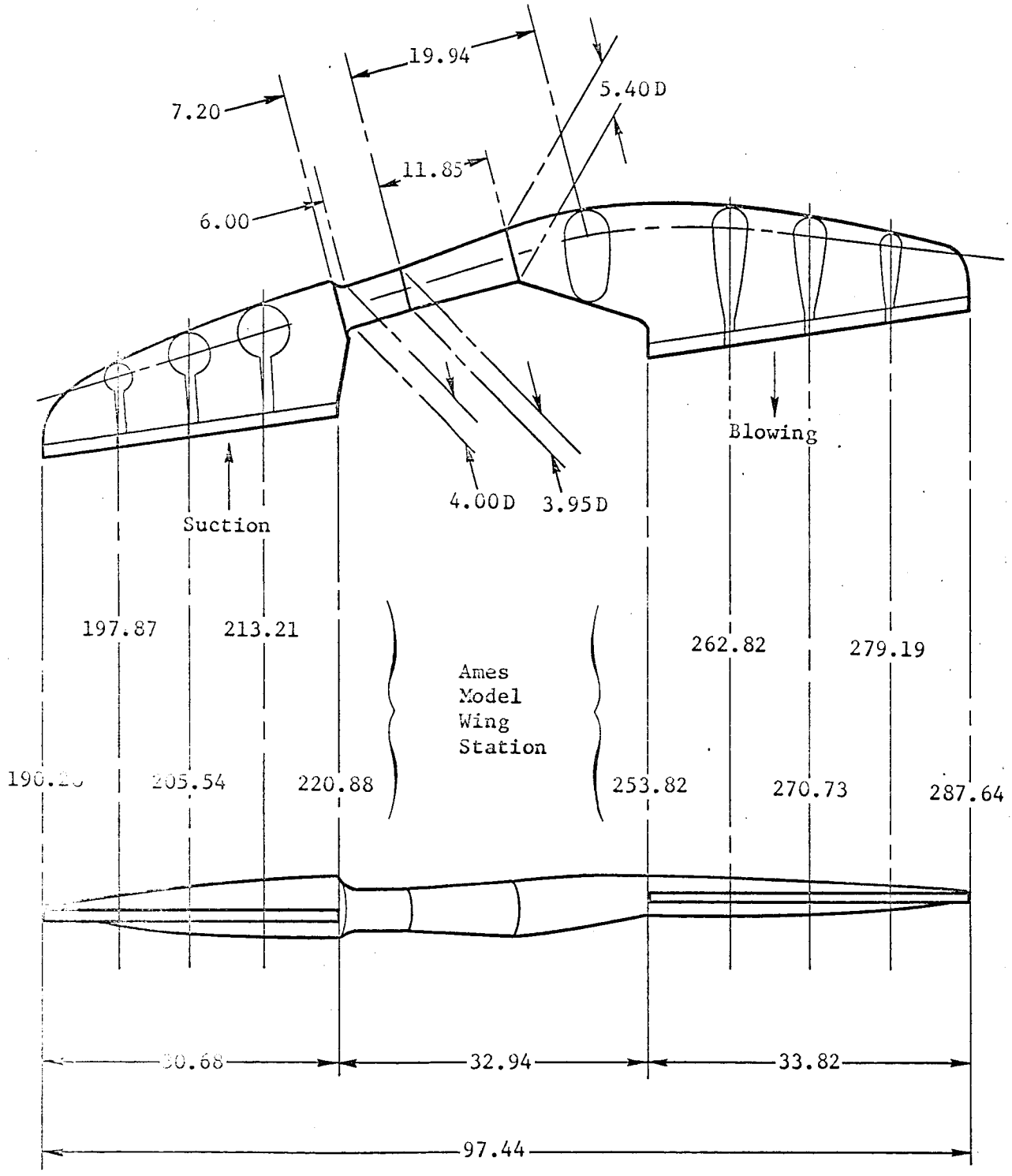

Note: All dimensions in inches

Figure 5.- Experimental jet pump dimensions.

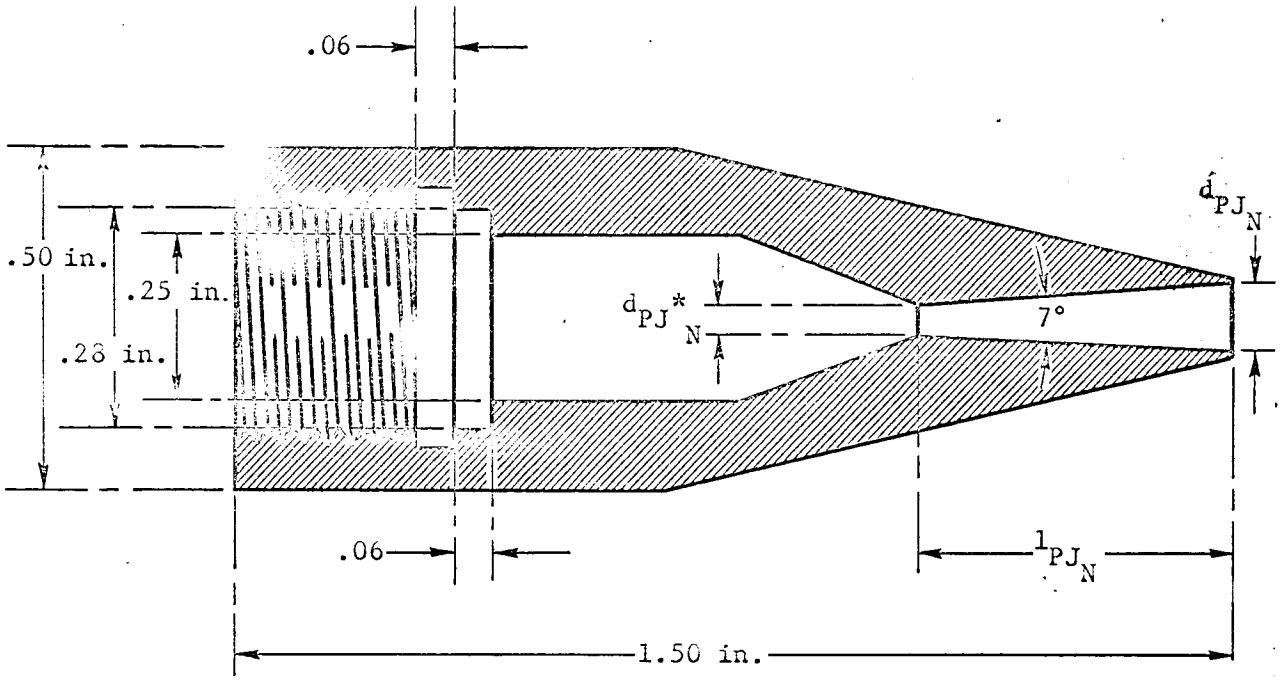

Nozzle Set	d_{PJ_N}, in.	$d^*_{PJ_N}$, in.	l_{PJ_N}, in.	Material
2	.083	.047	.311	2024 STAL
3	.145	.111	.276	Hastelloy "C"
4	.117	.0596	.474	310 Stainless
4A	.060	.063	.000	310 Stainless
5	.131	.063	.568	LT-1
5R	.131	.061	.568	310 Stainless

Figure 6.- Primary jet nozzle design dimensions.

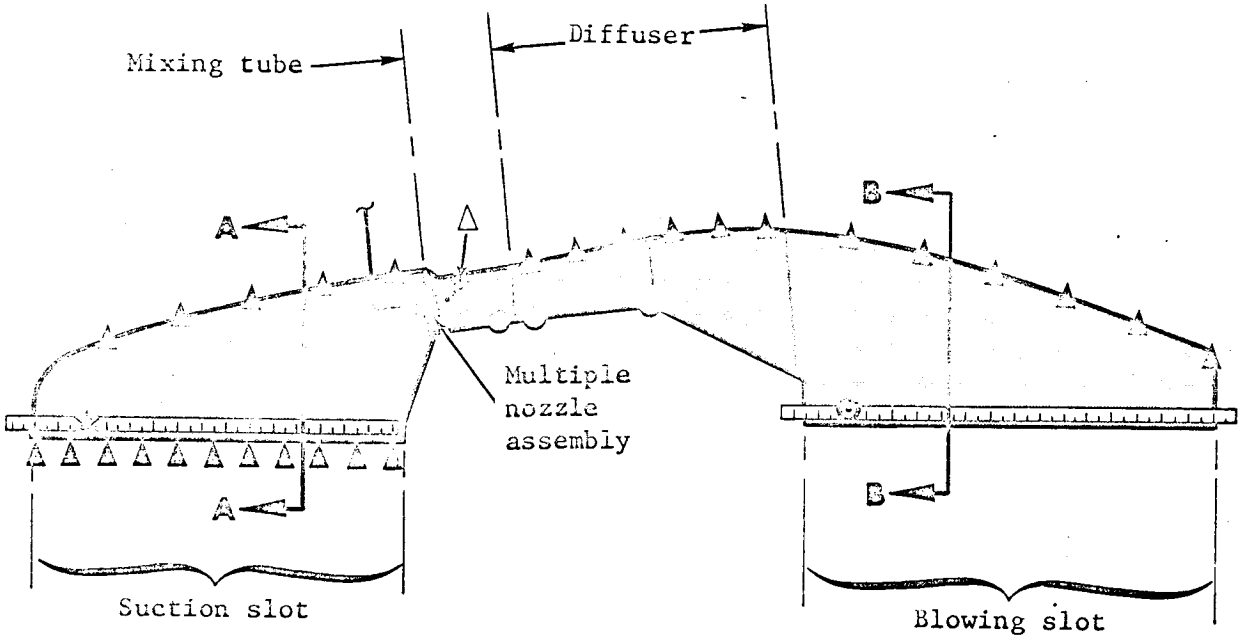

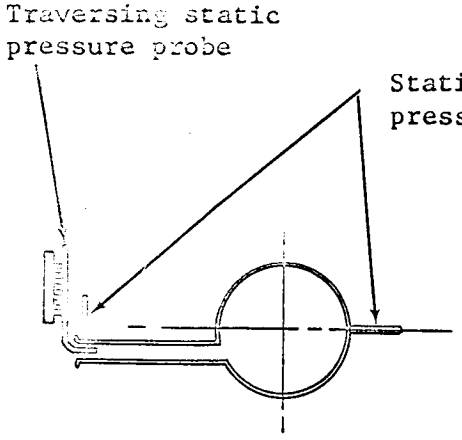

Section A-A suction chamber

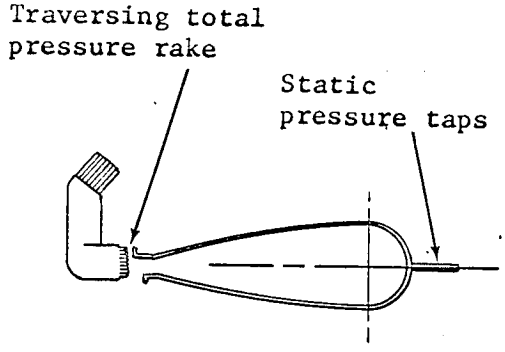

Section B-B blowing chamber

Legend:

- ⊙ Traversing total pressure rake
- ☆ Static suction pressure probe-traversing and vertical adjustment
- △ Static pressure tap
- △ Static pressure taps in mixing tube (20 locations)
- ○ Total pressure probe in mixing tube and diffuser

Figure 7.- Experimental jet pump instrumentation.

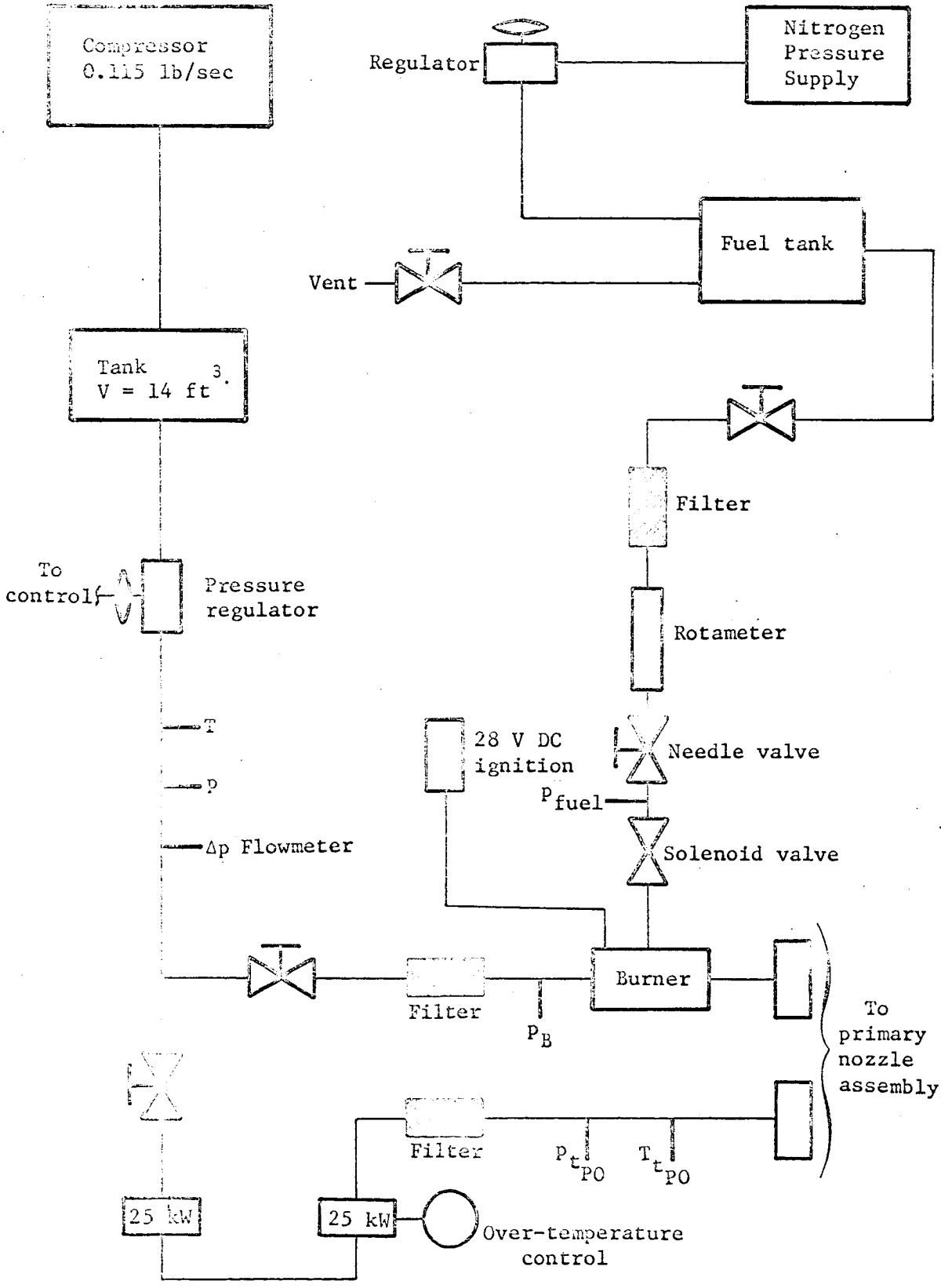

Figure 8.- Primary air and fuel system.

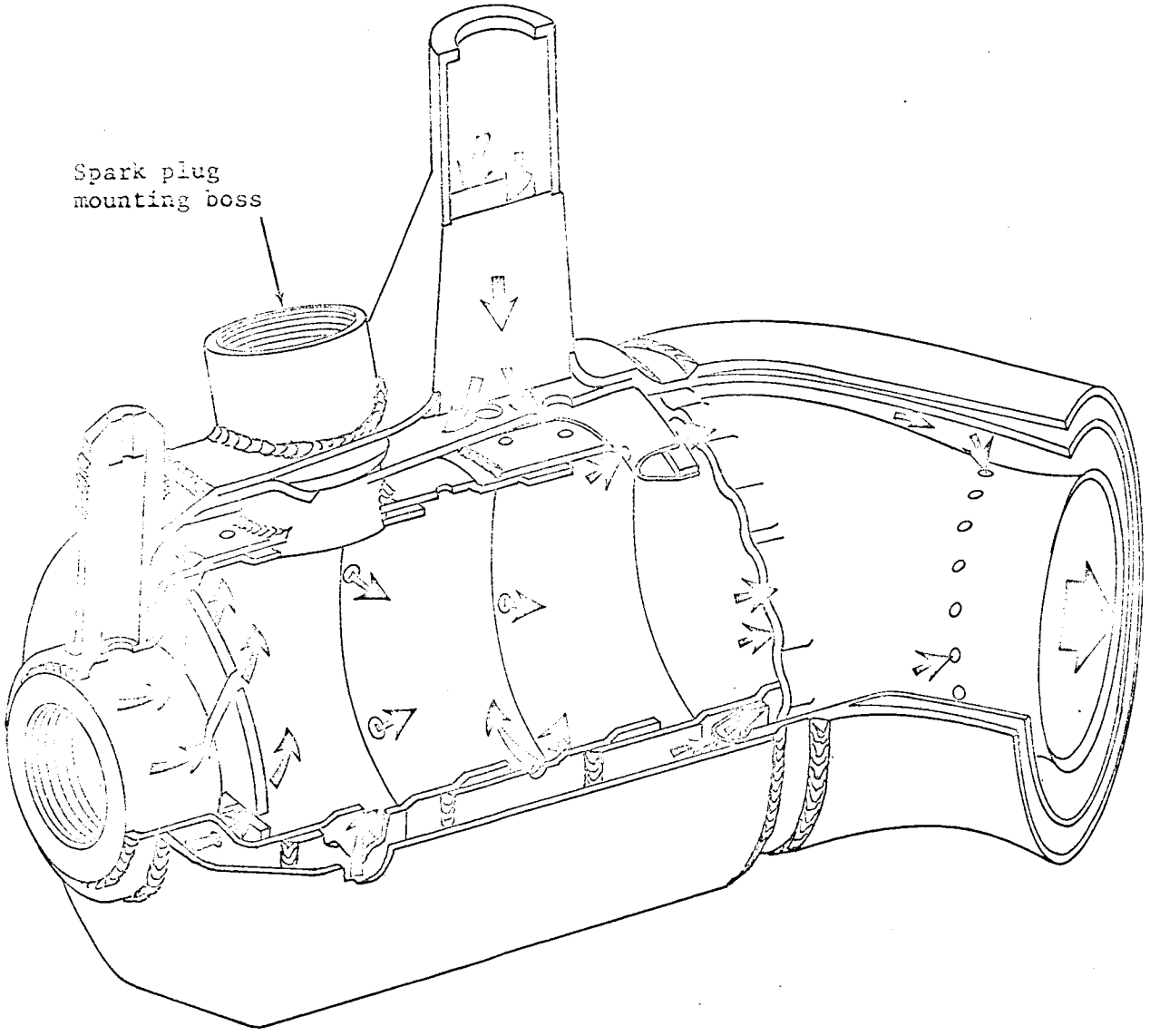

Figure 9.- Cutaway view of combustor.

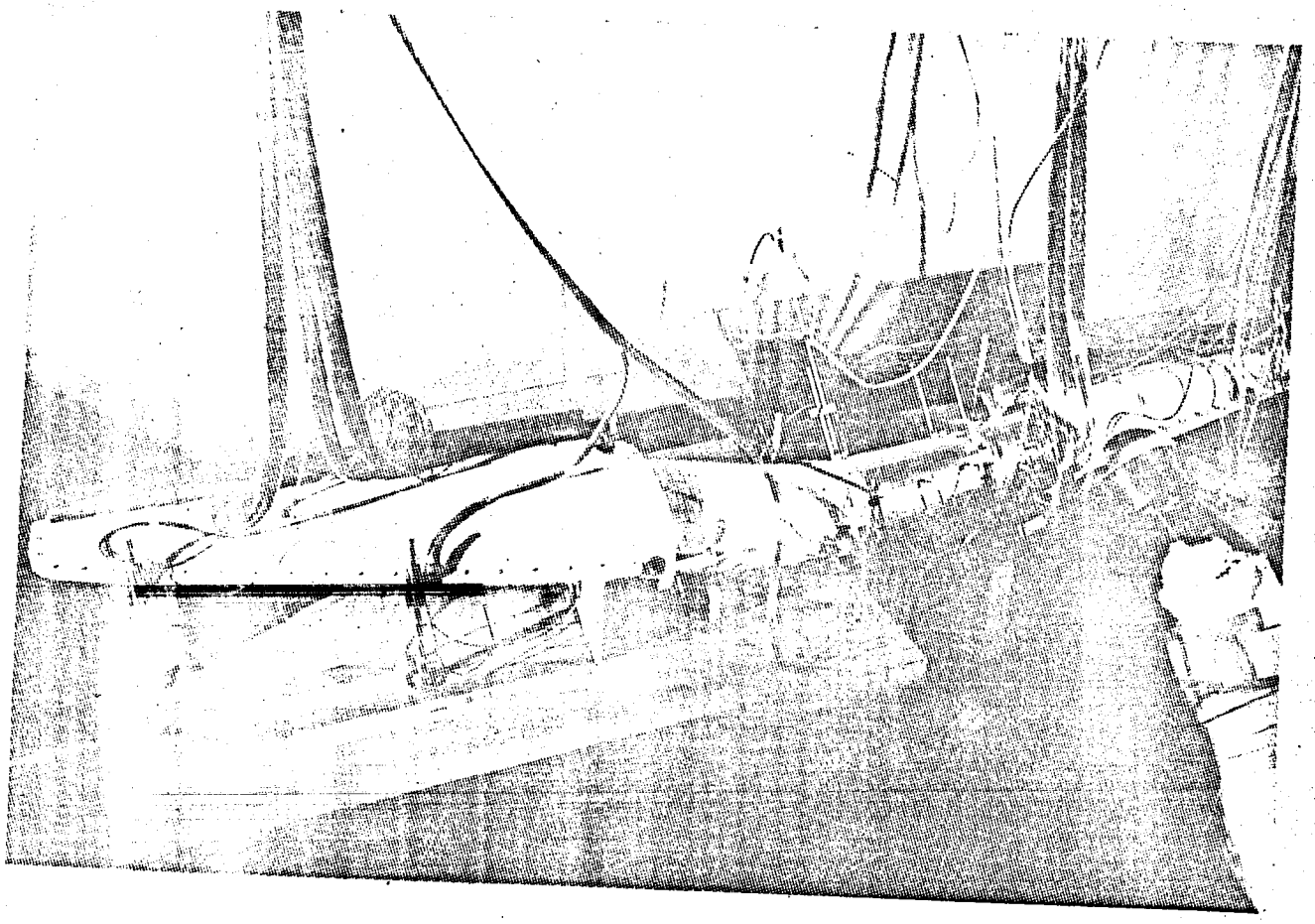

Figure 10.- Experimental jet pump on test stand.

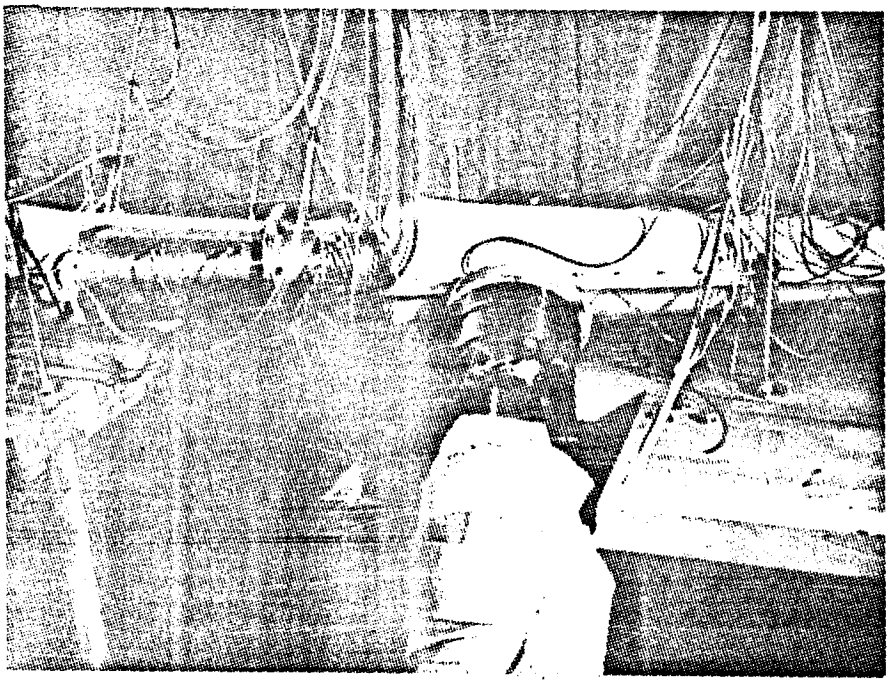

Figure 11.- Low temperature (60-1200° F) test installation (suction duct at right, mixing tube and diffuser to the left, nozzle feedpipe in foreground).

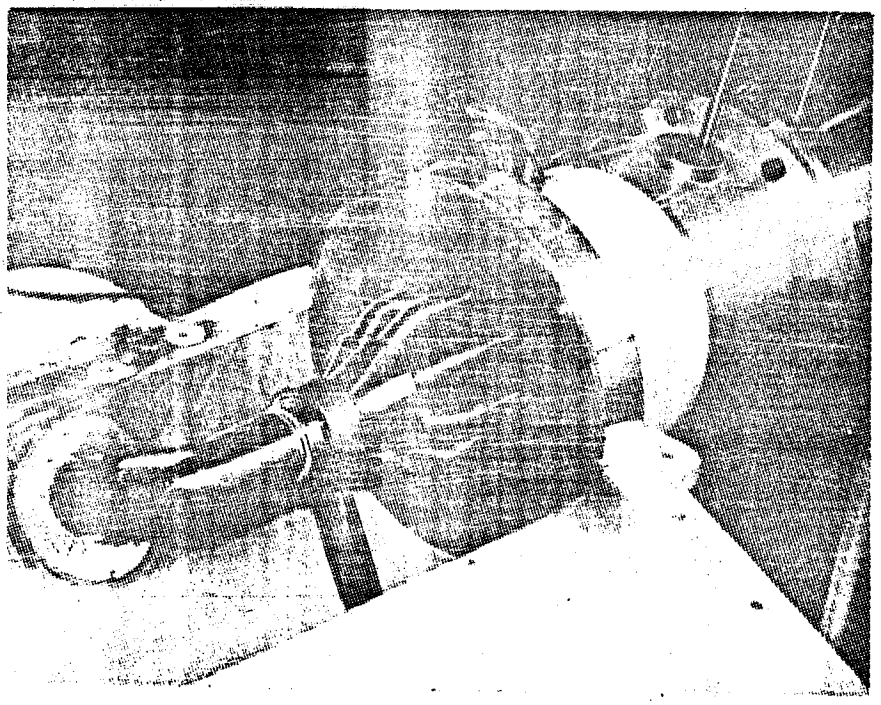

Figure 12.- Primary nozzle cluster installation (mixing tube to the right).

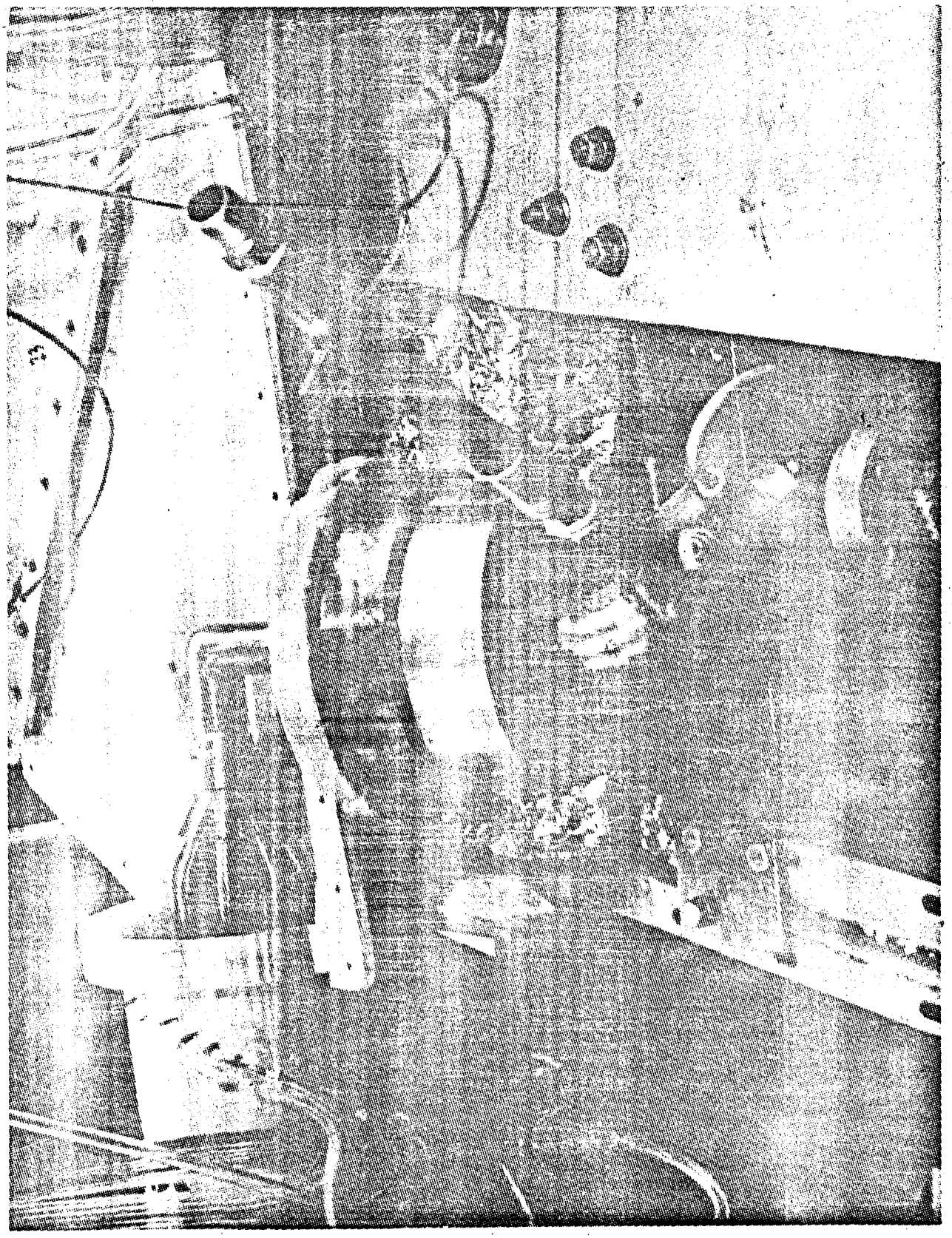

Figure 13.- Gas combustor installation.

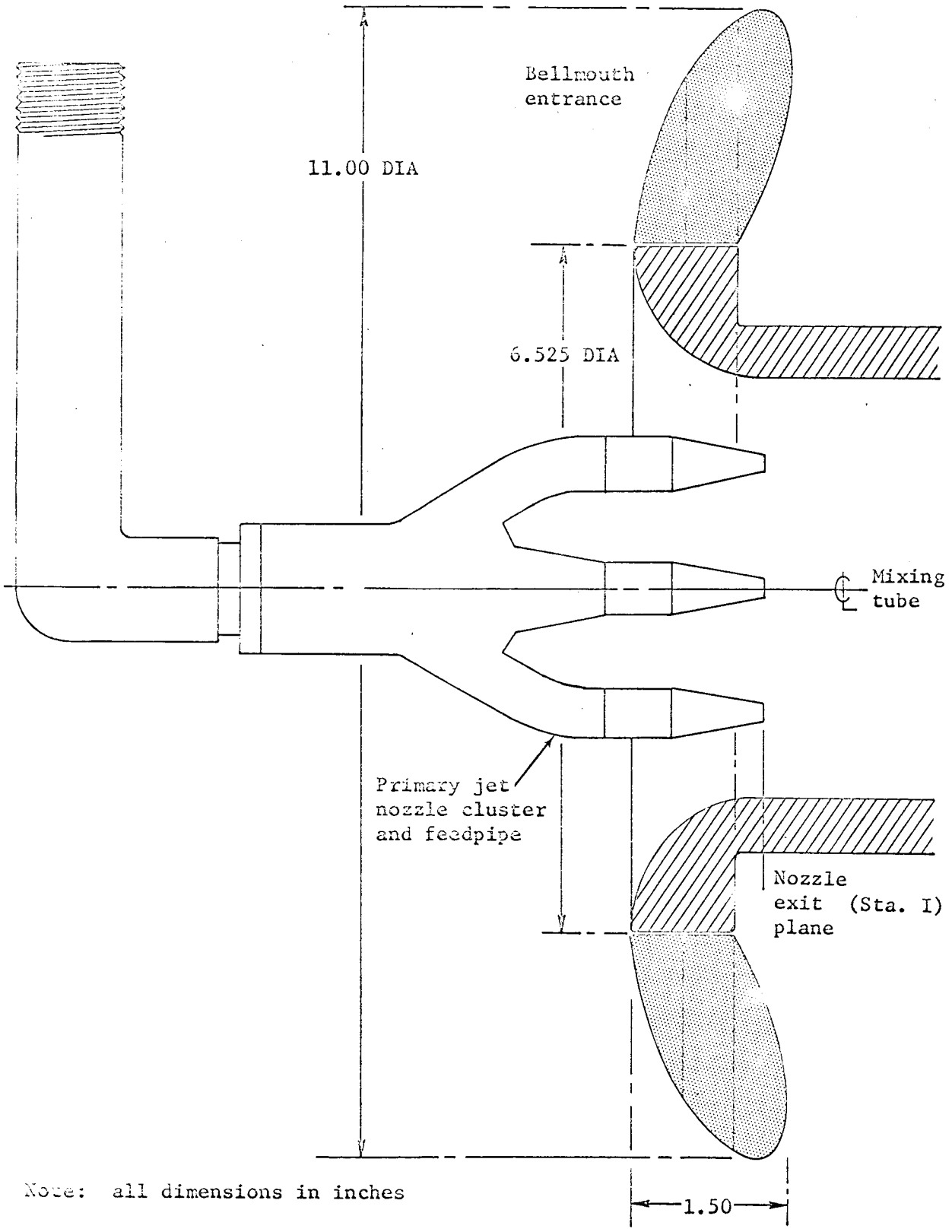

Figure 14.- Bellmouth entrance.

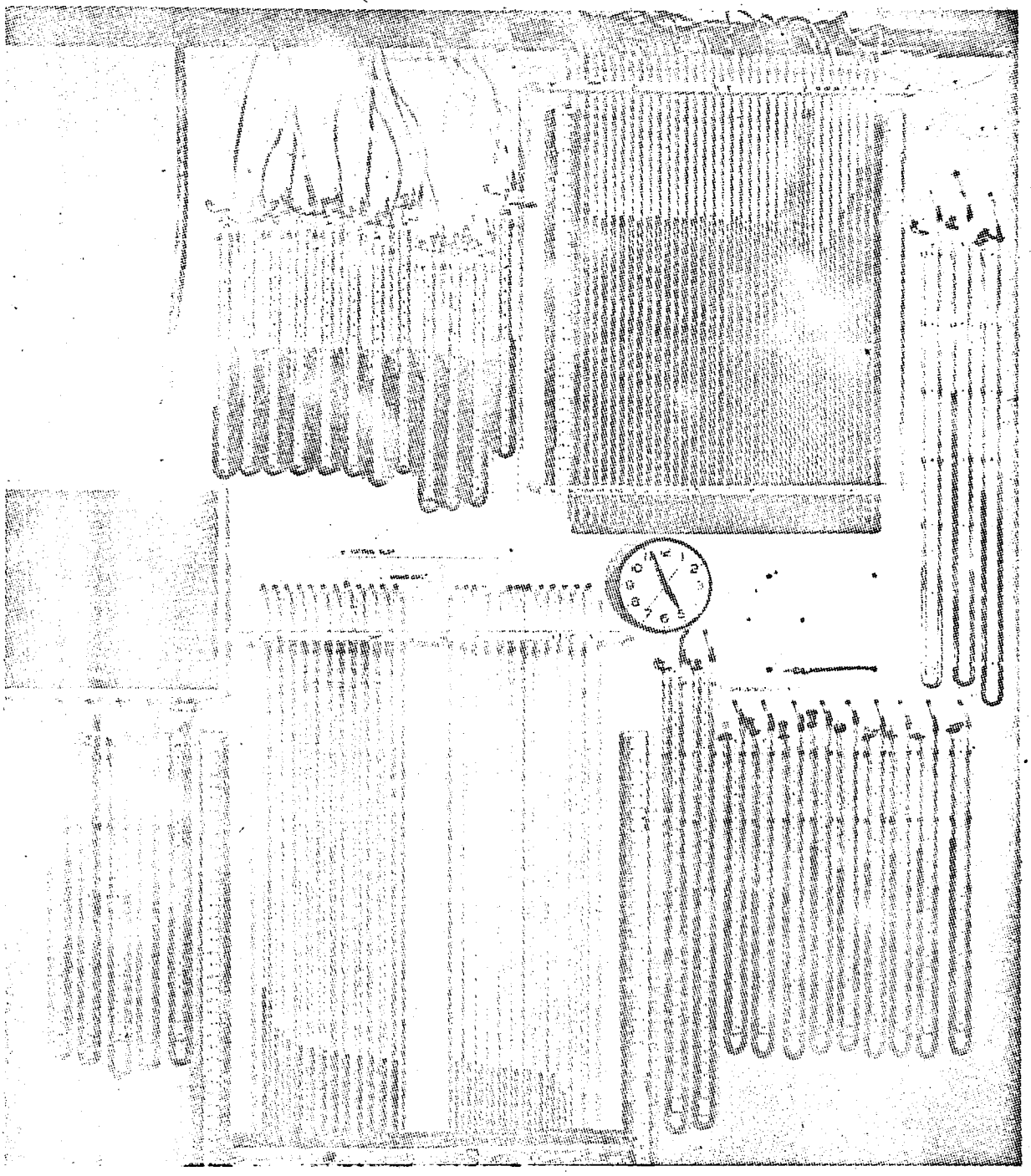

Figure 15.- Instrumentation bank.

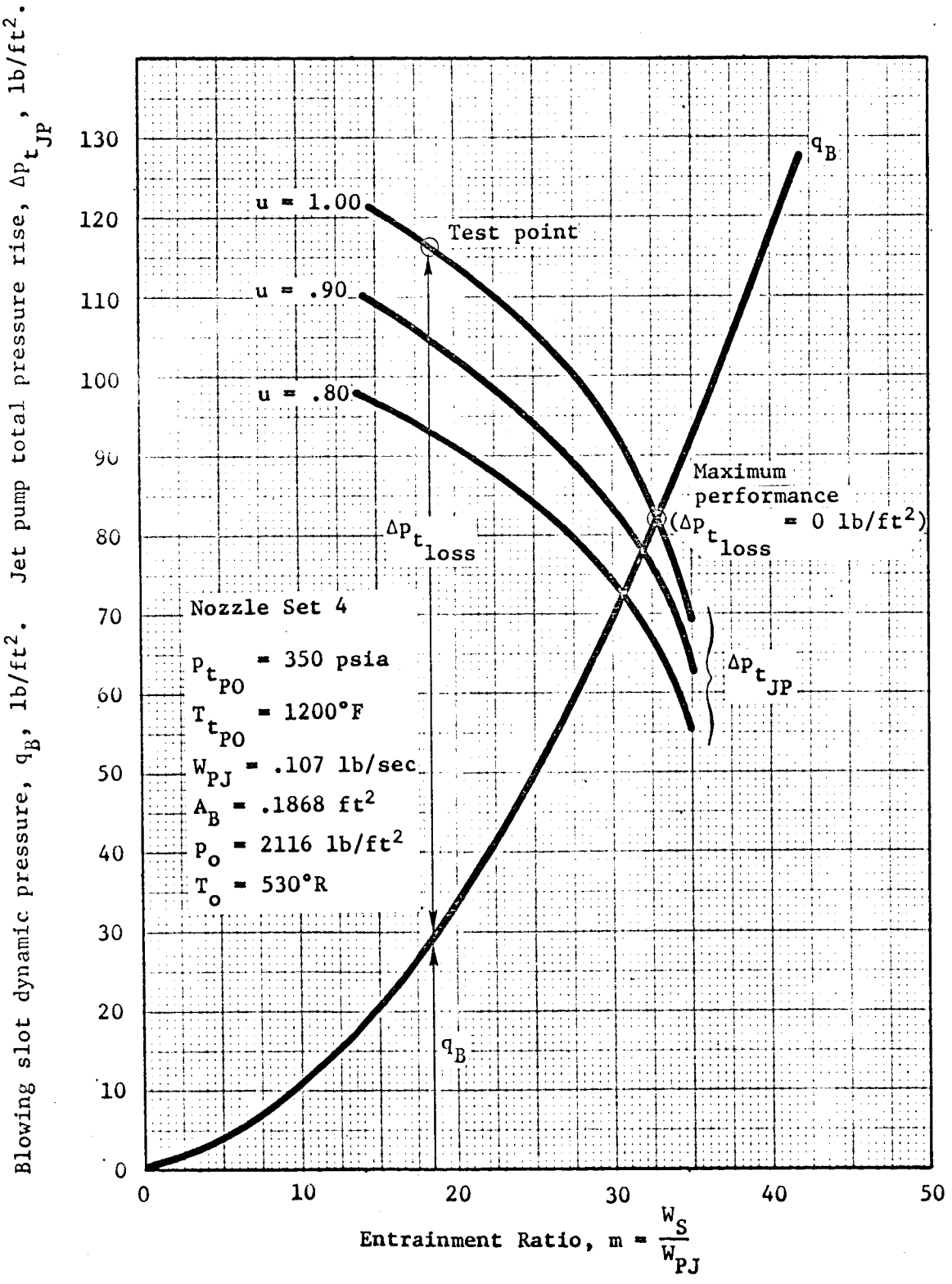

Figure 16.- Jet pump performance (test run 4-1).

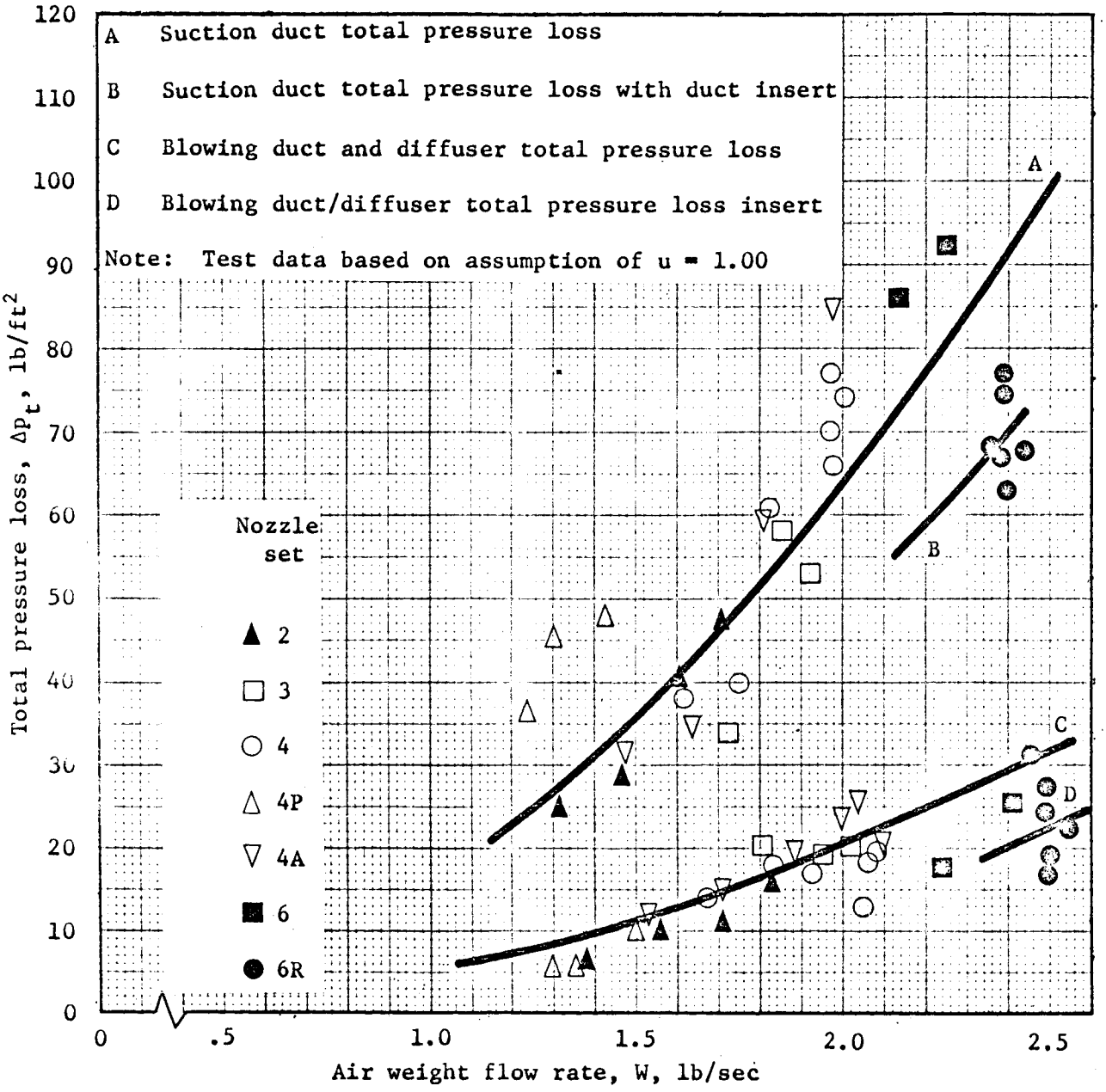

Figure 17.- Duct total pressure losses.

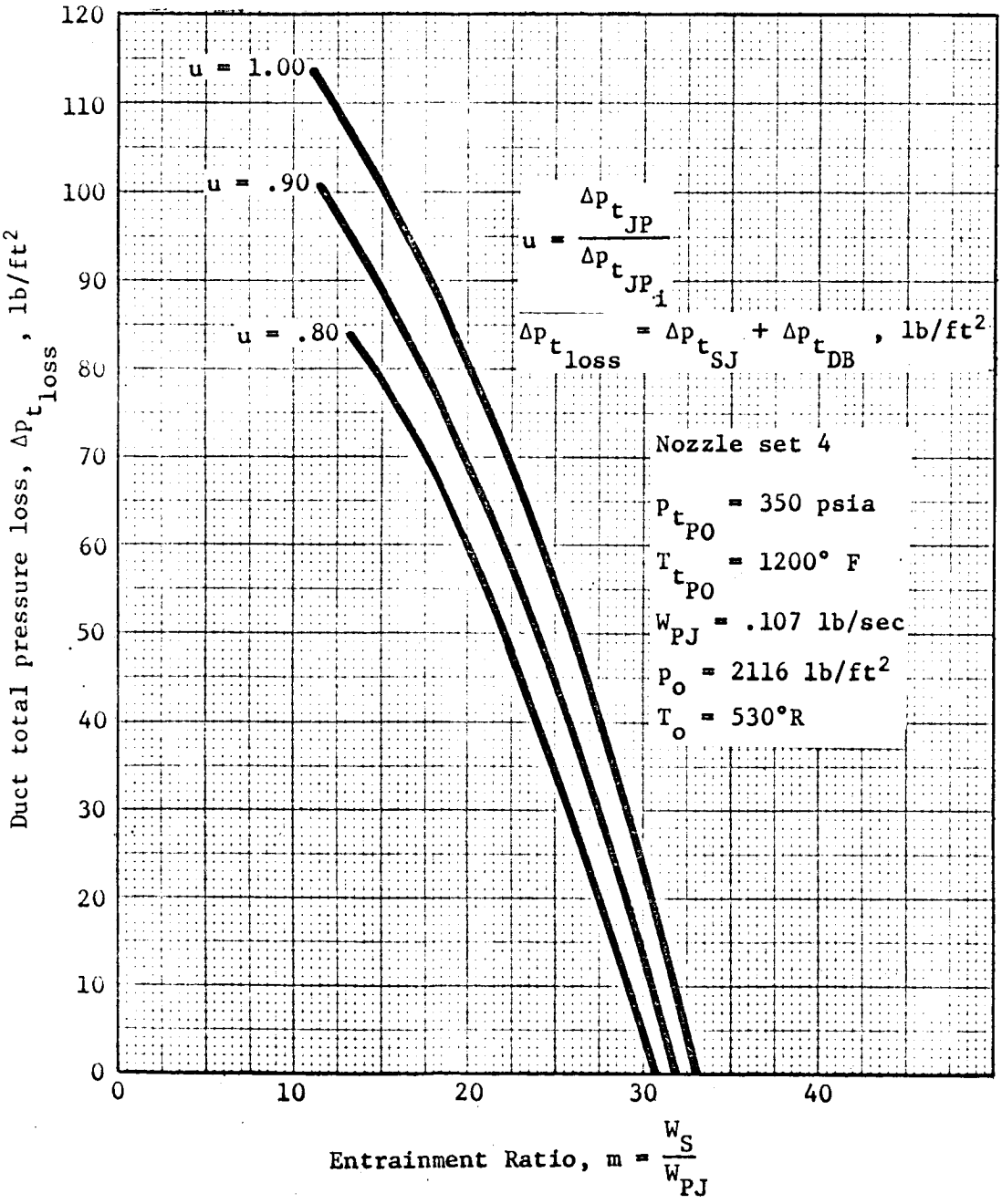

Figure 18.- Effect of total pressure loss on entrainment ratio (test run 4-1).

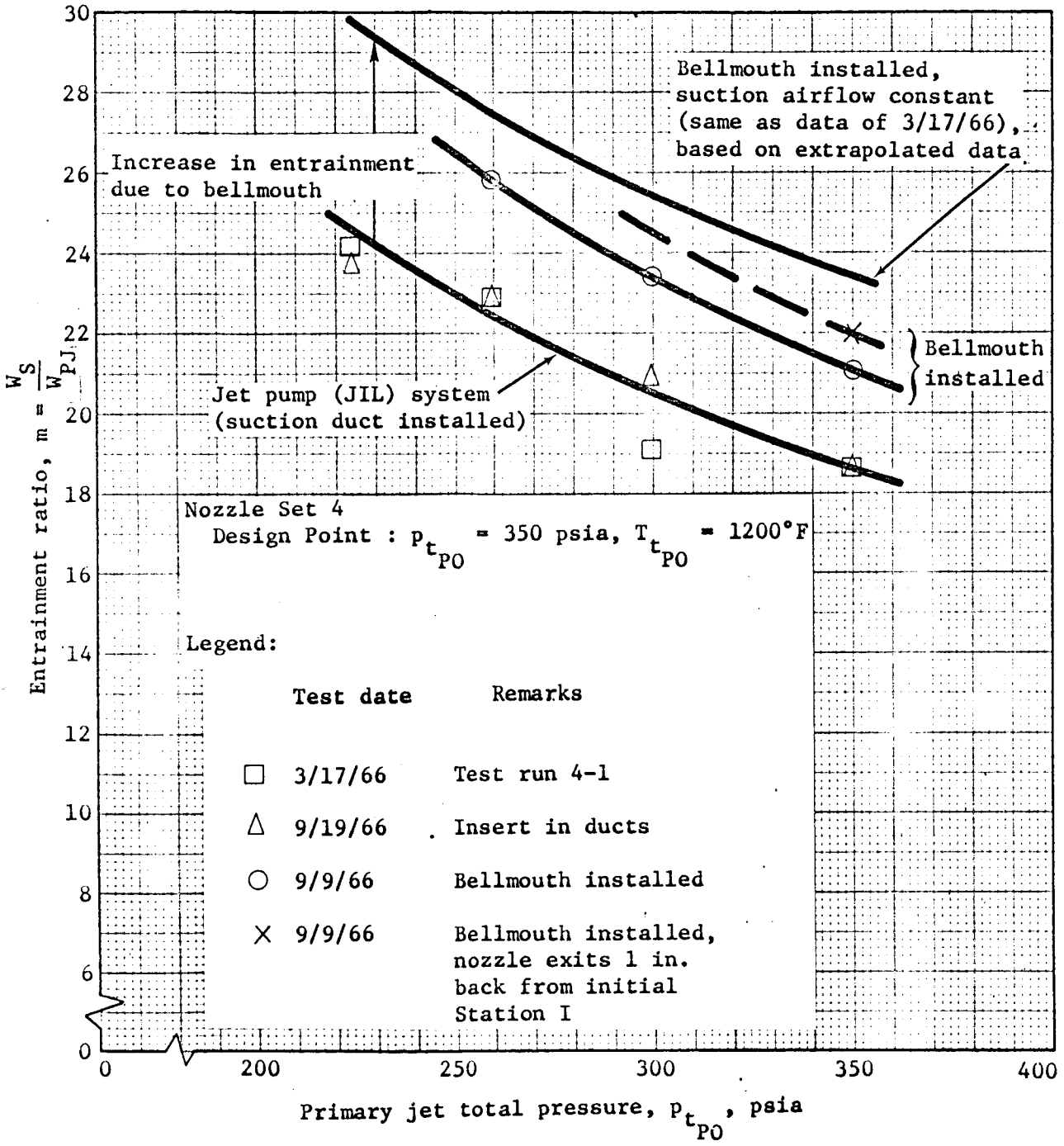

Figure 19.- Effect of bellmouth entrance on entrainment.

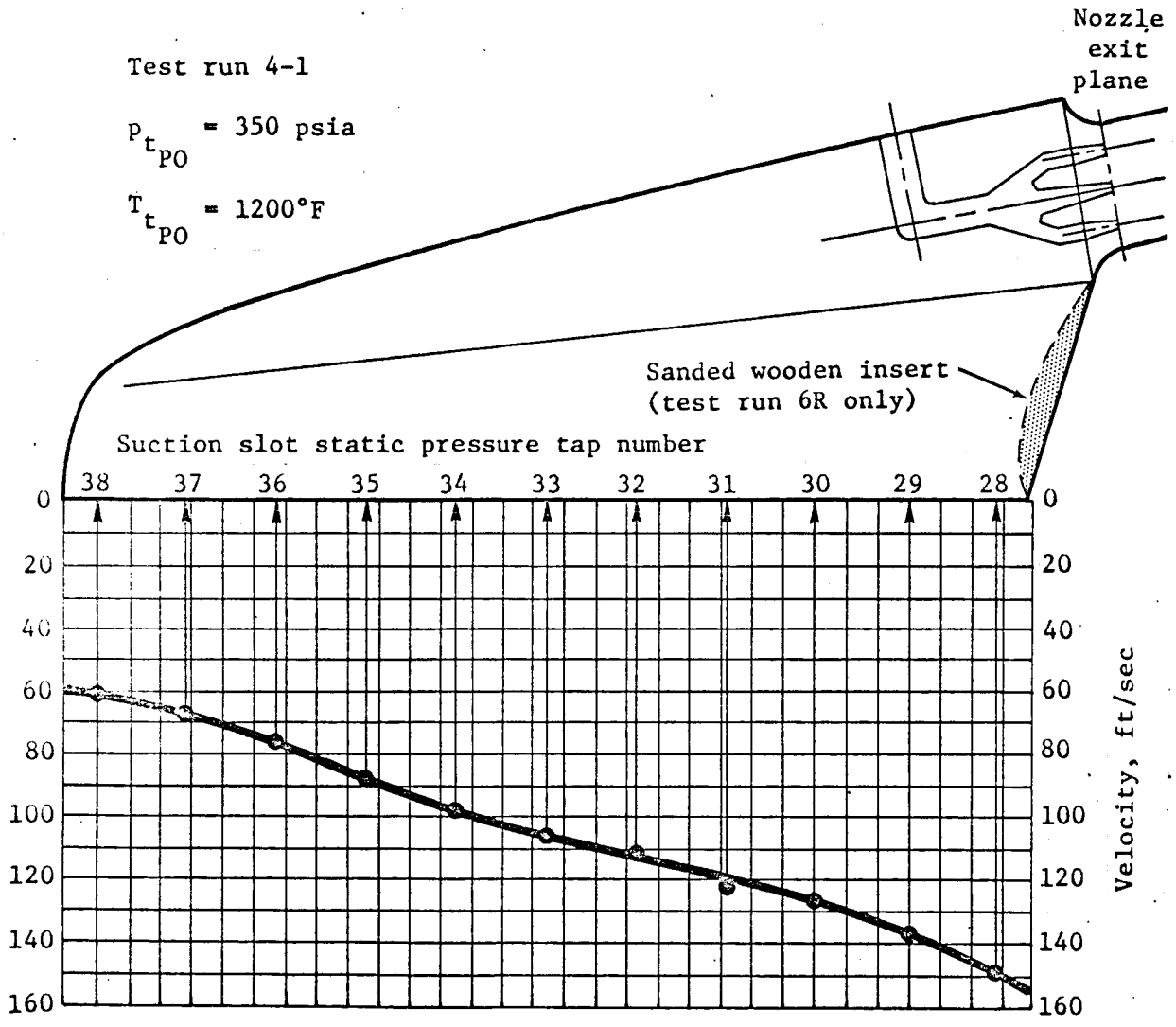

Figure 20.- Suction slot velocity distribution.

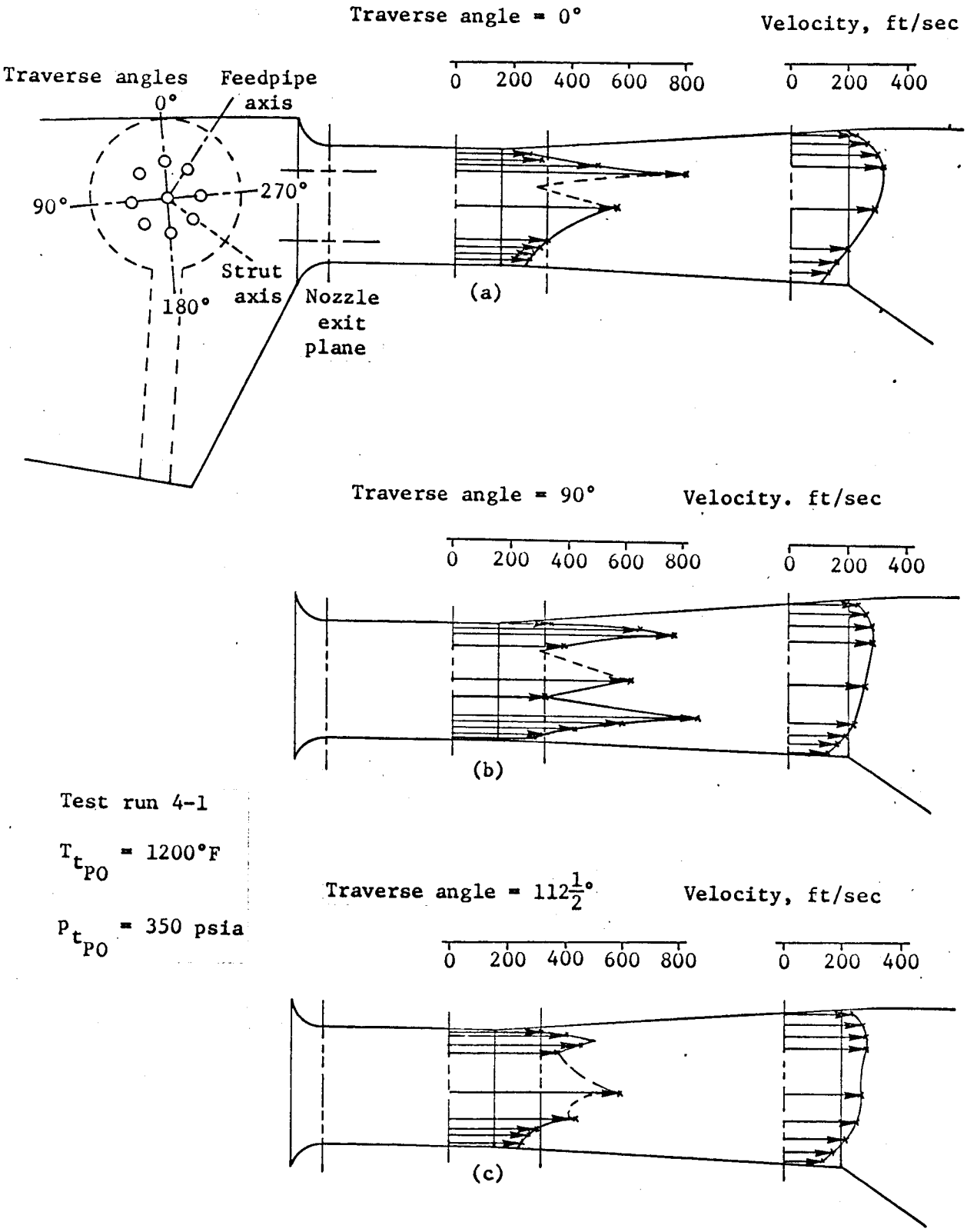

Figure 21.- Mixing tube and diffuser velocity profiles.

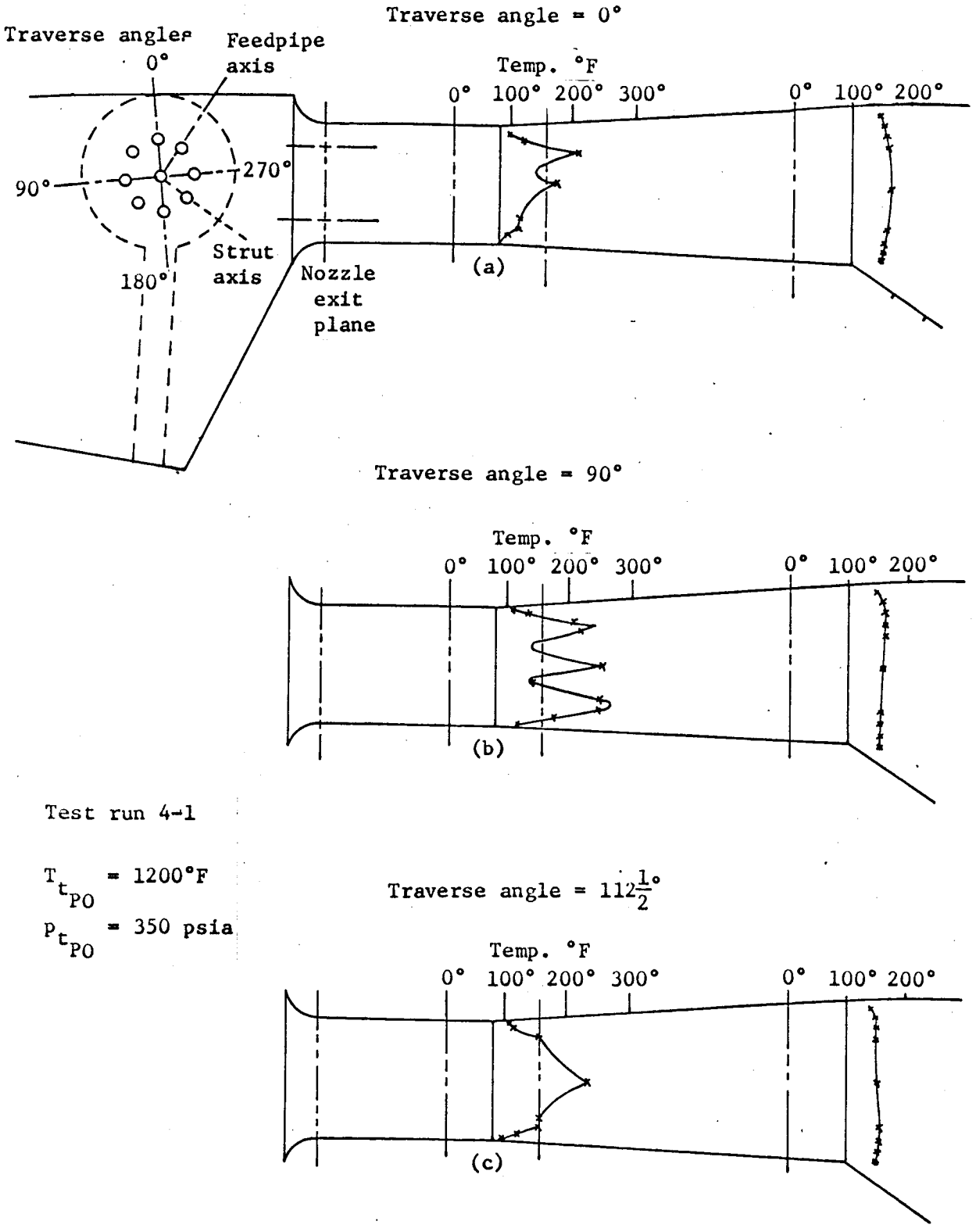

Test run 4-1

$T_{t_{PO}}$ = 1200°F

$P_{t_{PO}}$ = 350 psia

Figure 22.- Mixing tube and diffuser temperature profiles.

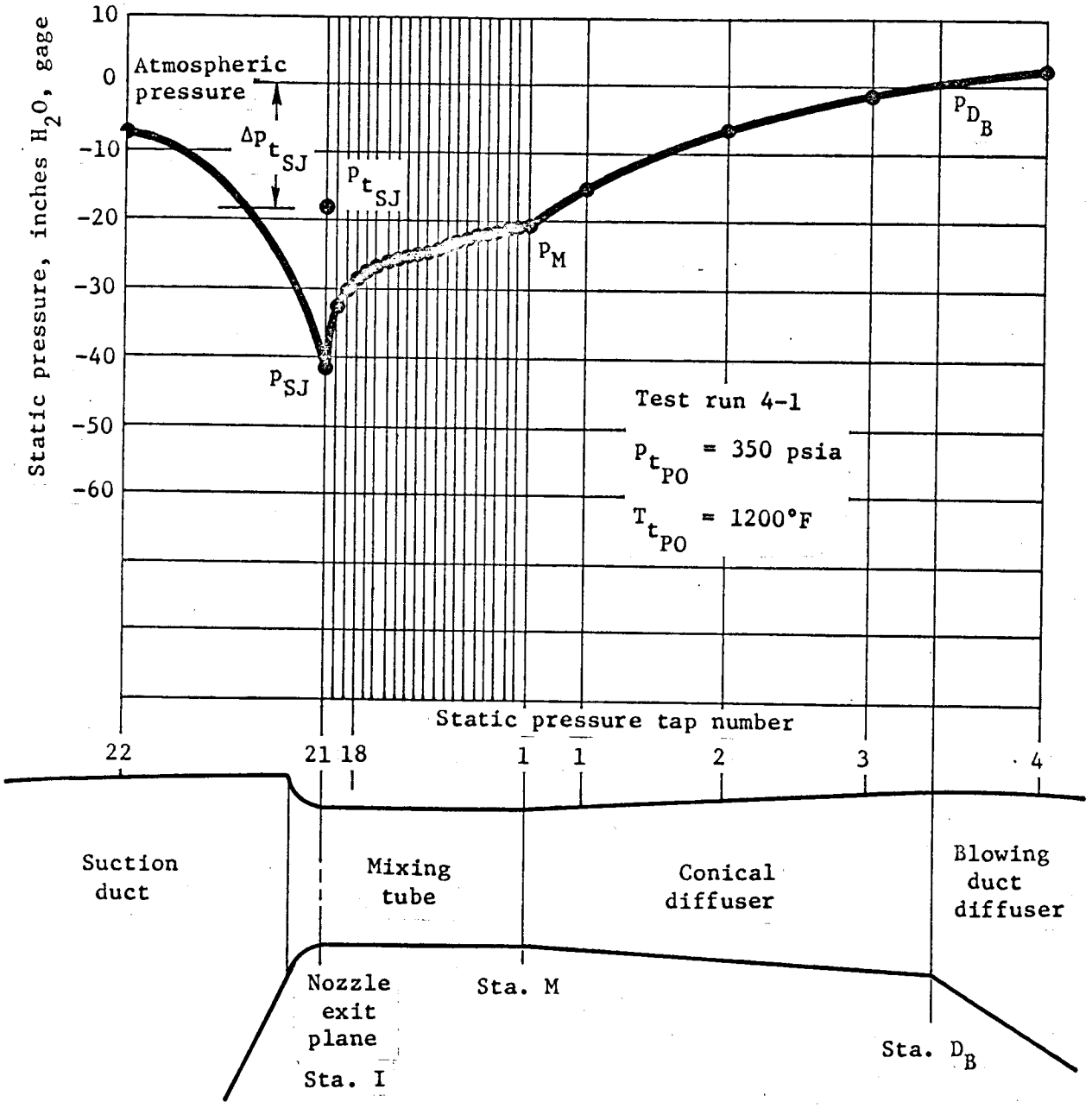

Figure 23.- Mixing tube and diffuser static pressure.

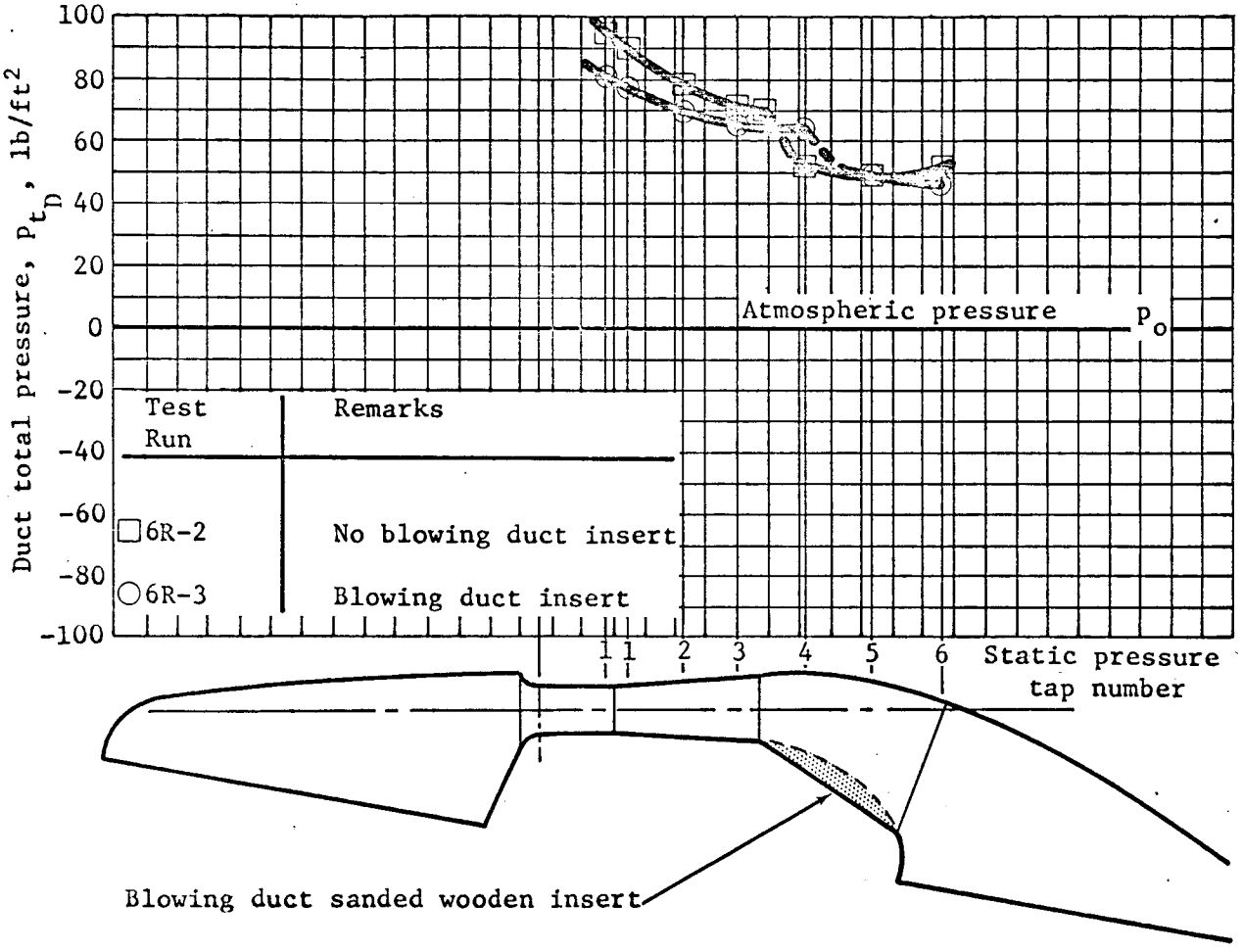

Figure 24.- Blowing duct total pressure distribution.

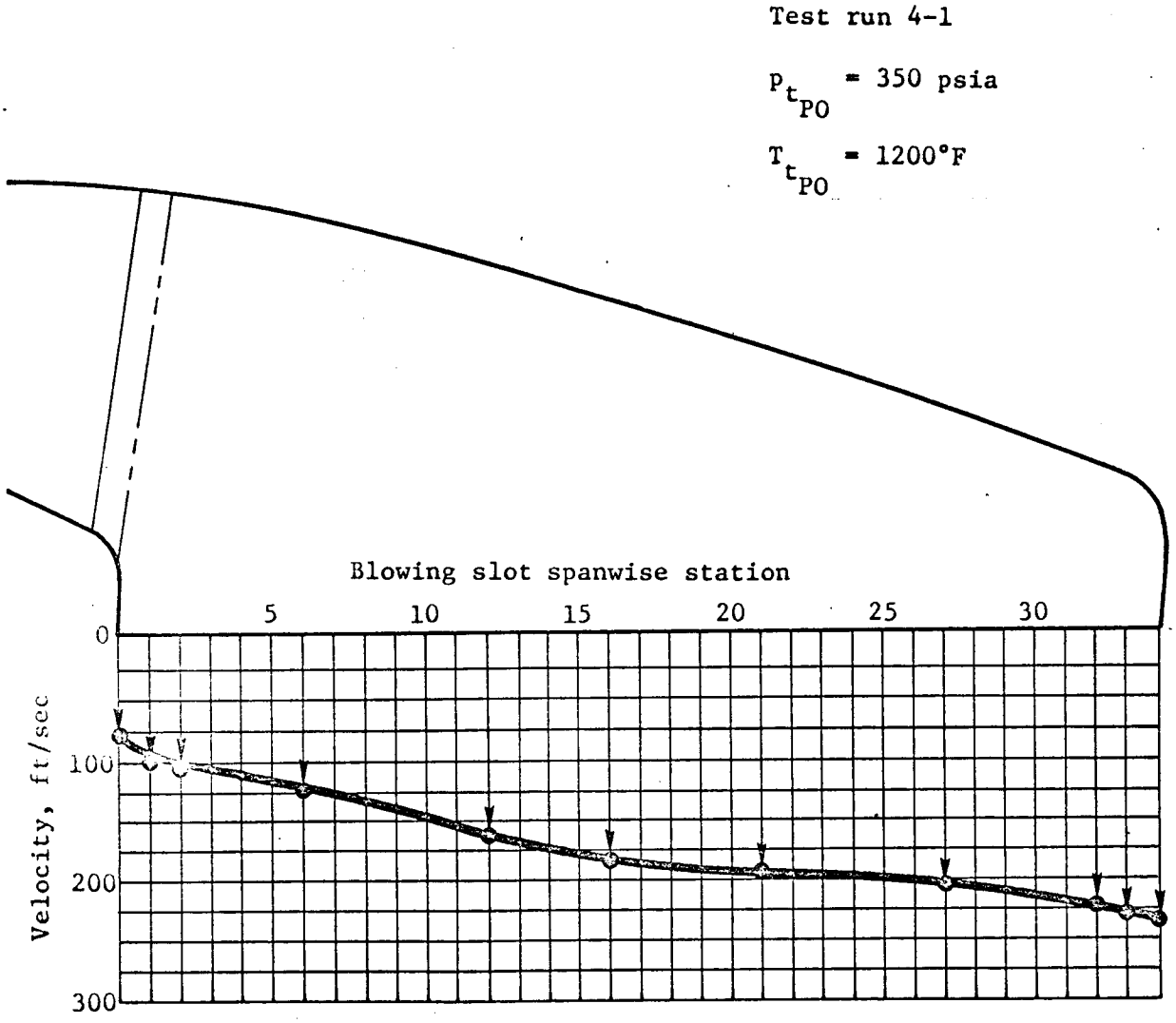

Figure 25.- Blowing slot spanwise velocity distribution.

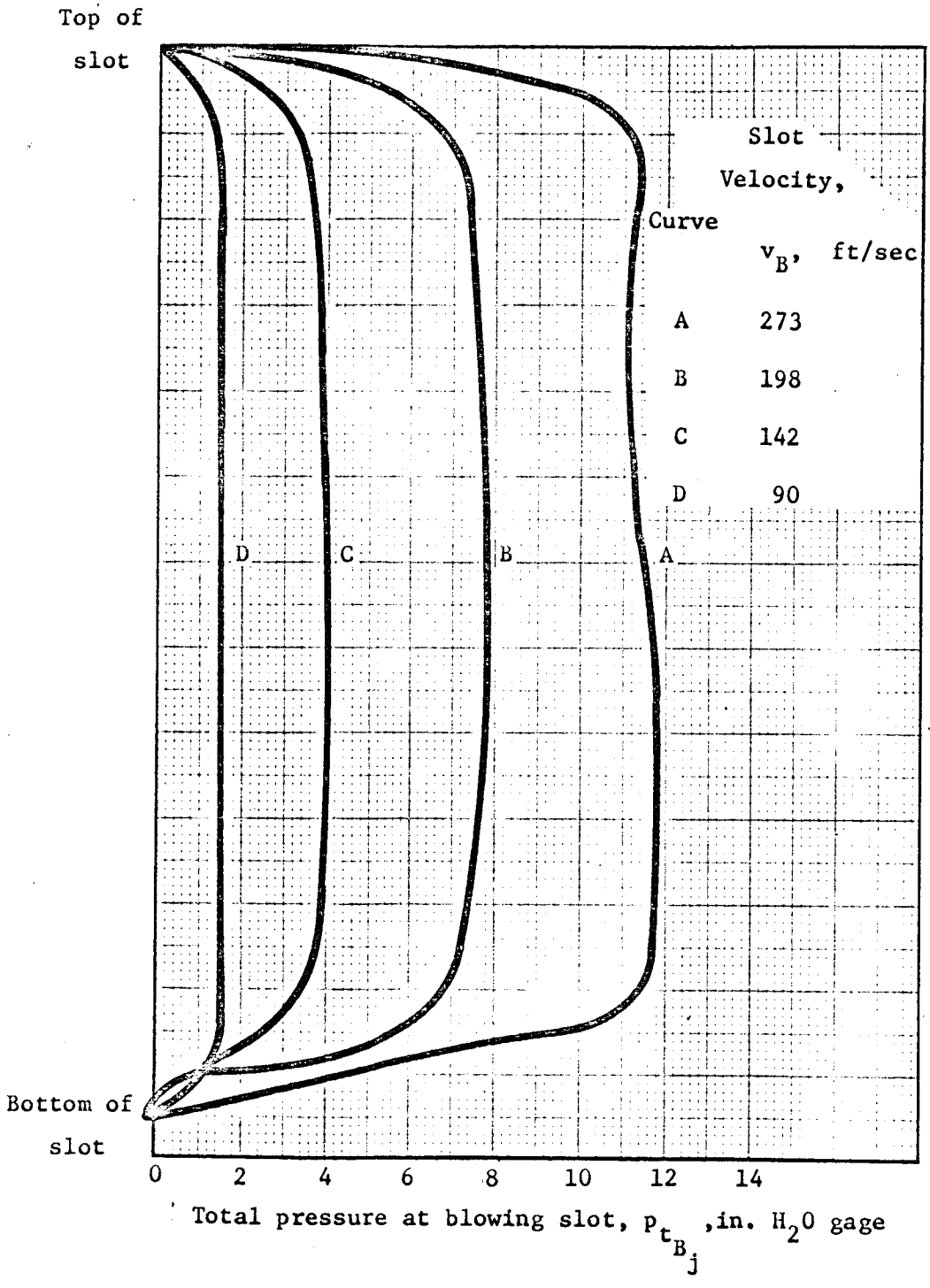

Figure 26.- Blowing slot total pressure profile.

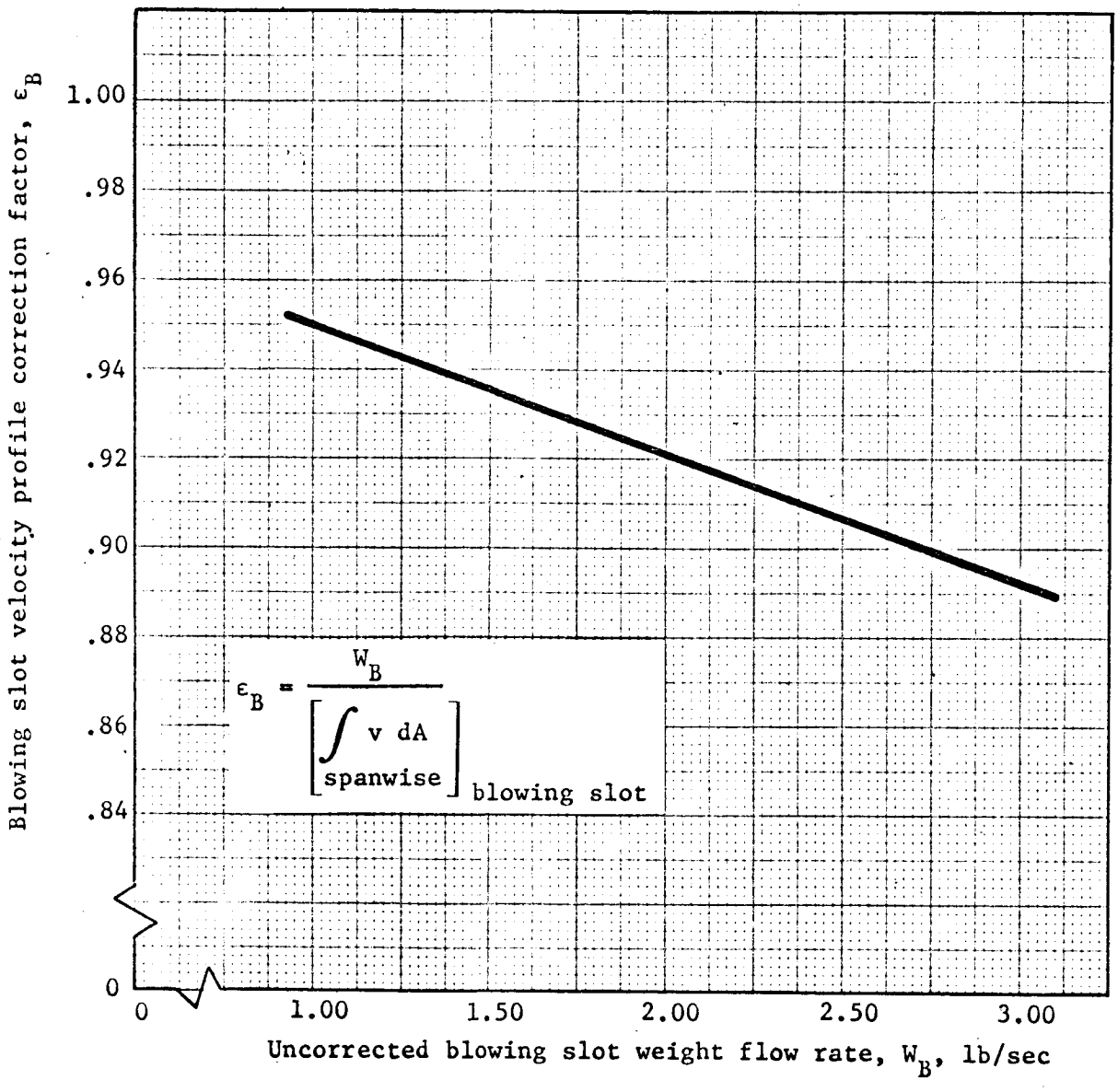

Figure 27.- Blowing slot velocity profile correction factor.

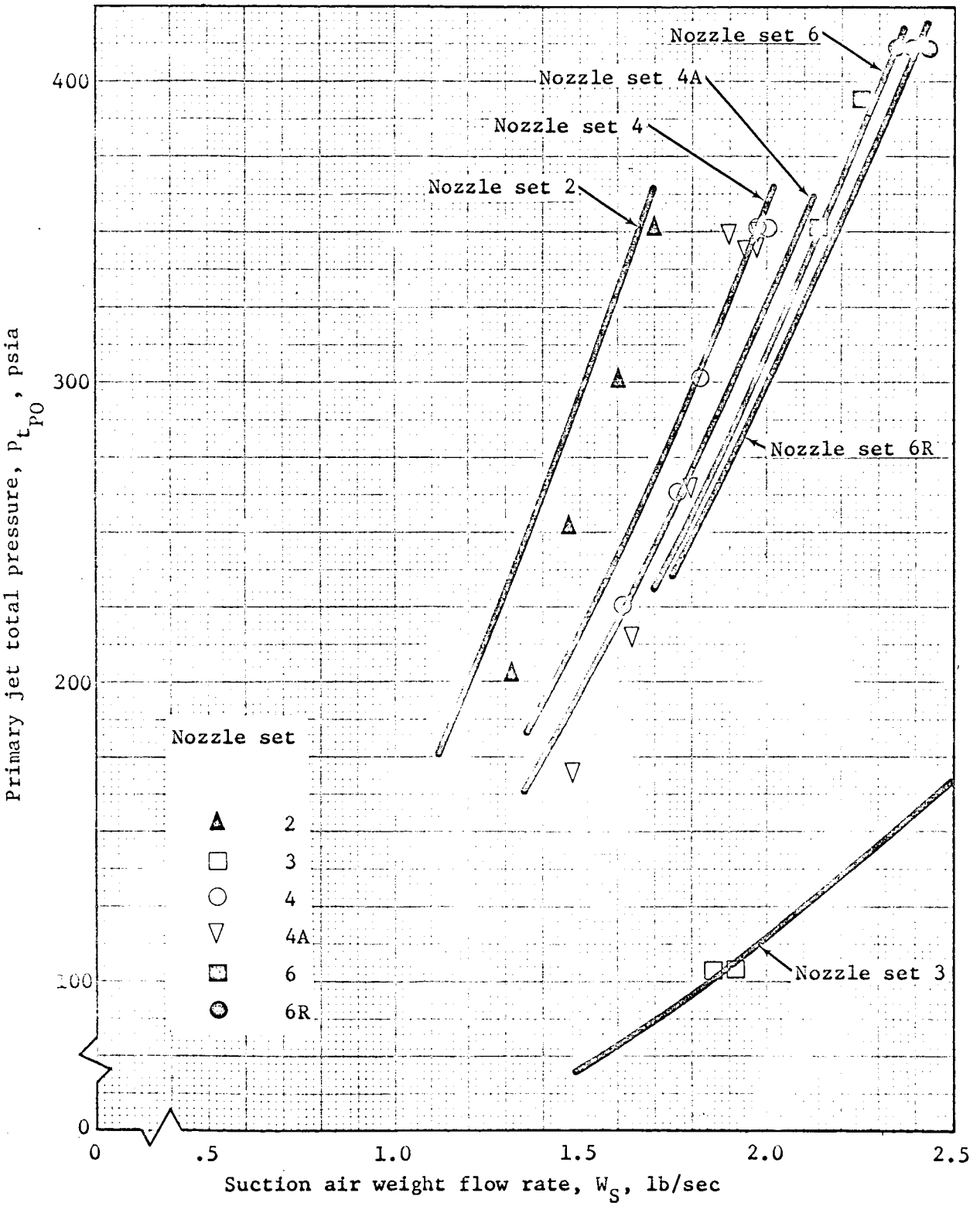

Figure 28.- Predicted jet pump performance.

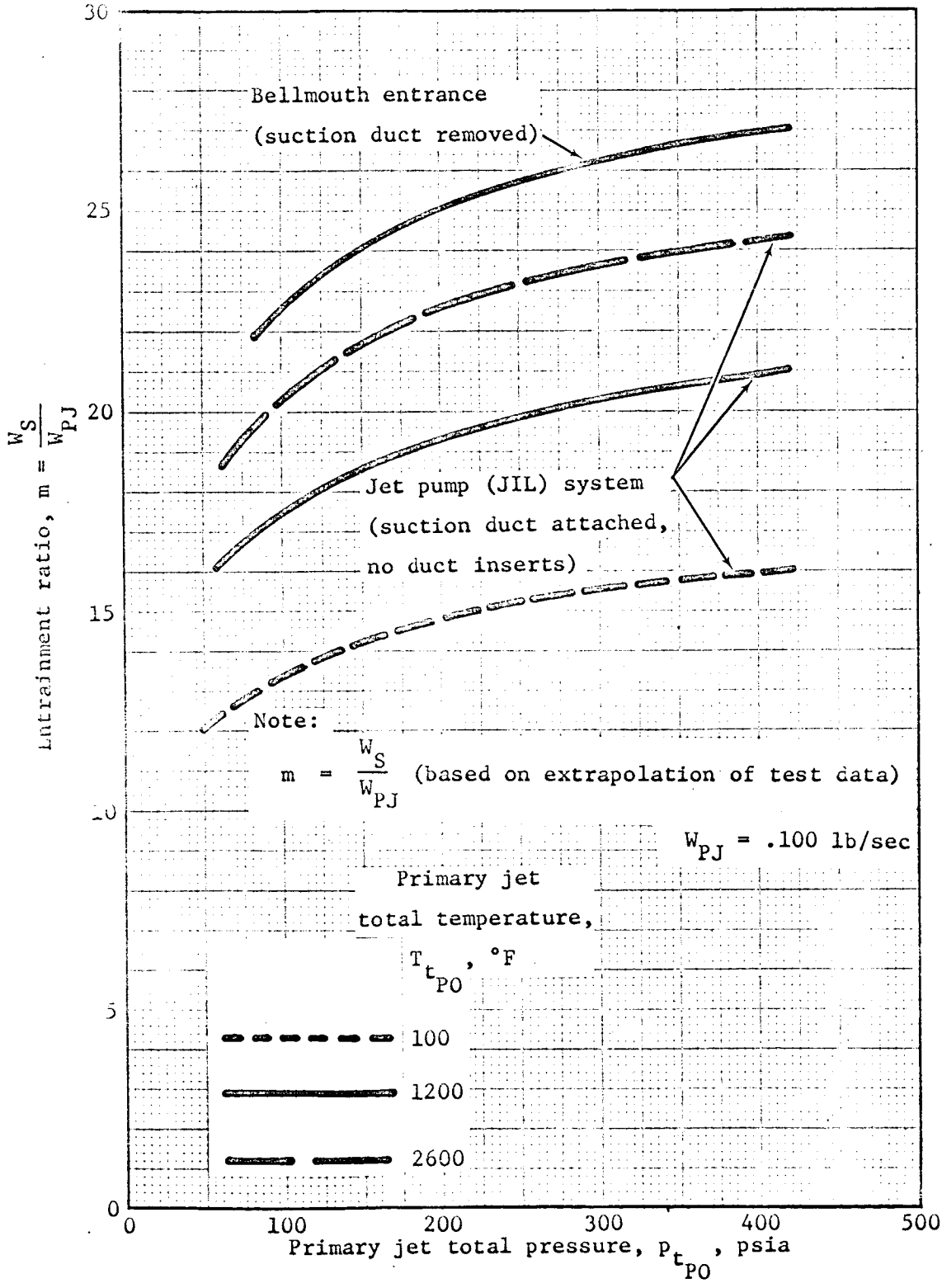

Figure 29.- Jet pump entrainment ratio.

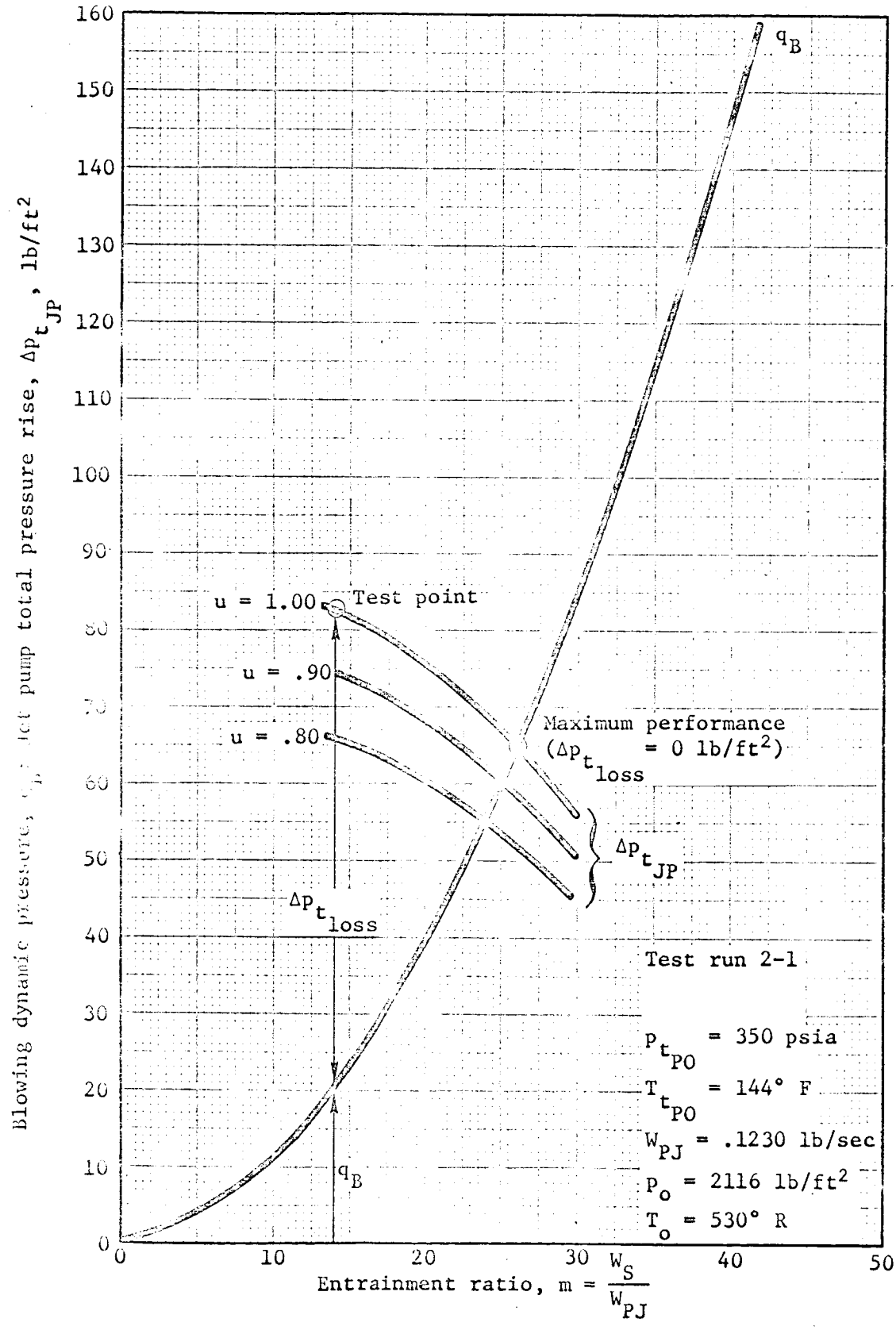

Figure 30.- Jet pump performance (test run 2-1).

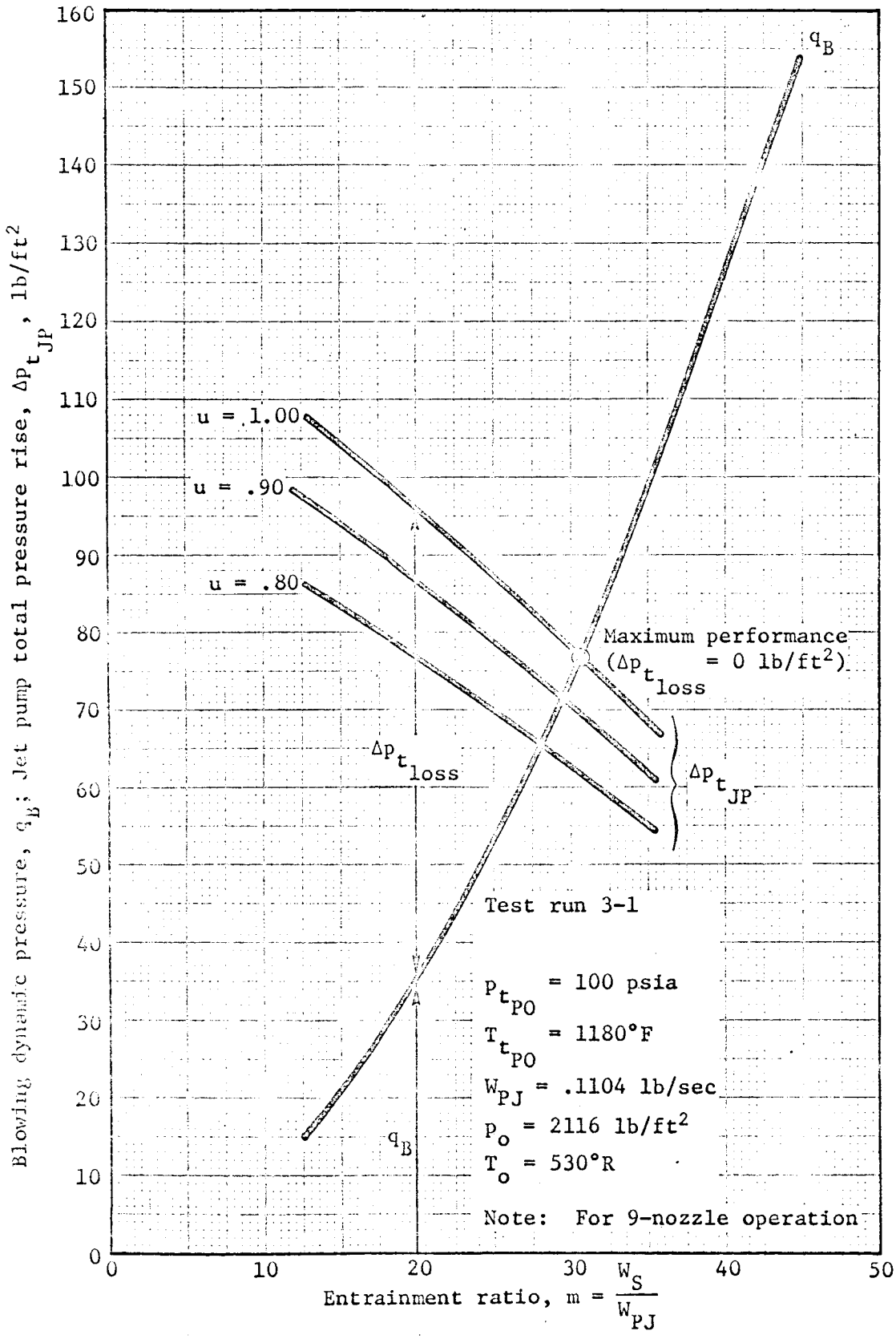

Figure 31.- Jet pump performance (test run 3-1).

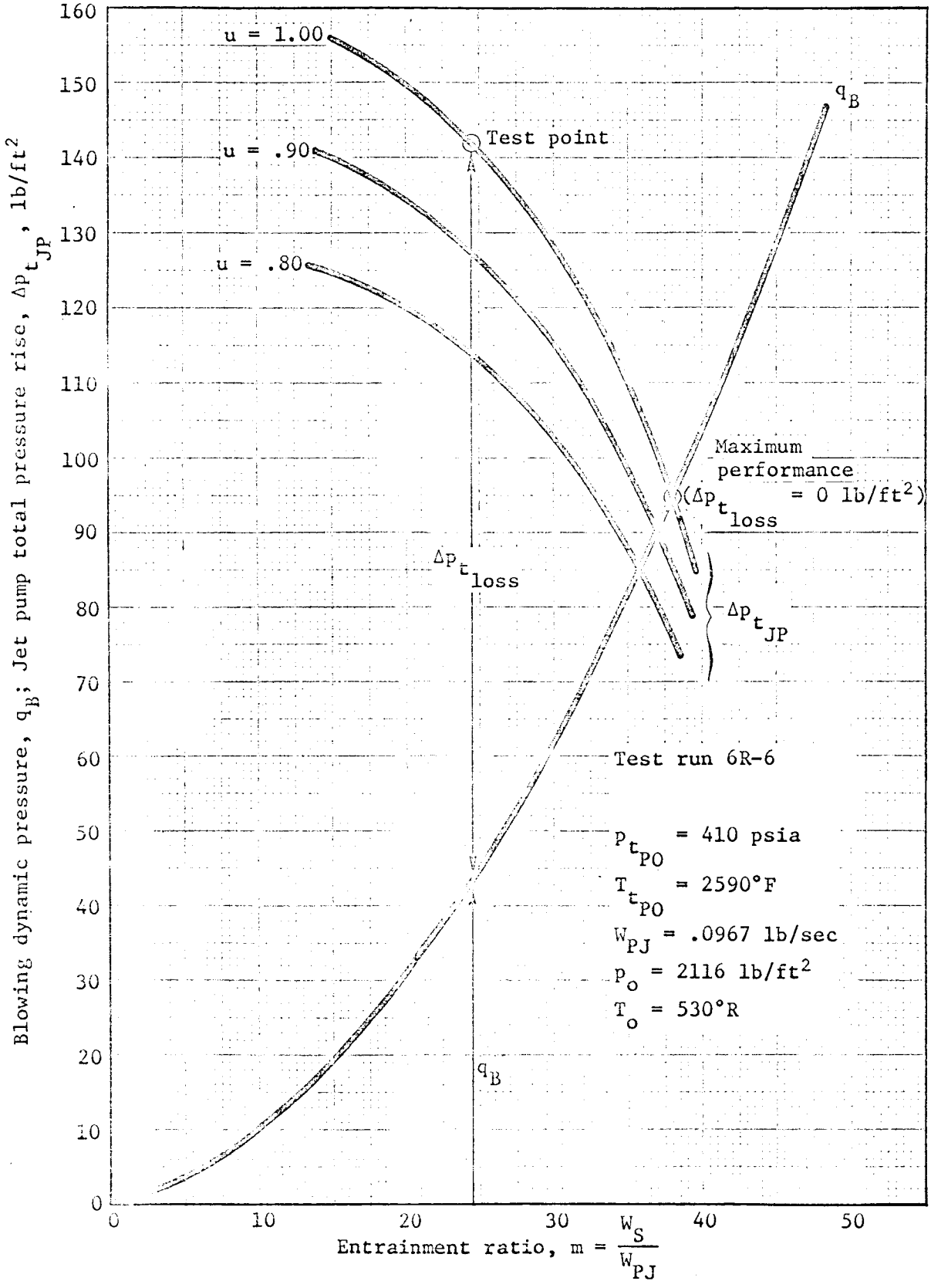

Figure 32.- Jet pump performance (test run 6R-6).

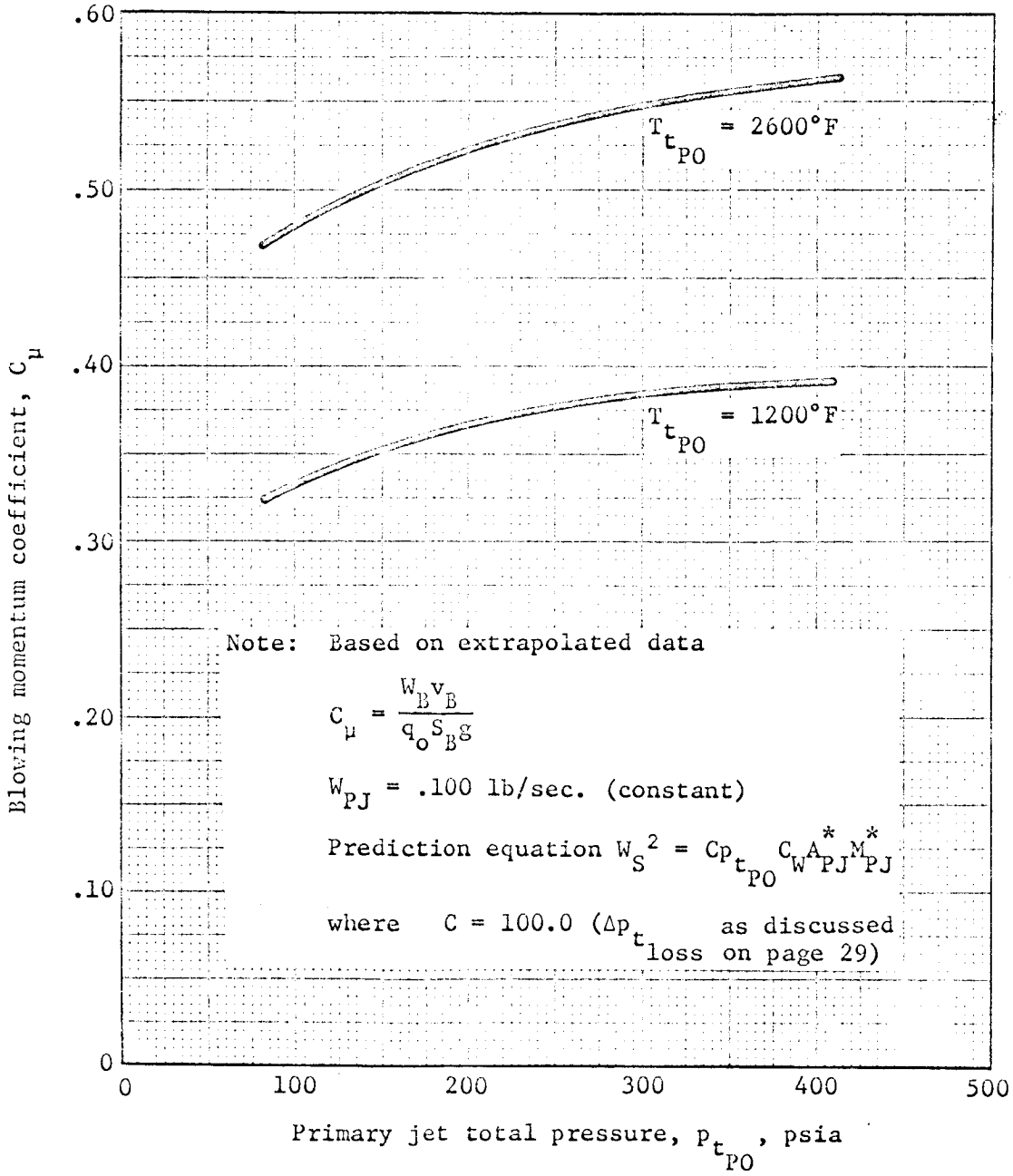

Figure 33.- Predicted maximum jet pump performance.

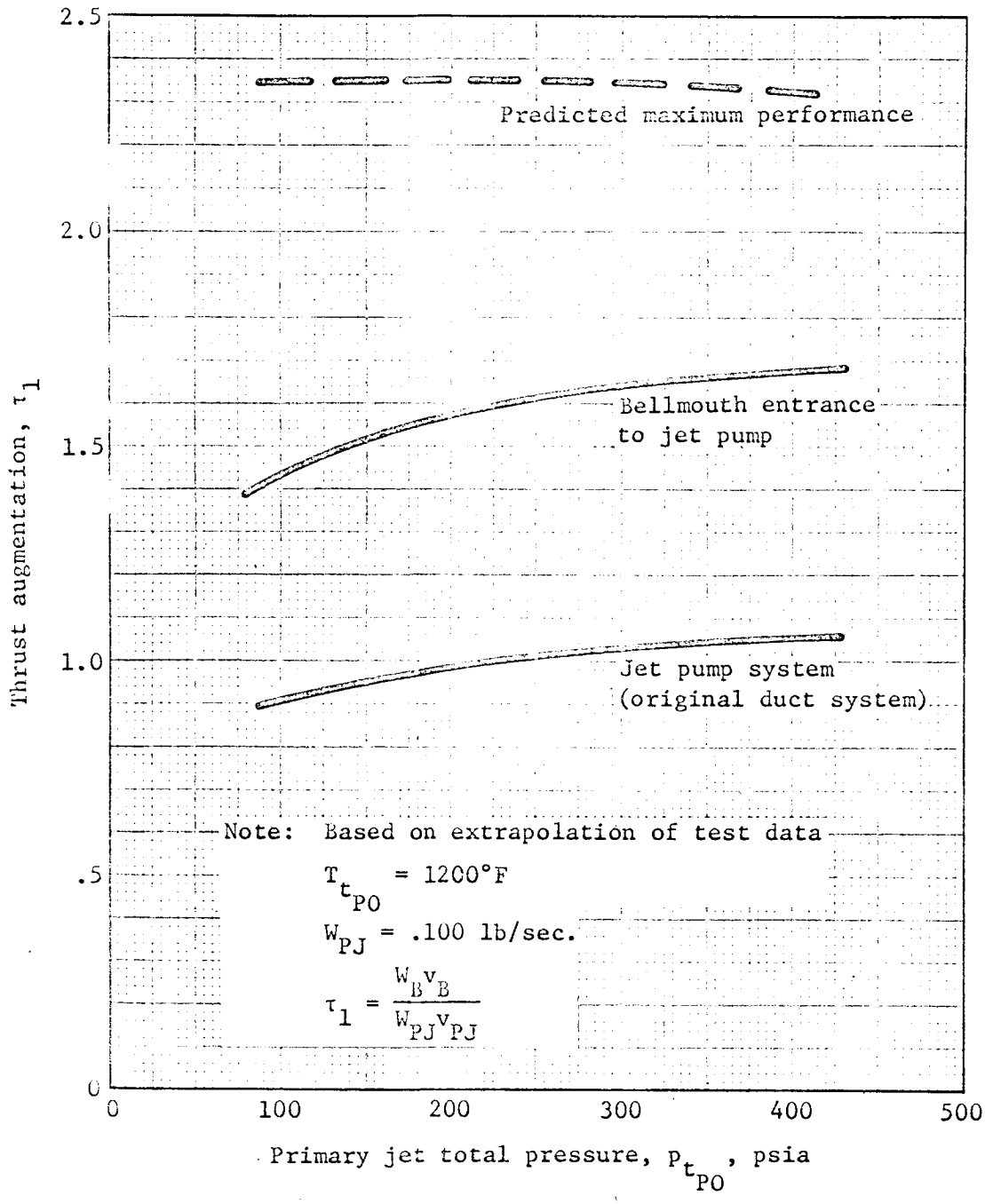

Figure 34.- Jet pump thrust augmentation.

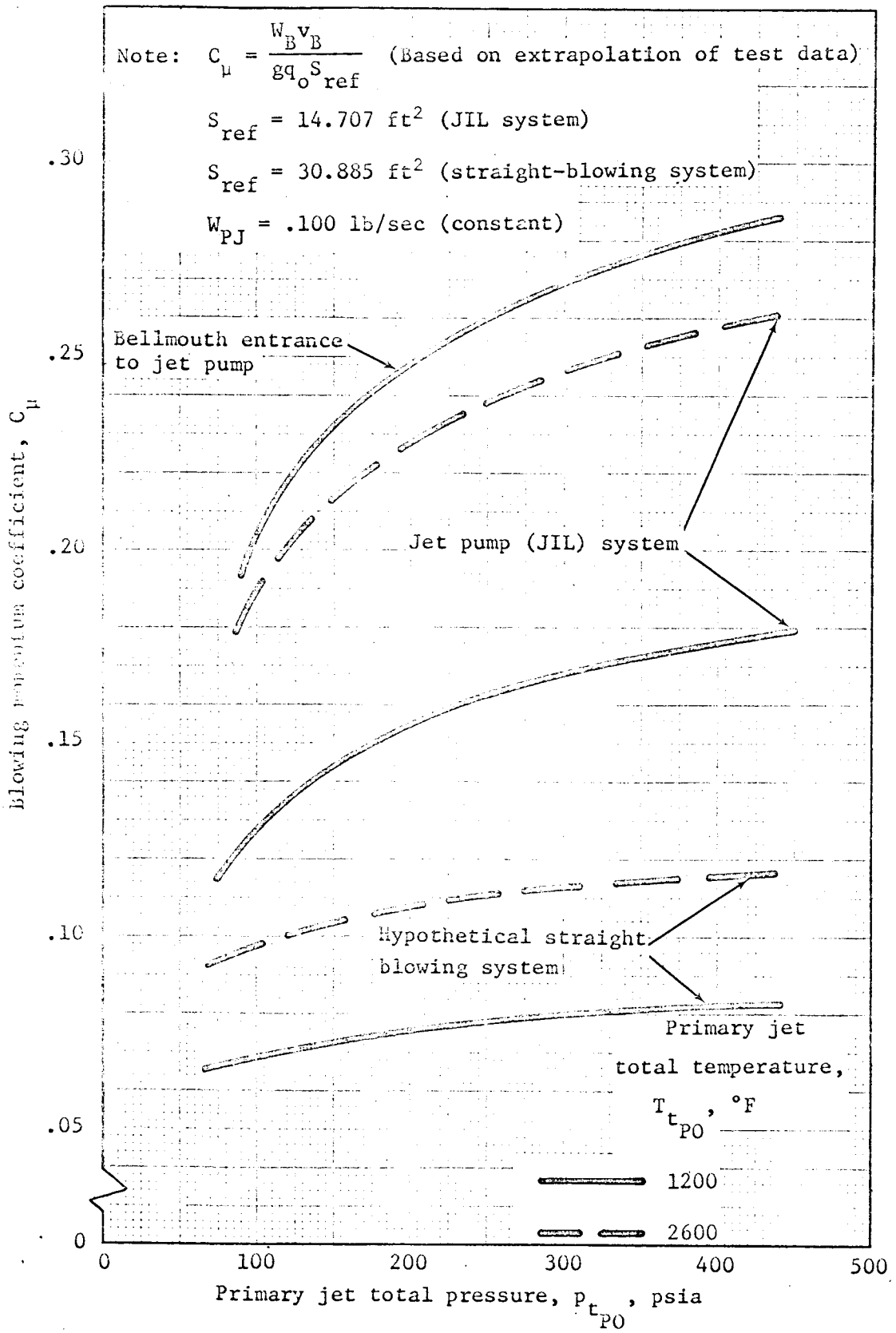

Figure 35.- Comparison of BLC systems.

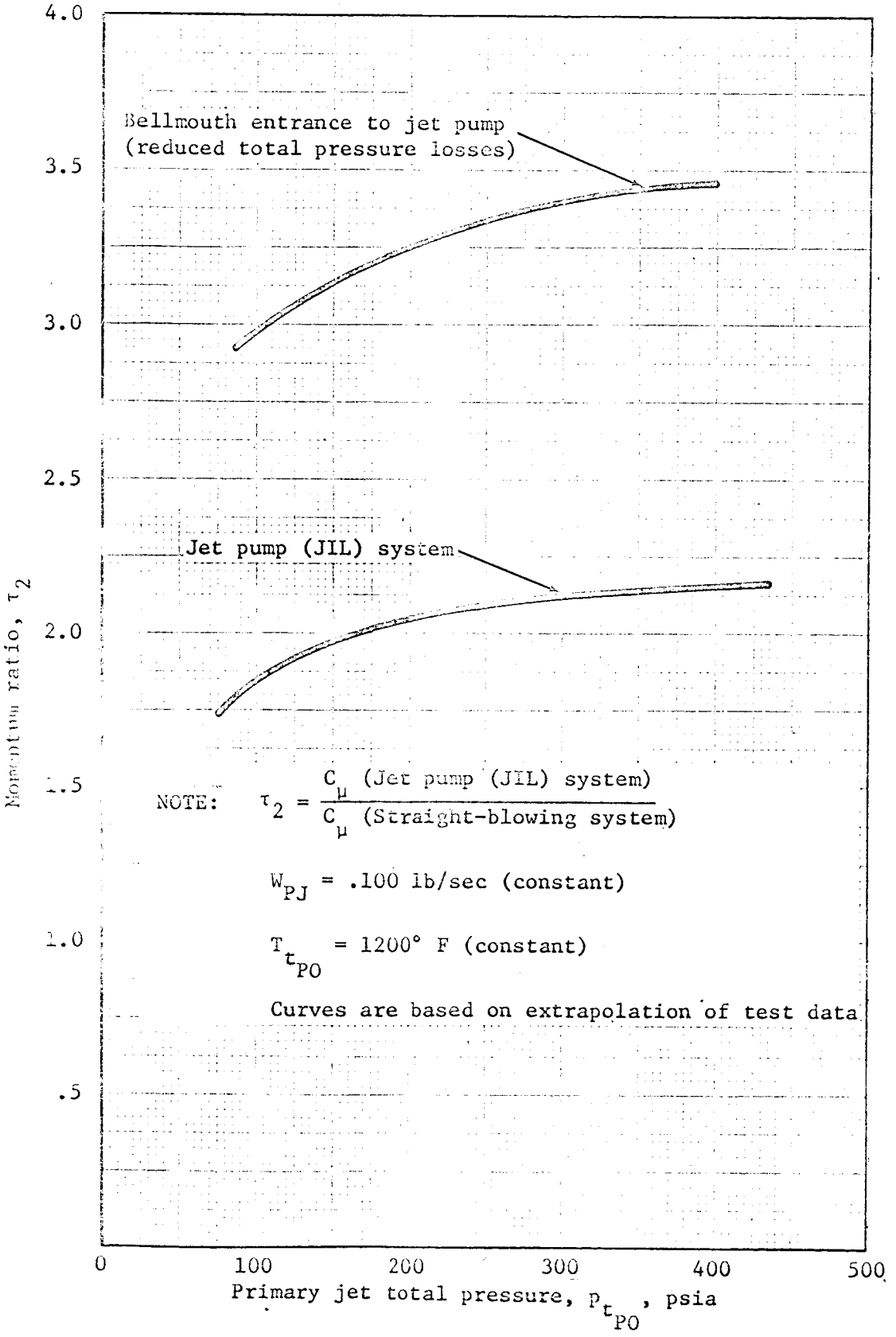

Figure 36.- Comparison of BLC systems.